ABSTRACT

NANDGAONKAR, AVINAV GHANASHYAM. Electrospinning of Chitosan and its Correlation with Degree of Deacetylation and Rheological Property. (Under the direction of Dr. Wendy E. Krause, TECS.)

Electrospinning is a technique that uses electric field to produced nanofibers in the range of 100 nm. Rheology of the polymer solution is one of the determining parameters for successful electrospinning. The electrospun nanofibers have found potential advantages in biomedical applications due to their high surface area to volume ratio and small pore size of the nonwoven mat, all of which helps cells grow, attach, and proliferate. In this project, chitosan is used to produce nanofibers via electrospinning. Chitosan was selected because of its biological properties, such as biocompatibility, biodegradability, and antibacterial, haemostatic and wound healing properties. Chitosan of different degrees of deacetylation were made using alkaline treatment. The degree of deacetylation and viscosity average molecular weight of three different chitosan samples were measured by acid-base titration and Ubbelohde viscometry method, respectively. Different solvents (formic acid, acetic acid, and trifluoroacetic acid) were used to electrospin the chitosan. Several material parameters: solvent, polymer concentration, and degree of deacetylation; and the process parameters: such as electric field (tip-to-collector distance and applied voltage) were investigated to optimize fiber consistency and diameter. The rheological properties of chitosan solutions (acetic acid) were measured using a rheometer. The morphology of electrospun nanofiber mats was observed using scanning electron microscopy (SEM). The entanglement concentrations of the two chitosan samples (deacetylation of 81% and 90%) in 90% acetic acid were determined. Below the entanglement concentration (1.8 wt%), only beads were formed and above entanglement concentration, the SEM images of electrospun

chitosan showed fiber formation. As the concentration and the degree of deacetylation increased, the average fiber diameter also increased as expected. At low electric field, there was more bead formation for chitosan sample having degree of deacetylation 81%, however, for 90% deacetylated chitosan sample, more smooth formation of nanofibers occurred.

Chitosan-TFA solutions were electrospun with different degrees of deacetylated chitosan, concentrations, and electric fields. Concentration below 3 wt% showed no fiber formation and concentration higher than 7wt% was not possible to extrude the polymer solution from the needle. Chitosan nanofibers were successfully electrospun from different degree of deacetylated chitosan having optimum concentration with lowest possible average diameter by varying the applied electric field. Chitosan dissolved in TFA solution with different degree of deacetylation were successfully electrospun onto a preexisting polysaccharide film that used for biomedical applications. The chitosan nanofibers are similar in size to the extracellular matrix (ECM) and could potentially be useful in tissue engineering and wound healing applications.

Electrospinning of Chitosan and its Correlation with Degree of Deacetylation and Rheological Property

by
Avinav Ghanashyam Nandgaonkar

A thesis submitted to the Graduate Faculty of
North Carolina State University
in partial fulfillment of the
requirements for the degree of
Master of Science

Textile Engineering

Raleigh, North Carolina

2011

APPROVED BY:

_____	_____
Dr. Wendy Krause Committee Chair	Dr. Russell Gorga
_____	_____
Dr. Samuel Hudson	Dr. Saad Khan

DEDICATION

To my *family* and *friends* for their constant support and encouragement.

BIOGRAPHY

Avinav G. Nandgaonkar was born on April 23rd, 1985 in Nagpur, Maharashtra. He did his schooling from Guru Nanak High School and Dr. Ambedkar College, Nagpur, India in 2003 and received an undergraduate degree in Textile Technology (B.Tech) from Veermata Jijabai Technological Institute (V.J.T.I.), Mumbai, India in 2007. After completing his bachelor of technology degree, he obtained professional experience as a service engineer at Sultex India Private. Limited, Mumbai. He came to the United States to pursue a Master of Science degree in Textile Engineering at North Carolina State University in Fall 2009.

ACKNOWLEDGMENTS

I would like to express my immense gratitude to Dr. Wendy Krause for her constant support, guidance, and encouragement during this research work. Dr. Krause has been an excellent mentor and great source of inspiration and motivation. She was always been there to point me in the right direction with great advice whenever I needed it. I would like to thank my advisory committee members Drs. Samuel Hudson, Russell Gorga and Saad Khan for their suggestions and reviewing my research work. The research was definitely a challenge for me and it has been a great experience working with them over the last two years.

I would also like to acknowledge my lab members especially Tianbin Zhou, Rebecca Klossner, and Mangesh Champhekar for their help, advice, fruitful discussions and smiles through the course of my research. I am grateful to Maria Ina and Abdelrahman Mohamed Abdelgawad, the Fiber and Polymer Science PhD students, for teaching me the synthesis and characterization techniques. I am thankful to Mrs. Judy Elson for training me on the Scanning Electron Microscope and for technical help and consultations. I would like to thank Ms. Angie Brantley for her help and coordination to make my graduate studies in NCSU more convenient.

It gives me immense pleasure to acknowledge all my friends and family back in India especially Sohail, Lokesh, Devesh, and Dilraj who supported and encouraged me through the difficult time of my life. Life here in NC State would not have been so easy without their unconditional love and timely help.

I would like to offer special appreciation to all my friends here in NC State especially Partha, Vidya Viswanath and to my roommates; Naren, Rupesh and Lalith for their love, help, guidance, and support throughout my graduate studies.

Finally, I would like to thank my parents Ghanashyam and Sheela Nandgaonkar, sisters and sister-in-laws who believed in my dreams and have been a blessing in my abilities. I lack the words to express my gratitude toward my brother, Rahul Nanadgaonkar who found my inner potential and inspired me to do higher studies.

TABLE OF CONTENTS

LIST OF TABLES

LIST OF FIGURES

ELECTROSPINNING OF CHITOSAN AND ITS CORRELATION WITH DEGREE OF DEACETYLATION AND RHEOLOGICAL PROPERTY

1. INTRODUCTION

1.1 Background and Significance

Nanofibers are the exciting new class of materials notable for their very small size (around 100 nm). These nanofibers have gained much attention in the last decade because of their very small size, large surface area to volume ratio, and small pore sizes of their non-woven mats as compared to regular fibers [1]. These special properties of nanofibers make them suitable in wide area of applications such as filtration for submicron particles,[2,3] protective clothing like military warfare,[4,5] and for biomedical applications such as tissue engineering scaffolds,[6-10] wound dressings,[11-13] and drug delivery [11,14,15].

Electrospinning is one of the methods used to produce nanofiber which was discovered by Zeleny, *et* al. in 1914 [16]. It is a simple technique and has gained much attention in the last two decades due to its versatility in spinning a wide variety of polymeric fibers. This spinning process is capable of producing nanofibrous structure of biopolymers which is similar to natural extracelluar matrix (ECM) for tissue engineering and scaffolding. The nanofibrous structure has very high surface area with certain porosity which helps the cells to attach, proliferate, and migrate. The cells on artificial ECM then help the tissue to grow and therefore, promotes wound healing [6,17,18].

Chitosan can be used as a component in the extracellular matrix to promote wound healing because of biological properties such as biocompatibility, biodegradability, and its antibacterial, haemostatic and wound healing properties [19-21]. Chitosan is a cationic (under acidic conditions) polysaccharide polymer which is a deacetylated product of chitin. The degree of deacetylation is the percentage of free amino group in the polysaccharide. A higher degree of deacetylation leads to higher number of positive amine groups under acidic conditions on the chitosan backbone due to the protonation of $–NH_2$. This property of chitosan found applications in tissue engineering scaffolds in which the protonated $–NH_2$ of chitosan allows cells matrix interaction with the negatively-charged group on the cell surface which facilitates to retain and increase the growth factor of cells [19,21-24].

A potential application of chitosan nanofibers is in the treatment for post surgical adhesions. A surgical adhesion is the formation of abnormal tissue linkages when two injured tissues come in contact with each other during the initial healing process after surgery [25]. Around 80% of patients suffer from adhesion after abdominal surgery. These post surgical adhesions affect the proper function of body, potentially causing intestinal obstruction, bowel obstruction, chronic abdominal pain, and female infertility. Moreover, they can even cause problems in future surgical procedures [26].

Even after careful surgical procedure, high chances of post surgical adhesions are possible. Various methods have been proposed to prevent and reduce the post surgical adhesion like

pharmacological agents and use of barrier films. The barrier film between the two injured tissues is a practical way to prevent post surgical adhesion [27,28]. Commercial barrier films are available for the prevention of surgical adhesion like Polyactive$^{(TM),}$ PRECLUDE Peritoneal Membrane$^{(TM)}$, Seprafilm^{TM}, and Tissucol^{TM} [29]. Seprafilm^{TM} is an anionic, bioresorbable polysaccharide membrane of chemically modified hyaluronic acid (HA) and carboxymethylcellulose that is biocompatible, nontoxic and nonimmunogenic which shows reduction in post-surgical adhesion after surgery [26]. One potential limitation is that the barrier can slip away; exposing the two damaged wound areas which may come in contact with each other forming an adhesion [30]. In one of the studies, 6% of patients showed no post-surgical adhesion without the use of Seprafilm^{TM}, while 51% who received Seprafilm^{TM} during surgery showed no adhesion formation. Though, the use of Seprafilm^{TM} greatly reduced the risk of developing post surgical adhesion, 49% of patients still developed some degree of adhesion even after the use of Seprafilm^{TM} [31]. This presents an opportunity to improve the efficiency of barrier product which promotes wound healing and increasing the effectiveness of film placement which further reduces the chance of post surgical adhesion to occur as a result of unsecured movement of barrier film. One method is by electrospinning a nanofiber layers of biopolymer such as chitosan on the barrier film.

The chitosan's haemostatic nature as it develop function with tissue will potentially increase the adherence of chitosan-seprafilm^{TM} and minimize the slippage of film to the wound site until the film absorb into the body. Additionally, the chitosan nanofibers will help in wound

healing and reduce the infection from the surgical site. Chitosan with higher amine group (higher degree of deacetylation) would interact with anions on bacteria cell wall and kill them due to its antibacterial property further reducing the chance for adhesion to occur [19-21,32].

The nanofiber web which is similar to an ECM would help the particular cell to attach and facilitates the tissue growth which promotes wound healing. At the same time, the chitosan nanofibers would increase the healing rate and reduce the chance of infection due to chitosan's biological and antibacterial properties. Decreased healing time by adding chitosan nanofibers on to Seprafilm^{TM} would further reduce the chance for damage tissue to form adhesions.

1.2 Objectives:

The objectives of this research project are to:

- Produce chitosan which has having different degrees of deacetylation by alkali treatment;

- Study and evaluate the rheological properties of chitosan solutions and their ability to electrospin as a function of different degrees of deacetylation and solvent (acetic acid, formic acid, and trifluroacetic acid);

- To study the effect of degree of deacetylation, solution concentration, applied voltage, tip to collector distance, and solvent on successful electrospinning; and

- To evaluate the electrospinnability of pure chitosan onto a pre-manufactured anionic, polysaccharide film (Seprafilm™) in the form of an ECM-like coating that could be useful for the prevention of post surgical adhesion.

2. LITERATURE REVIEW

2.1 History of Electrospinning

Electrospinning, earlier known electro-spraying which was discovered by Zeleny *et al*. in 1914 [16]; is a very simple and versatile technique to produce fibers by using electrostatic forces. From 1934 to 1944, Formhals e*t al*. patented various papers on producing nanofibers by different electrospinning set-ups using electrostatic forces [33-36]. In 1952, Vonnegut and Neubauer produced streams of highly electrified droplets having a diameter of 0.1mm with the help of high voltage supply varying from 5 to 10 kV [37]. The process of jet formation and how the jet behaves when an electrical field is applied was explained by Taylor in 1969 [38]. Taylor discovered that the polymer droplet at capillary end forms a cone (now called as Taylor cone) when an electrical field is applied which becomes a stable jet of polymer whose diameter is less than the diameter of capillary. In 1971, Baumgarten *et al*. [39] produced acrylic microfibers using electrostatic spinning. His work was focused on the fundamental parameters of the electrostatic spinning like the effect of feed rate, voltage, solution viscosity and humidity on fiber diameter and jet length. He found out that the jet length increased as the feed rate and voltage increased. The diameter of fiber also increased with the increase in the solution viscosity. With the help of high speed flash camera, he found that solution of polyacrylic forms a single continuous fiber which forms several loops before getting deposited on the grounded collector. His work has a lasting effect on electrostatic spinning process.

After establishing the relationships between various parameters and their effect on the electrostatic spinning process, many researchers tried to electrospin different polymer melts. Larrondo and St. John Manley Manley produced fibers from polyethylene and polypropylene melts using electrospinning [40,41]. They have found out that the diameter of melt electrospun fibers were larger than the solution spun fibers. In 1986, Hayati and co-workers studied the role of electrical shear effects on the jet stability and atomization. They also determined that the conductivity of the electrospun solution plays an important role in jet stability and fiber diameter [42]. Reneker and his co-workers have established relationships between the governing process parameters (applied voltage, tip to collector distance, feed rate), solution parameters (viscosity, surface tension), and atmospheric parameters (humidity, temperature) with the morphology of fibers produced. Because of the simplicity and versatability of electrospinning process, they were able to produce nanofibers from twenty different polymers (solution and melt) by adjusting the process conditions [43-46]. Soon after this, a considerable increase in the number of research publications observed in the past 15 years regarding the ability to electrospin different polymers and the application of nanofibers in many fields such as filtration [2], tissue engineering scaffolding [7], drug delivery devices [14], and protective clothing [5]. Companies such as Donaldson Company, Inc and Freudenberg Filtration Technologies has found the application of electrospun nanofibers and been using this technology to developed filtration products from the last two decades [47].

2.2 Electrospinning Set-up

Electrospinning is a very simple and easy technique to carry out on the laboratory scale. The typical laboratory setup consists of a syringe with needle, syringe pump which extrudes the polymer solution from syringe- needle assembly at defined flow rate, a high DC voltage supply usually in the range of 1-40 kV with positive and negative polarity for charging the polymer solution, and the conducting collector which can be of any shape like plate, rotating drum and parallel electrode for collecting the nanofibers. A typical horizontal electrospinning setup is shown in Figure 1.

The electrospinning process is generally carried out at room temperature. The polymer solution is taken into the syringe-needle assembly and a high voltage supply is connected to the metal needle to charge the polymer solution. The solution emerges from the tip of the needle with the help of syringe pump at desired flow rate in horizontal setup. When the DC high voltage power supply is turned on and reaches the threshold voltage, the solution at the tip of needle extrudes due to electrostatic forces within the solution and forms a Taylor cone. The Taylor cone gets stretched forming a jet of polymer which gets attracted towards the collector plate of opposite polarity [1,48].

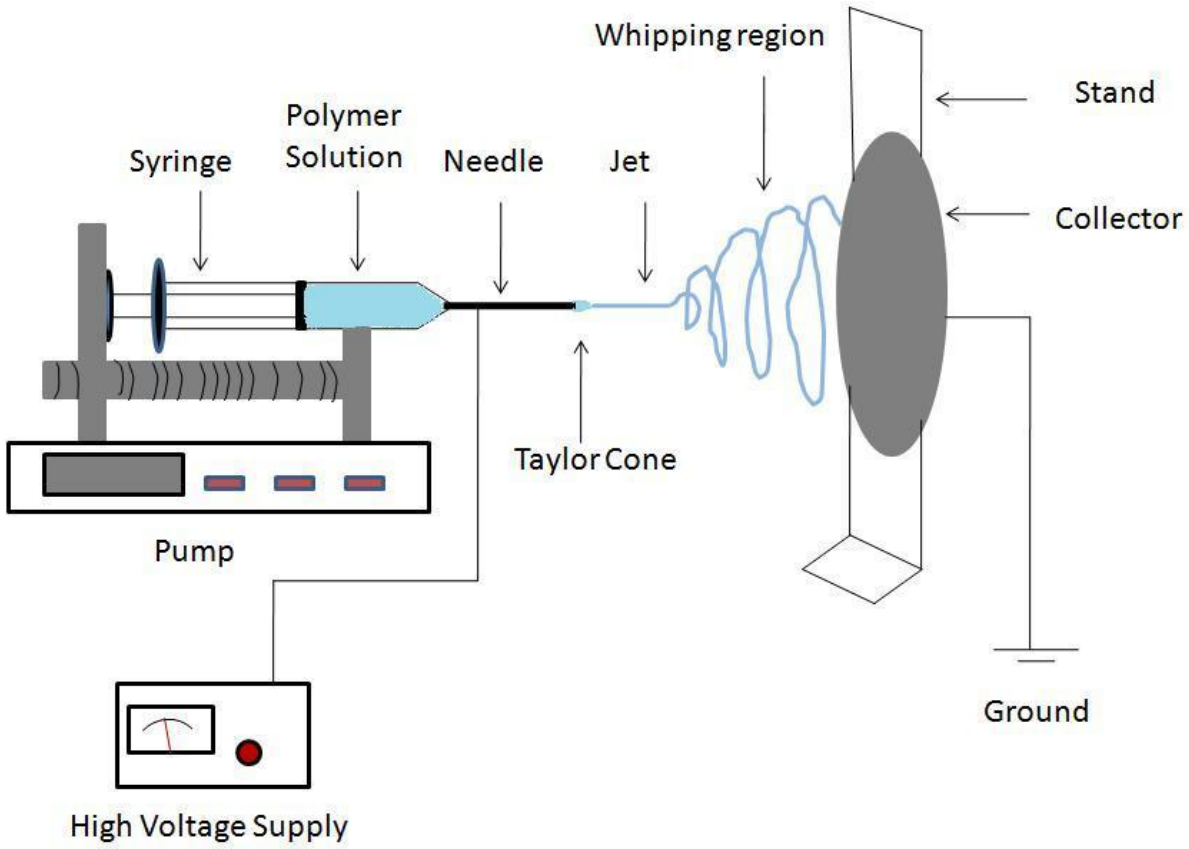

Figure 1 Illustration of a typical horizontal electrospinning setup consists of a high voltage power supply, syringe pump and the collector

2.3 Electrospinning Process

Electrospinning is a technique which uses high electric forces to generate fibers (μm to nm in diameter) from polymer solutions or melts. The resulting fibers have an extremely high surface area to volume ratio.

The electrospinning process can be explained by dividing the process into several stages namely, droplet generation, Taylor cone and jet initiation, jet and thinning of jet, and whipping instability region.

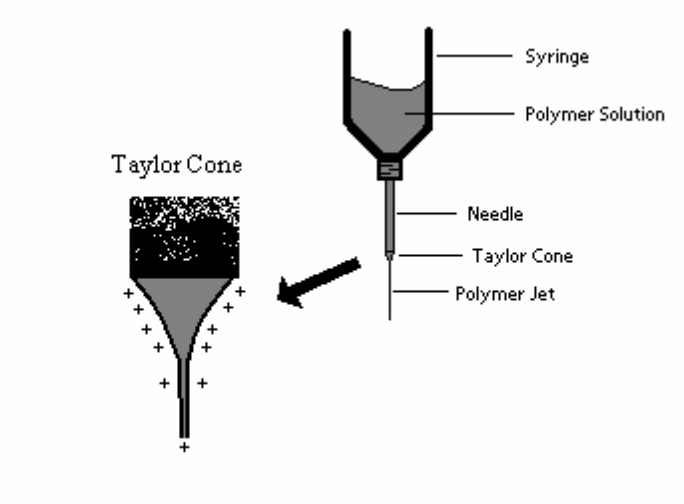

Figure 2 Taylor cone formation and origin

When the DC high voltage is turned on, the solution at the tip of needle comes out and gets charged. Because of strong electric field, the solution causes a repulsive attraction between the like charges in the liquid and attractive charges between the opposite charged liquid. When the voltage reaches the threshold value, the repulsive electrical forces overcome the surface tension of the solution and the droplet forms a conical shape called Taylor cone (see Figure 2) [38]. When the applied voltage increases further, the cone becomes unstable and a fine jet of polymer emerges from the Taylor cone. The diameter of the jet continuously reduces because of stretching of fluid filament as it travels towards the grounded collector. The jet remains stable over a certain distance and spraying of fibers occur called as whipping of fibers (see Figure 1). This happens because of high charge density on surface of jet

causing instability in fibers. The whipping region generally looks like many fibers were coming out from single point. But actually, it is just the single fiber which whips around randomly very fast as seen by the high speed photography [49]. Because of the very high speed of spinning, high voltage, suitable distance and very small diameter of fibers; the solvent from the fibers gets evaporated during whipping action and only fibers with some conductivity gets collected on the oppositely charged collector [1,47,50].

2.3.1 Droplet Generation

Charging the polymer droplet at the tip of the needle is the first step in electrospinning. The polymer solution is pushed through the capillary needle at the desired flow rate. Typically the positive end of a high DC voltage supply is connected to the metal needle to charge the solution. When the electric supply is off or low, the solution from the tip of needle drip offs under the influence of gravity. At this time, the hemispherical shape of the droplet at the end of needle tip will have two forces acting on it, surface tension of the liquid γ and the gravitational force, $F_{G.}$ The radius of the droplet $r_{o,}$ formed by inner radius of needle will be

$$r_o = \left(\frac{3R\gamma}{2\rho g}\right)^{1/3} \qquad \textbf{Equation 2.1}$$

where R is the inner radius of needle, ρ is the density of liquid and g is the gravitational force. When the voltage is increased, the radius of the droplet reduced to r because of high electric force F_E. The expression for the electric field is given as,

$$F_E = 4\varepsilon\pi V^2/[\ln(4L/R)^2] \qquad \textbf{Equation 2.2}$$

where V is the voltage applied, L is the distance between the tip of needle and the collector plate and ε is the permittivity of the air [51].

When the voltage reaches a certain value, charge separation takes place, depending upon the polarity of the applied voltage and the conductivity of the polymer solution. Free ions and charges will move to the surface of the droplet and the charges with opposite polarity will move to the interior of the droplet when they reach the equilibrium. This creates repulsive electrostatic forces which will be encountered by the surface tension of the polymer solution.

2.3.2 Taylor Cone and Jet Initiation

Under the influence of high electric field, the droplet at the end of the needle tip held by surface tension of the polymer solution forms a conical shape called as Taylor cone [38]. The polymer solution at the tip of needle held equal number of positive and negative charges on surface and the interior of the droplet, respectively. When the voltage reaches the threshold value, this charges of the polymer solution moves and concentrate inside the droplet. The surface of the droplet becomes big due to charge accumulation and because of this; the charge per unit area at the tip of needle is highest causing pulling of polymer droplet into conical shape (Taylor cone). The change of shape from spherical droplet into conical shape causes further increase in charge per unit area at the tip of cone. When the applied voltage

overcomes the surface tension of polymer solution, a jet of polymer liquid emerges from the cone [44]. The point, at which the jet initiates, is a very complex phenomenon and subject to many process parameters. It is the basic step toward the fiber formation and there has been many research carried on how the Taylor cone forms and jet initiate [52-54].

Taylor had determined the cone angle of 49.3°, when the critical voltage was reached and electrostatic forces and the surface tension were in equilibrium. He proposed this based on the hyperboloidal approximation of the initiating droplet shape. But this cone angle varies according to the different hyperboloidal shapes and can have a sharper cone with a half angle of 33.5° [52]. Even different polymer solution has different cone angle. For example, a molten polypropylene has an angle of 37.5° [53]. The shape and angle of cone will define the droplet formation or fiber formation which leads to electrospraying or electrospinning, respectively. The solution with low viscosity gives droplet generation and the solution with high viscosity gives a stable Taylor cone geometry. The Taylor cone is difficult to maintain throughout the electrospinning process because it depends upon the feed rate and evaporation of solvent from jet during collection [54].

When the spherical droplet forms a conical shape, the charges accumulate at the tip of cone and there is no additional area for charge accumulation. So, a very thin jet of fiber from tip of cone emerges creating an additional area to accommodate additional charges on the surface of jet. These charges on the surface of jet get attracted towards the collector of opposite

charge. Many parameters affect the jet initiation such as concentration, viscosity, applied voltage and the flow rate.

2.3.3 Jet and Thinning of Jet

The jet emerging from the Taylor cone follows a linear path to certain distance before the bending instability starts. The jet diameter decreases as it travels towards the collector because of both stretching of polymer solution and evaporation of solvent [55]. The diameter of jet is less than the tip of the cone because of stretching and orientation of polymer molecules in the direction of elongation causing crystallization of molecules inside the jet [43]. The stretching of polymer jet increases the surface area per unit mass while the surface charge per unit area reduces. The continuous solvent evaporation from the surface of jet increases the surface charge density compensating with the increase in surface area by extension.

Various factors like flow rate and applied voltage affects the stability of jet. Many researchers proposed theories on parameters affecting the thinning of jet. One such important parameter is the elasticity of jet which was explained by Jian Yu *et al.* [56]. They tried to correlate the Rayleigh instability with the Deborah number (ratio of the fluid relaxation time to the instability growth time) in the electrospinning process. The Figure 3 shows the images of jet having different diameter depending on different flow rate and electric field.

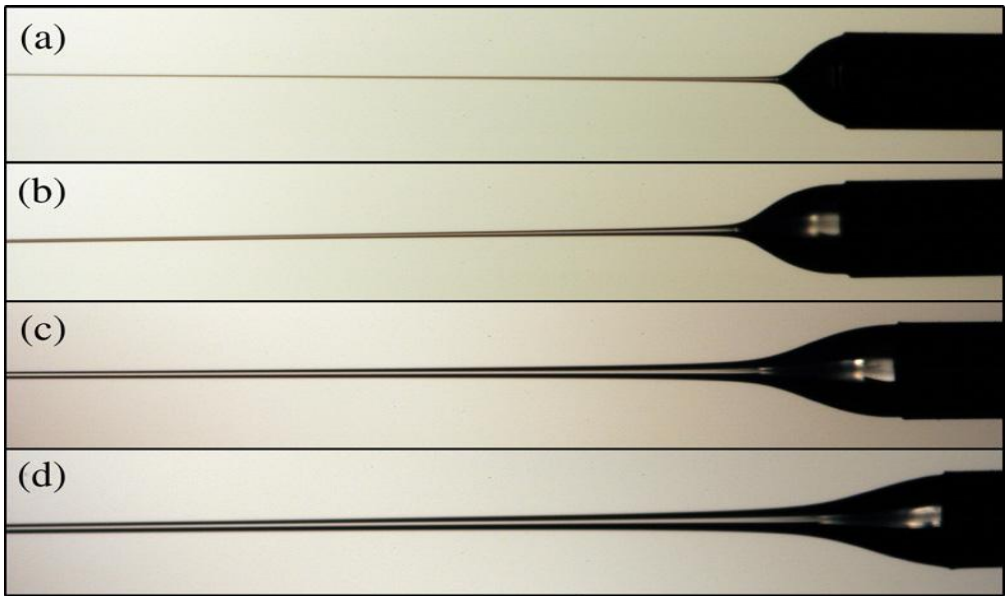

Figure 3 Effect of flow rate (Q) and applied voltage (E) on jet of 2% solution of PEO in water. a) Q=0.02 ml/min, E=0.282 kV/cm; (b) Q=0.10 ml/min, E=0.344 kV/cm; (c) Q=0.50 ml/min, E=0.533 kV/cm; (d) Q=1.00 ml/min, E=0.716 kV/cm [48]

Theoretical model has been proposed to predict the diameter and length of thinning jet at different points. The characteristic length (L) of jet where initial thinning of jet start can be derived by the Equation 2.3.

$$L^5 = \frac{K^4 Q^7 \rho^3 (In\ \chi)^2}{8\,\pi^2 E\, I^5 \acute{\varepsilon}^{\,2}} \qquad \textbf{Equation 2.3}$$

where Q is the flow rate, ρ is the density of solution, χ is aspect ratio of the jet, E is the local electric field, I is the electric current and έ is the dielectric constant of the polymer. Here, the length is directly proportional to the flow rate and inversely proportional to the electric field.

The jet thins more slowly beyond this point and approaches the asymptotic regime where only electrostatic and inertial exits. In this regime the viscosity plays a very major role and a scaling relationship exists in between the electrostatic and the viscous forces. The diameter of the jet (*h*) is given by the Equation 2.4, where η is the viscosity and z is axial coordinate. The diameter of jet is directly proportional to the flow rate. It means that the diameter of jet increases as the flow rate increases.

$$h = \left(\frac{6\,\eta\,Q^2}{\pi E\,I}\right)^{\frac{1}{2}} z^{-1} \qquad \textbf{Equation 2.4.}$$

.

2.3.4 Whipping Instability Region

The jet which was originated from the Taylor cone follows a linear path and then become unstable and undergoes bending and stretching called as whipping of jet [43,49,57]. The jet carrying the charges moves towards the collector of opposite charge following a chaotic motion because of origination of repulsive forces from the charged element of the jet [49]. The chaotic motion was first thought to be bending of jet and then splitting of jet into multiple jets. Doshi and Reneker proposed that the diameter of jet decreases due to stretching and evaporation of solvent and because of this the surface charge density on the jet increases which splits the jet into smaller jet splay. The diameter of jet then further reduces and this process occurs repeatedly which produce jet of very small diameter to form fibers [43]. Few years later, Reneker and coworker work on the bending instability and they have experimentally showed with the help of high speed photography, that the jet does not split

into smaller jets. Instead, it is the single jet that follows a straight path first and then with growing amplitude, it follows a bending, winding spirally and looping path in three dimensions. This motion occurs so fast that the jet appears to be breaking into several jets which result into smaller diameter fibers. Figure 4 shows the whipping motion of single jet whose diameter decreases continuously with the increase in loop diameter.

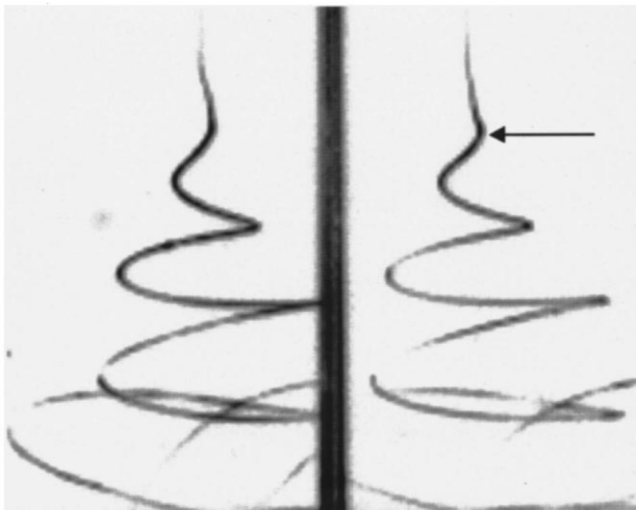

Figure 4 Starting of jet instability with growing spiral loops [49]

Reneker and coworker developed an experimental model to explain the bending instability behavior of a viscoelastic electrified jet. They used mathematical approach and developed a theory on the jet path and onset of bending instability. The rectilinear electrified jets have electric charges which interact because of coulomb's law. This interaction leads to instability according to Earnshaw's theorem. They have used Earnshaw's theorem to explain the bending instability. Figure 5 in which they have consider three point charges in a straight line at A, B and C. The interaction of this charges causes perturbation due to repulsion of like

charges. The coulomb forces acting on B pushes it on opposite direction. The perturbation causes charge B to move a little offline by a distance δ and a net charge acts on B in direction perpendicular to the line which cause charge B to move further in direction to perturbation away from jet axis. If the perturbation occurs in liquid jet, the Coulomb force caused by bending instability counteracts and overcomes with the forces like surface tension and viscoelastic. The charges on the jet get attracted towards the grounded collector in a helical path with growing diameter resulting in whipping action [49].

Rutledge and coworkers [57] have worked on different types of instability. Due to the interaction between electric field and charges on jet give rise to competition between the different kinds of instabilities. This instability grows at different rates depending upon the operating and fluid parameters. They have proposed the possibilities of three instabilities namely; 1) classical Rayleigh instability (axisymmetric), 2) at high electric field axisymmetric instability and 3) a nonaxisymmetric instability due to fluctuation in dipolar component of charge distribution. The latter two conducting mode instabilities were independent of surface tension but depend upon the conductivity of fluid. The two main reason for whipping instability which bend the jet are the lateral fluctuation of dipolar charge which interact with external field and the mutual charge repulsion on the surface of jet. They have investigated both the fluid properties and the operating parameters for obtaining stable jet. Viscosity and conductivity (fluid properties); electric field and flow rate (operating parameters) are the most important characteristic they have found.

Fridrikh *et al.* proposed a model on the forces which determines the jet diameter during electrospinning process as a function of electric field, flow rate and surface tension. The model predicts the terminal diameter of jet had a $10^{2/3}$ fold variation and this 2/3 scaling with the inverse volume charge density is experimentally proved using several concentration of PCL solution [58].

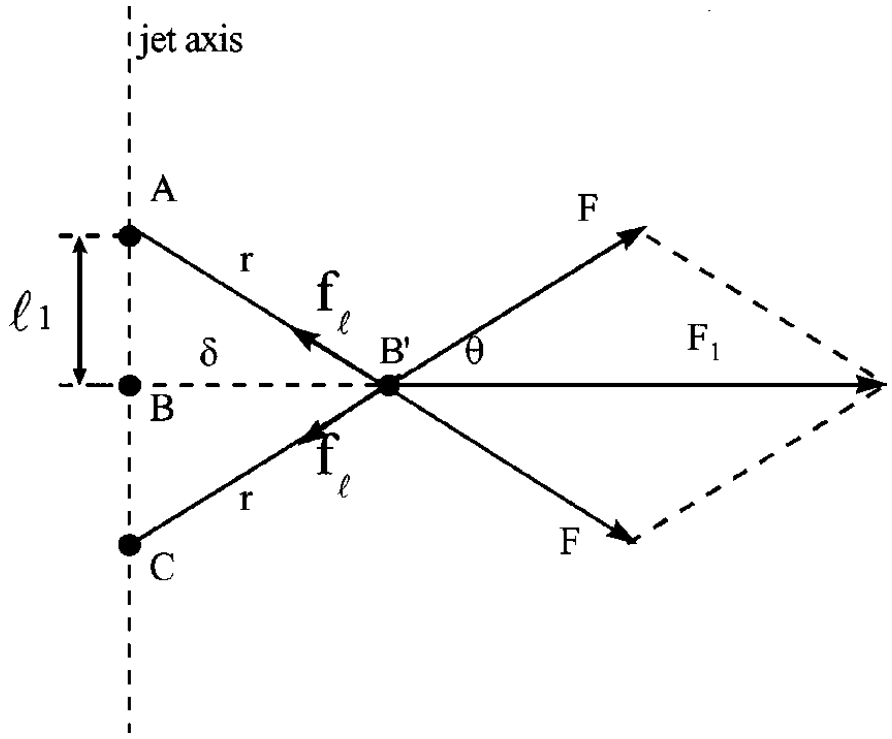

Figure 5 Representation of Earnshaw's Instability causing bending of jet [49]

2.4 Parameters Affecting Electrospinning Process

Many researchers have been trying to understand the parameters that affect the electrospinning process and the resulting nanofibers [55,59,60]. These parameters can be classified into three types; material parameters, process parameters, and environmental

parameters. Figure 6 shows the general classification of these parameters and Table.1 shows the effect of these parameters on fiber morphologies.

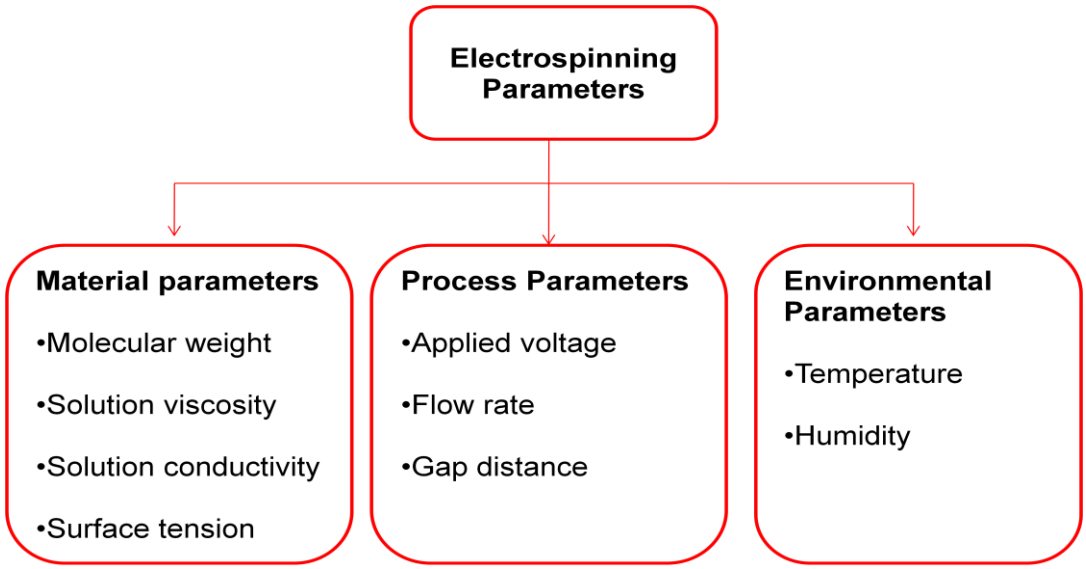

Figure 6 General classification of electrospinning parameters

2.4.1 Material Parameters

2.4.1.1 Molecular Weight, Polymer Concentration and Solution Viscosity

Molecular weight, polymer concentration and viscosity are interrelated. A liner-chain polymer solution has four different concentration regimes: dilute, semidilute unentangled, semidilute entangled, and the concentrated regime. McKee *et al.* found out that the defect free nanofibers can be obtained from a polymer solution when the polymer concentration is atleast 2 to 2.5 times the entanglement concentration (critical concentration, C_e). The entanglement concentration is the point in between the semidilute unentangled regime (where

polymer chains starts to overlap) and the semidilute entangled regime (where the polymer chains overlap one another and topologically constrain each other's motion). In their study, they have found out that the polymer solution having viscosity in semidilute unentangled regime produce only droplets, while the polymer solution having viscosity in semidilute entangled and above entanglement concentration produces bead free fibers. A high polymer concentration will have high solution viscosity indicating a higher entanglement of polymer chains if the molecular weight is high enough [61].

The electrospinning process is possible only above the critical concentration. Much research has been done to find out the upper and lower concentration boundary for producing the nanofibers without any defects [59]. At low concentration (low viscosity), the polymer solution drips from the tip of the needle because of low surface tension. At this concentration (semidilute unentangled), it is called electrospraying process which forms beads or droplet instead of fibers. At concentration above entanglement concentration, the polymer droplet stretches out into conical shape and a thick strand of jet emerges from it producing nanofibers. In general, it has been observed that as the solution concentration increases, average fiber diameter also increases and has a scaling relationship. Increasing the concentration sometime also increases the surface tension of solution which prevents the electrospinning process and tends to form some beads [59]. But for some polymer solution like polystyrene, even if the surface tension remains constant with increasing polymer concentration, it gives bead formation with increased viscosity [62]. This result indicates that the polymer concentration and viscosity affect the fiber forming process and its morphology.

The molecular weight has a profound effect on fiber formation [63]. Koski *et al*. studied the effect of molecular weight [9000 to 186,000 g/mol] to produce nanofibers of PVA. The concentration is varied depending upon the molecular weight of that polymer. They have found that for each molecular weight, fibers can be formed when concentration/viscosity is $[\eta]\ C > 5$, where $[\eta]$ was the intrinsic viscosity and C was the concentration. The average fiber diameter was increased with increase in molecular weight and concentration.

Table 1 Effect of electrospinning parameters on fiber morphology [50]

Parameters	**Effect on fiber diameter**
Applied voltage increases	Decreases
Flow rate increases	Increases (if flow rate is too high, gives beaded fibers)
Gap distance increases	Decreases (if distance is too short, it gives beaded fibers)
Polymer concentration/viscosity increases	Increases (if viscosity is high, drying of solution at tip of needle occurs preventing electrospinning)
Solution conductivity increases	Decreases (with broad distribution of fiber diameter)
Solvent volatility increases	Fibers with microtexture having high surface area.

2.4.1.2 Surface Tension

A polymer solution having higher surface tension forms bead or beaded fibers. This happens because the surface tension tries to make the area per unit mass smaller by changing the jet into spheres. The jet which emerges from the Taylor cone has a decreasing surface area because of surface tension. The jet eventually breaks into spherical droplet giving rise to droplet formation which are collected as bead or beaded fibers on the collector. The viscoelastic force of the polymer solution is necessary for the stretching and the stability of jet. Therefore, the surface tension should be low enough than the viscous forces of the polymer solution for successful electrospinning [64].

2.4.1.3 Solution Conductivity

The polymer solution with high conductivity will have a tendency to form a stable jet because of charged ions. These ions produce high surface charge density on the jet under the influence of electric field which affects the elongation force on jet causing charge repulsion. The higher charge repulsion enhances the bending instability causing more whipping and elongation of jet producing more uniform and finer fibers [45,65,66]. For high conductivity solution, even a small electric field is enough to produce a stable jet. The ionic conductivity of the solution can be altered by adding some ionic group like salt [45], alcohol [64], or surfactants [67].

2.4.2 Process Parameters

2.4.2.1 Applied Voltage

Voltage or the field strength has a profound effect on the fiber morphology. Under the influence of electric field, the surface of hemispherical liquid droplet suspending in equilibrium at the tip of needle will be distorted. Above the critical voltage a stable jet of polymer solution is ejected from the Taylor cone tip. At low voltage (below the critical voltage), the polymer droplet at the tip of needle remains suspended and a jet of polymer solution will come out and form the Taylor cone producing fibers with some beads. As the voltage increases, the Taylor cone reduces in size (change of shape of polymer droplet) because of volume of fluid at tip needle decreases producing bead or beaded fibers [59].

2.4.2.2 Flow Rate

The speed of polymer solution flowing from the tip of the needle is very important parameters in determining the jet stability and the resulting nanofiber morphology. At low flow rate, the fibers will have small diameter [68]. The fiber diameter increases with an increase in feed rate. After certain limit, the solvent does not evaporates completely which results in wet or fused fibers with residual solvent remaining. If the flow rate is too high, the fibers will have beaded structures. Also if the feed rate is too slow, then the polymer solution will not be enough for a stable electrospinning process, resulting in beaded fibers or beads [69-71].

2.4.2.3 Gap Distance

The tip-to-collector distance is one of the parameters that affect the fiber diameter and morphology because it depends upon the solvent evaporation rate, the deposition time for nanofibers, and the whipping instability region. If the distance is too high or too low it will form beaded fibers [72]. So there should be enough distance from tip-to-collector for the solvent to evaporate and for the fibers to dry off before reaching the collector. The solvent volatility also affects the fiber morphology. If a polymer system having highly volatile organic solvent then the tip-to-collector distance should be less for solvent evaporation and dry fiber formation than the aqueous polymer system [73].

2.4.3 Environmental Condition

Environmental conditions such as humidity and temperature affect the electrospinning process. If the humidity of the spinning environment is more than 60 %, the fibers will not have enough time to dry properly (fused fibers) because of high water absorption [74]. The average fiber diameter of the nanofibers decreases with increasing humidity. But, beyond a certain limit, fusing of nanofibers occur giving larger nanofibers. The increase in temperature can cause a decrease in solution viscosity which provides more stretching of jet and giving thinner nanofibers [74].

2.5 Nanofibers Formation by Electrospinning and its Properties

The polymeric fibers that were formed by electrospinning have the diameter in the range of submicron to nanometer. In fiber science, the fibers diameters below 100nm are considered as nanofibers. These nanofibers has gain much attention from the last decade because of their very small size, larger surface area to volume ratio, and small pore sizes as compared to regular fibers [1]. The surface morphology of these nanofibers can be varied by the material and process parameters as explained above. Because of very small size as compared to melt blown and conventional textile fibers, the nanofibers have big difference in thermal and mechanical properties. As compared to traditional fibers, the nanofibers have lower glass transition temperature because of high surface area to volume ratio and lower crystallinity because of high evaporation rate of solvent during the electrospinning [75]. The small diameter also influences the mechanical properties of fibers like tensile strength and Young's modulus. A 40% reduction in tensile strength peak and 60% reduction in elongation at maximum applied stress were observed for electrospun elastomer nanofibers as compared to cast films [1].

2.6 Application of Nanofibers

Because of the enhanced properties of nanofibers like high surface area to volume ratio, they have gained much attention in the field of filtration for submicron particles [2,3], protective clothing like military warfare [4,5], and for biomedical applications such as tissue engineering scaffolds [6-10], wound dressings [11-13], and drug delivery [11,14,15]. Number of patents has been published in US only on polymeric nanofibers. Many of the

patents deal with the application for biomedical purposes (see Figure 7).The tissue's natural extracellular matrix is in nanofibrous form. The electrospinning method helps to build this three dimensional scaffolds and tissue templates which can mimic the natural extracellular matrix (ECM) for the treatment of tissue or organs.

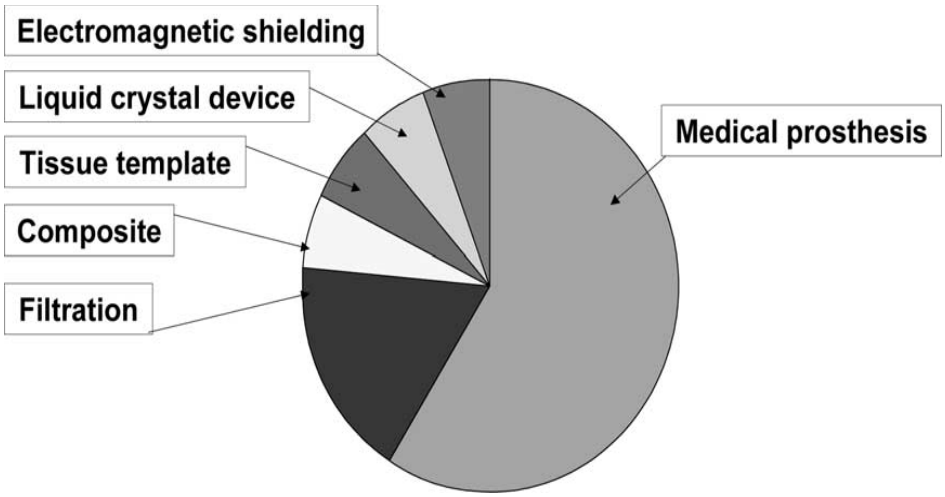

Figure 7 Application of electrospun nanofibers targeted by US patents [76]

2.6.1 Biomedical Applications of Nanofibers

Tissue engineering is one of the particular interests for producing biocompatible and three dimensional scaffolds similar to natural extracellular matrix (ECM) which can help in cell generation for tissue repair and replacement with sufficient biological and mechanical properties. The scaffolds with drug loading capacity such as antibodies and anticancer agents are useful for wound healing applications. These functions and properties of nanofibers make them suitable for biomedical application [6,7,14].

2.6.1.1 Tissue Engineering Scaffolds

The tissue engineering is “an interdisciplinary field that applies the principles of engineering and life sciences toward the development of biological substitutes that restore, maintain, or improve tissue function” [77]. It is working to solve the problem of limited donor tissue or organs for transplantation. All living organisms have extracellular matrices which control the cell behavior. The ECM is a physically and chemically cross linked three dimensional network of protein and glycosaminoglycans. The dimension of ECM is less than the cells, usually in nanometer range [6]. Nanoscale fibers influence cell behavior and the cells attach and proliferate on the fibers with diameters less than the diameter of cells [17]. Therefore, the artificial scaffolds which can mimic the natural ECM for tissue engineering should have certain properties like biodegradability, biocompatibility, and mechanical properties that can mimic natural tissue. Apart from that the scaffolds should provide a matrix cell attachment, proliferation, and migration which are controlled by the scaffold architecture, porosity, and size of pores [6,18].

Wan-Ju Li and coworkers electrospun a novel scaffold of poly(D,L-lactide-*co*-glycolide) (PLGA), which is morphologically similar to natural extracellular matrix (ECM) of natural tissue [8]. They have characterized the mechanical properties, porosity, and the cell activities of the nanofibers such as cell proliferation assay and cell-matrix interaction. In this study, they used two types of cells fibroblasts and bone-marrow-derived mesenchymal stem cells (MSCs) on scaffolds because of their skin and cartilage tissue replacement properties.

The results showed that the nonwoven electrospun mat had a very high porosity of 91.63% which helps to provide more space for cell accommodation and makes the exchange of nutrient and metabolic waste between a scaffold and environment. The tensile modulus and the ultimate tensile stress of the structure were found to be 323.15 MPa and 22.67 MPa, respectively which is more than human cartilage and skin. These mechanical properties make the scaffolds a suitable candidate for tissue engineering scaffolds which maintain its structural integrity, stability and biomechanical support before and after the surgery for tissue regeneration and structure degradation. The cell proliferation assay showed that the cell population increases with time on scaffolds which indicates cell growth because of high surface area to volume ratio. The cell matrix and cell-cell interaction was been observed by the SEM images in which they used BALB/c C7 mouse fibroblasts on scaffolds.

The dimension of cells of particular tissue varies in size. So the artificial ECM should have proper pore size, architecture, porosity, and fiber diameter for facilitating cell attachment and proliferation. If the pore size doesn't match up with the cell diameter then no infiltration or nonadherance of cells will occur [18]. By changing the electrospinning parameters, one can change the pore size, its distribution, fiber diameter and its surface properties for a given type of cell to attached and migrate [78-79].

2.6.1.2 Wound Dressing

The polymer nanofibers also have been used for wound dressing material because of their extremely high surface area to volume ratio and small pore sizes. They have been used for

the treatment of wounds or burn to repair the damage tissue [76], removal of exudate, inhibition of exogenous microorganism invasion, and improved appearance [13]. The electrospun matrix has high gas permeability, and good barrier property to infection and dehydration which are useful for wound dressing material. Polyurethane is being used for wound dressing material for good barrier and oxygen permeability properties; and it also protects the wound from infection and dehydration [13]. Apart from that, the nanofiber matrix shows good biocompatibility and support proliferation and normal function of fibroblast. Nanofibers membrane have high wound healing rate than the commercial collagen sponge wound dressing [12]. The pore size (usually 500nm to 1µm) of nanofibrous membrane plays a very important role in wound healing applications as it protects the wounds from bacterial penetration. The high surface area is requirement for fluid absorption and dermal delivery [76].

2.6.1.3 Drug Delivery

The high functional characteristic of nanofibers makes them suitable for drug delivery carriers. These drug delivery systems are very advantageous because of controlled drug release at a definite rate for a definite period of time on a localized area [1]. This system can be incorporated with tissue engineering scaffolds to prevent infection and to regenerate the tissue. Drug and carrier can be mixed for the electrospinning of nanofibers. The drugs then can be in the form of particles attached to the surface of nanofibers; blend of drug and carrier in the form of one kind of fiber contains both elements; and the carrier material electrospun in the form of tubular structure in which the drug is encapsulated. Because of very small size

of the drug particles and the coating material which helps to encapsulate the drug, the drug gets easily absorbed by human being [76]. The high porosity of nanofibers provides rapid diffusion of degradation byproducts. Even the release rate of drug can be controlled by having fibers with suitable diameter. Therefore, the electrospinning process and choice of material provides various techniques that can be used for drug loading in the various forms as mentioned above which gives a better control over the drug release kinetics [50].

2.7 Polymeric Material for Bio-medical Applications

Both natural and synthetic bio-polymers can be used for bio medical applications. Because of biocompatibility, antibacterial and biodegradability of bio-polymers, these polymers are being used in the industries like medicine, agriculture, textile, and paper. The electrospun biopolymer mats found many applications in field like filtration, pharmaceutical, wound dressing, tissue engineering scaffolding (vascular grafts and extracellular matrix). The artificial extracellular matrix (ECM) must mimic the natural ECM in terms of osteoconductivity, biocompatibility, degradability, high surface to volume ratio and mechanical properties. The surface of artificial ECM having nanofibers and nanopores influenced the cell attachment activation, proliferation, alignment and orientation. It is found out that the cell attach and organize well whose diameter were less than the fiber diameter [17,80].

The biopolymers (both natural and synthetic) that have been electrospun for biomedical application is listed in Table 2.[76,80]. The synthetic material is been widely used because of

advantage over natural polymers. This polymer can be process to meet the biodegradation kinetic profiles and mechanical strength properties. The synthetic polymer does not require any complexity in processing like purification, immunogenicity, and pathogen transmission [19]. However, the natural polymers are very difficult to process, because they had to be extracted from their base source. For example chitin has to be extracted from crust shell, yeast, or fungal biomass. Even they vary a lot in their properties like molecular weight, crystallinity, charged distribution and purity. They require some prior processing for cleaning which complicate controlled manufacture. But, because of their biological properties, they have been used widely in medical industries [80].

Table 2 Polymer/solvent systems with their applications [76,80]

Polymer	Solvent	Application
Nylon6, 6 , PA-6.6	Formic acid	Protective clothing
Polylactic acid, PLA	Dimethyl formamide, Methylene chloride and dimethyl formamide	Membrane for prevention of surfery induced adhesion
	Dichloromethane	Drug delivery system.
Collagen-PEO	Hydrochloric acid	Wound healing, tissue engineering, haemostatic agents
Silk-like polymer with fibronectin functionality	Formic acid	Implantable device
Silk/PEO blend	Silk aqueous solutions	Biomaterial scaffolds
Poly vinyl phenol, PVP	Tetrahydrofuran	Antimicrobial agent

Table 2 (Continued)

Polymer	Solvent	Application
Cellulose acetate, CA	Acetone, acetic acid, dimethylacetamide	Membrane
PLGA	Tetrahydrofuran:dimethylformamide (1:1)	Scaffold for tissue engineering
	Hexafluoro-2-propanol	Scaffold for tissue engineering
Poly(ethylene-co-vinyl alcohol)	Isopropanol/water: 70/30 (%v/v)	Biomedical
Chitin	1,1,1,3,3,3-hexafluoro-2-propanol (HFIP)	Tissue scaffolding, wound dressings
Chitosan	70/30 TFA/Dichloromethane (MC)	Wound dressings
Chitosan/PEO Blend	Acetic acid, water	Bone tissue engineering, controlled drug release, tissue repair

2.8 Chitosan

Chitosan is the *N*-deacetylated derivative of chitin and chitin is second most abundant polysaccharide. Chitin is found in the exoskeleton of arthropods and cell walls of fungi and yeast. The source of chitin and chitosan is given below [22]. The commercial production of chitin and chitosan comes from the crustacean shell which is the byproduct of food industry. Around 10^{11} tons of chitin are processed for general application but only around 1,50,000 tons of chitin is used for commercial purpose. Regardless, of the huge production and availability, chitin still remains underutilized material because of its intractable molecular

structure. Its molecular weight usually may range from 10,000 to 10^6 (Da, g/mol, or Daltons) [81].

Source of chitin and chitosan

- Insects
  - Cuticle
  - Ovipositors
  - Beetle cocoon
- Crustaceans
  - Crab shell
  - Shrimp Shell
- Squid
  - Ommastrephespen
  - Loligo stomach wall
- Fungi
  - Mucorrouxi(60-90% deacetylated)
  - Aspergillisnidulans
- Deacetylated chitin
  - Shrimp shell (Molecular weight upto $1.6 * 10^6$ Dalton)

2.8.1 Structure of Chitosan

Chitin consists of 2-acetamido-2-deoxy-β-D-glucose through a β (1-4) linkage. It resembles as cellulose in chemical structure with hydroxyl at position C-2 replaced by an acetamido group. The chemical structure of cellulose, chitin and chitosan is shown in Figures 8 and 9 respectively.

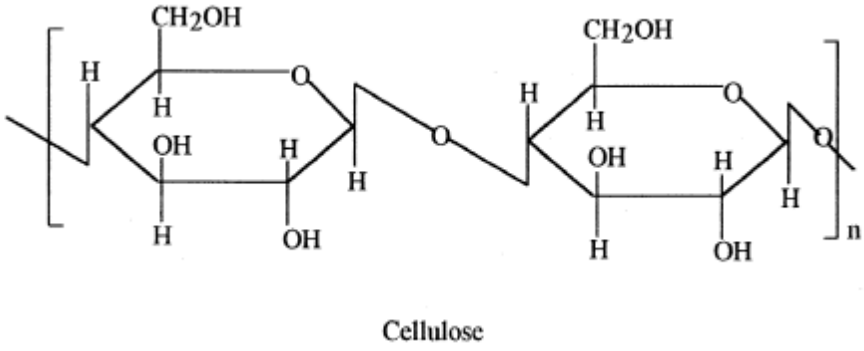

Cellulose

Figure 8 Chemical structure of cellulose [21]

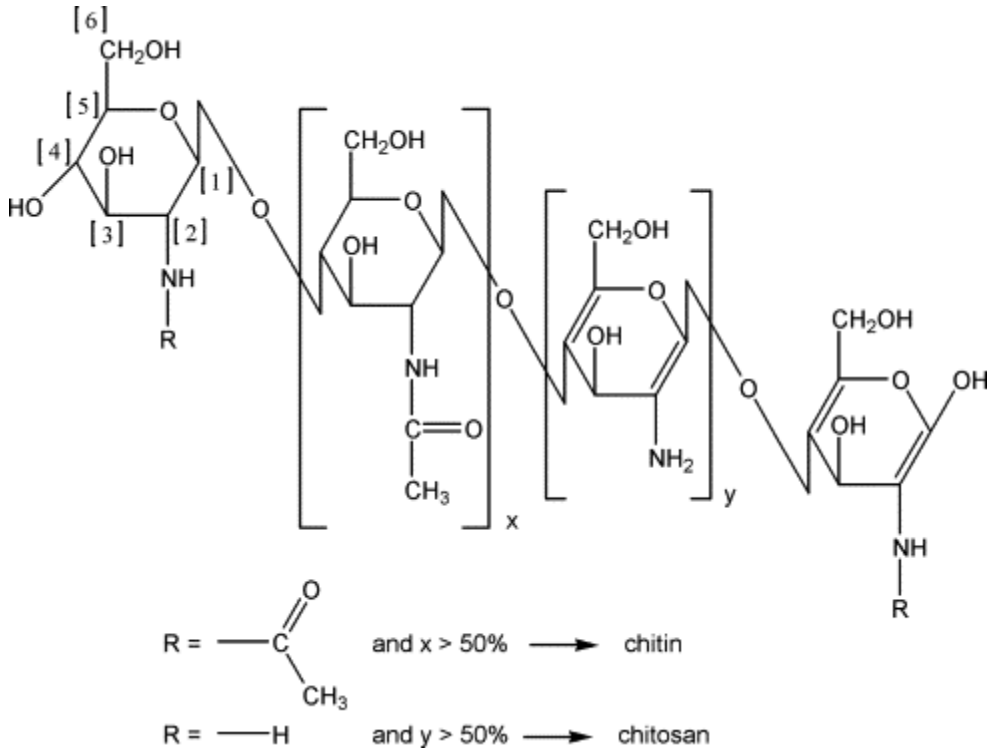

Figure 9 Chemical structure of chitin and chitosan [81]

The chitosan is *N*-deacetylated derivative of chitin. The deacetylation results in a primary – NH_2 amine on the C-2 of the *D*-glucosamine repeat unit. Chitosan is composed of glucosamine and *N*-acetyl glucosamine linked in a β (1–4) manner. If the acetyl group and the x unit (see Figure 9) is more than 50% then it is considered as chitin. And if the amine group and the y unit are more than 50% then is called as chitosan [81]. Thus, the chitosan is copolymer composed of glucosamine and *N*-acetylglucosamine. The ratio of glucosamine/*N*-acetyl glucosamine is referred as degree of deacetylation. When the chitin is deacetylated in 40% sodium hydroxide at 120° for 1-3 hour, the treatment produces chitosan of around 70% deacetylation (y=70%) (Figure 10**)** [21].

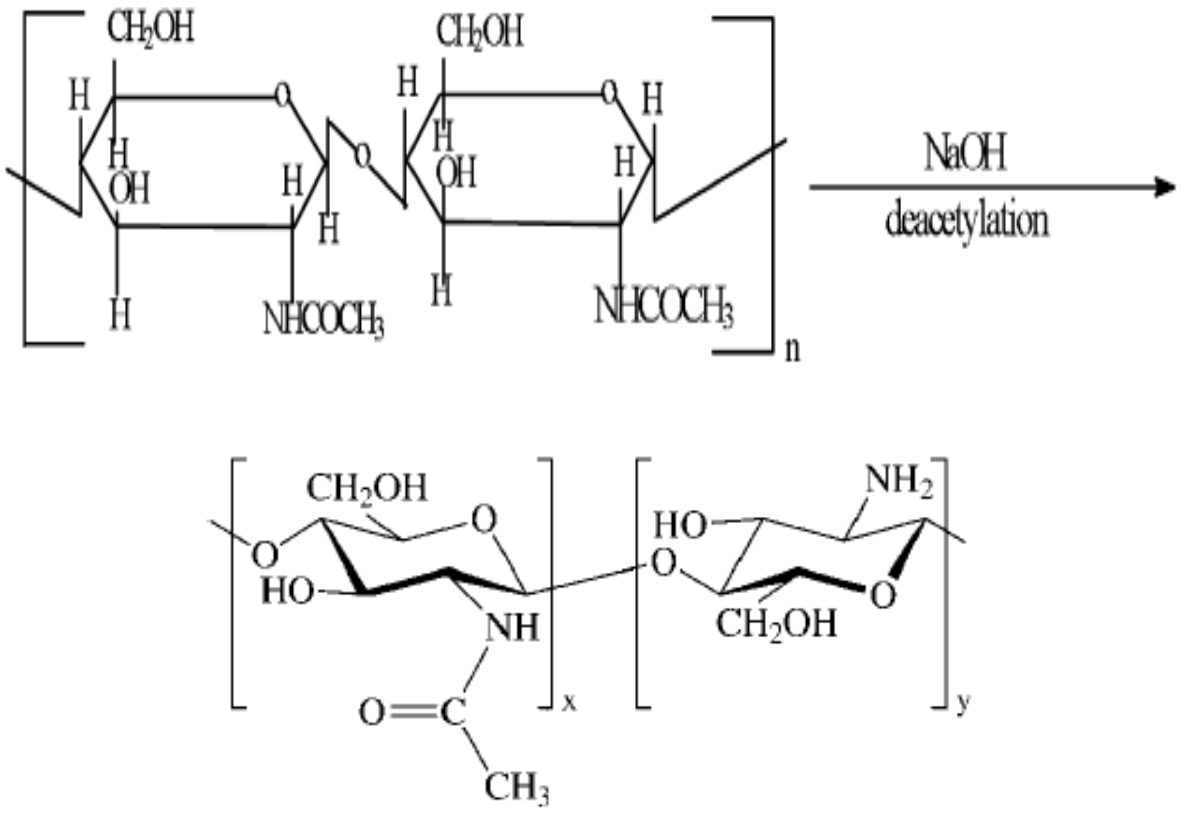

Figure 10 Deacetylation of Chitin to form Chitosan [21,22]

2.8.2 Properties of Chitosan

Most of the biopolymers found in nature such as cellulose, dextran and pectin are neutral or acidic in nature. Chitin and chitosan are the example of basic polysaccharides. The quality and properties of chitosan varies depending on the method of manufacturing process. The process generally affects the viscosity, deacetylation, molecular weight and purity. The degree of deacetylation is one of the most important properties of chitosan. The deacetylation decides the amount of free amino groups in the polysaccharide. The nitrogen in the amino group makes chitosan a cationic polymer. The degree of deacetylation and the molecular

weight determines the solubility of chitosan. The chitosan has high hydrogen bonded network in solid state which requires solvents to introduce some interchain repulsion or break the intermolecular hydrogen bonding for dissolution. It is generally soluble in aqueous acidic media if the degree of deacetylation is more than 50%. The protonation of $–NH_2$ on the C-2 position of the *D*-glucosamine repeat unit occurs when chitosan dissolve in aqueous acidic media [21-23,82].

2.8.3 Applications of Chitosan

Chitosan is a nontoxic and biodegradable material and because of these properties it has found many applications in water treatment, cosmetics, agriculture and food processing. Due to its unique set of properties such as tumor inhibition, wound healing acceleration, and stimulation of immune system, chitosan is been a suitable candidate for biomedical applications such as for artificial skin, surgical dressing, and controlled drug release. Chitosan is been used for the chelation which can bind specific material such as cholesterol, fats, metal ions and proteins [21-23].

2.8.3.1 Water Treatment

Chitosan is been used for chelation to remove harmful metal elements like copper, lead, mercury, and uranium from wastewater because of the free amino group content in the chitosan molecule which acts an electron donor. The primary amine can bind with the metal ions. So in general if the chitosan has higher number of primary amine then it will have

higher adsorption of metal ions. The effectiveness of chitosan to remove the harmful ions depends upon the degree of deacetylation, pH, and surface area of chitosan substrate. Chitosan is also a good coagulating agent and flocculant because of high amino group on the backbone of chitosan chain which can interact with other negative charged elements such as proteins, dyes and solids [21-23].

2.8.3.2 Food Processing Application

Chitosan has found many applications in food industry because of its antibacterial and antifungal properties which reduces the use of synthetic food preservatives. It can be used either as a packing wrap or directly as food coatings. Synthetic wraps could be replaced with chitosan films because of low oxygen permeability and high moisture transfer of synthetic wrap which increases the chance of fungal growth. The oligomers of chitosan have been observed to lower cholesterol and showed antitumor activity in term of nutrition value. The chitosan can be used to remove the proteins and peptides from cheese whey. The electrostatic interaction between the protonated charged amine group of chitosan and negatively charged milk fat globule membrane fragments facilitates to remove the lipids from cheese whey [22,83].

2.8.3.3 Tissue Engineering

The tissue engineering scaffolds should be porous to provide cell seeding and proliferation onto polymer matrix. The porous structure of scaffolds then direct the host cells to migrate

into the matrix for growth and to regenerate tissue. The polymer scaffolds should be biodegradable such that it should degrade into nontoxic product in to the body [20]. Chitosan is used in tissue engineering scaffolds because of its novel properties like biocompability, biodegradability, antibacterial and wound healing. Also, chitosan has the ability to form porous structure, gel formation, and chemical modification. The interconnected porous structure helps the cells to seed, migrate inside and multiply. A positively charged matrix chitosan scaffold allows cells matrix interactions with the negatively-charged group on the cell surface [19]. Also, the chitosan interacts with anionic glycosaminoglycans (GAG) and proteoglycans which are distributed widely in the body. The chitosan-GAG complex helps to retain and increase the growth factor of cells. The degradation of chitosan is inversely related to chitosan crystallinity and also on the degree of deacetylation. Also, the degree of deacetylation of chitosan is directly related to cell adhesion [32]. The choice of chitosan for tissue support material for various tissue engineering applications like bone, skin, nerve and blood can be controlled and engineered by many ways by which its biological, physical and chemical properties can be changed [84].

2.8.3.4 Wound Healing

The biomaterial for wound dressing material should be biocompatible and promote the growth of dermis and epidermis. The amino group of chitosan shows high effect against bacteria and fungi. The positive charge on chitosan targets the cytoplasmic membrane of bacterial cells [85]. The new tissue generation, granulation must be occurred when an open wound treated with chitosan, it shows accelerated granulation and migration of inflammatory

cells. The macrophage is known as glucan which is present in chitosan. It stabilizes the growth factors and affects the wound healing. The glucan accelerates the production of cytokine which promotes tissue repair. Chitosan helps in fibroblast proliferation and extracellular matrix (ECM) production which require for reformation of connective tissue. All these biological effects were also studied with the chitin but its effects were lesser than chitosan. The difference in the biological effects is due to the degree of deacetylation [86]. Chitosan has antibacterial property which reduces the infection rate. The cationic charge of amino group of chitosan interact with anions on bacterial cell wall which control biosynthesis and it also kills the bacteria [32]. Chitosan's derivatives such as water soluble chitin shows good healing rate as compares to chitin and chitosan powder. Chitosan and its different forms like hydrogels, films, nanofibrous membranes and in conjunction with other materials like bandages and cotton shows good wound healing capability [20].

2.8.3.5 Drug Delivery

Chitosan can be used as a carrier for various active agents like drugs and biologics because of its physicochemical and biological properties. The hydrosoluble and positive charged on chitosan enables chitosan to interact with other negative charged polymers, macromolecules, and polyanions which are essential requirement for drug delivery. The degradation rate of chitosan can be controlled by controlling the degree of deacetylation of chitosan [87]. Chitosan can be used as colloidal delivery vehicles like (microparticles, microsphere, nanopartilces, beads, and hydrogels) for the potential application of controlled drug delivery [88]. The drug loading into nanofibers can be used with the help of electrospinning process.

The high surface area and short diffusion passage length give the nanofibers higher release rate than the bulk material. The chitosan nanofibers found to be useful for controlled drug delivery application [85].

2.8.3.6 Surgical Adhesion

Adhesion occurs due to the surgical repair or inflammatory disease after the initial healing process of surgery like pelvic and abdominal operations. An adhesion is the formation of abnormal tissue linkages. Generally, when two injured tissue surfaces come in contact with each other during healing process then it forms an adhesion. The natural healing of wound requires the body to deposit fibrin on damages tissue and fibrin promotes healing and helps to bind the tissue [30]. Around 80% of patients suffer from adhesions after surgery. These post surgical adhesions can affect the proper function of body, causes intestines obstruction, bowel obstruction, chronic abdominal pain, female infertility and can even cause problem in future surgical procedures [25]. The abdominal adhesion was responsible for many people to hospitalization during 1994 and the procedure causes around $1.3 billion in hospitalization and surgeon expenditures [26]. Various methods have been proposed to prevent and reduce the post surgical adhesion like surgical techniques, pharmacological agents and use of barrier film. The solid barrier placed between two injured tissues is a practical way to prevent post surgical adhesion. The barrier should be noninflammortory, nonimmunogenic, remain in place and should be biodegradable. The physiochemical barrier prevents the contact between the damage tissue and non-damage tissue for up to seven days after surgery [89,27]. There are some commercial barrier films available for the prevention of surgical adhesion like

Polyactive(TM), PRECLUDE Peritoneal Membrane(TM), Seprafilm™, and Tissucol(TM). A comparative study of these barrier materials on rat model shows that Seprafilm™ or PRECLUDE Peritoneal Membrane(TM) prevents post surgical adhesion better [28].

Regardless of using these barrier films, there are high chances of post surgical adhesion to occur. In one of the animal studies, several barrier film were tested to prevent the post surgical adhesion, but despite of using barrier film, there were incidences of adhesion due to slippage of barrier film exposing a wound area [29]. A review indicates that wrapping a suture or staple line from an inflammatory bowel disease operation with Seprafilm™ increases the chance of anastomotic leaks and intraabdominal abscesses [26,30].

When the barrier film adhered to the wound site without stapling or suturing it, then it could potentially eliminate the chance of film shifting which lead to surgical adhesion. Electrospinning a layer of chitosan nanofibers on barrier film would improve the adhesion of film to the wound site because of haemostatic and wound healing properties of chitosan [20,90].

2.9 Electrospinning of Chitosan and Complications Associated with it

Because of many useful properties of chitosan, many researchers had tried to further utilize it and attempted to electrospin chitosan and its blend with other polymers [10,21,91-97]. Chitosan has rigid *D*-glucosamine structure, high crystallinity, and has high hydrogen bonding which leads to its poor solubility in most organic solvents. In acidic pH, it behaves

as a linear cationic polyelectrolyte and shows high net charge density on chitosan backbone because of protonation of its primary amines [97,98]. The degree of protonation is proportional to the amount of NH_2 groups which is directly related to the degree of deacetylation [98]. Due to these properties, the chitosan has high solution viscosity at low concentration which limits its electrospinnability.

Considerable research has been done on electrospinning of chitosan/PEO blend since 2004. Daun *et* al. was first to attempt electrospinning of pure chitosan but failed. He incorporated PEO with chitosan with a molar ratio of 1:1. The ultrafine fibers were mostly consists of chitosan while the microfiber consists of PEO because of phase separation of chitosan/PEO solution [91]. Subramanian *et al*. electrospun aligned chitosan/PEO blend fibers and studied the chondrocyte cell behavior on nanofibrous surface. The tensile strength of aligned nanofiber scaffold has higher modulus than to the cast film of same material. Also, the nanofiber showed good cell adhesion, proliferation and viability [92]. Kossovich *et al*. electrospun ultrafine fibers of chitosan/PEO blend for burn dressings. The chitosan dressing helps in fast preparation of wound and skin transplantation and also reduces the pain while removing or changing the dressing [95]. Bhattarai *et al*. was able to electrospun chitosan/PEO blend for studying cellular compatibility of the nanofibrous structure for tissue engineering application by incorporating Triton X-100TM into solution as a nonionic surfactant and dimethylsulphoxide(DMSO) as a cosolvent. The average diameter of the nanofibers was in the range of 40 nm to 110 nm. From the cellular attachment and viability study, they have found out that cell attached more easily and efficiently on nanofibers than

on cast film of same material [10]. In similar studies where they have used three different kind of surfactants; anionic, cationic, and nonionic. When any kind of surfactant added to chitosan solution it resulted in lesser bead formation. The nonionic surfactant when added to chitosan/blend solution containing 90% acetic acid, nanofibers in the range of 60 to 250 nm were obtained. When anionic surfactant was used, smaller diameter fibers (70-200 nm) were formed [94]. Klossner *et al*. produced nanofibers of chitosan/PEO blend. They had studied the effect of acetic acid concentration, polymer concentration and polymer molecular weight. They used three different molecular weight chitosan (600000, 400000 and 148000 g/mol) each with a degree of deacetylation of 75-85%. However, only chitosan with the lowest molecular weight (148000 g/mol) was able to electrospin with an average fiber diameter ranging from 62 to 129 nm [96].

Desai *et al*. studied the metal binding capacity and anti-microbial property of chitosan/PEO blend having chitosan with various degree of deacetylation (67%, 70% and 80%). The higher DD gives uniform beadless fiber formation with higher fiber diameter [99,100]. This phenomenon was also obtained with chitosan/PVA blend solutions [97]. The metal binding capacity increases with the increase in DD while the antimicrobial activity decreases with the increase in DD because of larger fiber diameter.

The successful electrospinning of pure chitosan has been reported by using trifluroacetic acid (TFA) [104] and 90% acetic acid [101-103]. TFA is been used for the successful electrospinning of pure chitosan. Ohkawa *et al*. used TFA/dichloromethane (70/30) to

electrospin chitosan having a viscosity average molecular weight of 210,000 and degree of deacetylation 78% at 8 wt%. The mean diameter of fibers was found to be 330 nm [104]. In a later article of Ohkawa, they used four different kind of commercial chitosan with a viscosity average molecular weight ranging from 210,000 – 180,0000. They have studied the effect of solution viscosity on electrospinnability and fiber morphology [105]. Geng *et al*. used a solvent system of 10-90% acetic acid and a three different chitosan samples having a molecular weight of 30,000, 106,000 and 398,000 g/mol with a DD of 54%, 56% and 65% respectively. However, only chitosan solution of molecular weight of 106,000 (degree of deacetylation DD 54%) at 7% concentration in 90% acetic acid gives uniform bead-free nanofibers having average fiber diameter of 130 nm [101]. De Vrieze *et al*. also studied the same solvent system of 90% acetic acid, but they were able to produce chitosan nanofibers of 3 wt% with a molecular weight ranging from 190,000 – 310,000 having a degree of deacetylation 75-85%. The average fiber diameter of chitosan nanofibers were about 70 nm to 45 nm [102]. Homayoni *et el*. used an alkali treatment which hydrolyzes the chitosan chain and reduce the molecular weight to produces chitosan nanofibers using a solvent system of 90% acetic acid. The original sample had a viscosity average molecular weight of 1,095,000 g/mol with a DD of 75-85%. After alkali treatment for 48 hours, the viscosity average molecular weight was found to be 294,000 g/mol, however they haven't measured its degree of deacetylation. By lowering the molecular weight by this method, they were able to electrospin more amount of chitosan (5 wt% instead of 2.5 wt%) with an average fiber diameter of 140 nm [103].

In all of the above mention articles of electrospinning of pure chitosan, they have studied the effect of molecular weight and the solvent system. None of the articles discussed the effect the degree of deacetylation on electrospinning, which is the most important property of chitosan as mention in the above literature review. In this study a medium viscosity chitosan having a viscosity average molecular weight of 1.0×10^6 is used, which is deacetylated to certain percentages by alkaline treatment having nearly same molecular weight as original sample. This study will address the effect of solvent such as acetic acid, formic acid, and TFA on the electrospinning process of chitosan solution having different degree of deacetylation, and resulting fiber morphology, fiber diameter and concentration of chitosan. In this study, the chitosan nanofibers will be directly electrospun on a preexisting barrier product (SEPRA film) to address the practical use of chitosan nanofibers for wound healing application (prevention of post surgical adhesions).

3. EXPERIMENTAL WORK

This chapter deals with the materials, electrospinning setup, deacetylation of chitosan, characterization techniques, initial trials and the experimental designs to achieve the research goals.

3.1 Materials

The materials used in this study include two different types of chitosan and three different solvents. Low molecular weight chitosan (CS-Sigma) obtained from Sigma-Aldrich Company, with the reported viscosity of 20-300cp, deacetylation of 75-85%, and molecular weight of approximately 50,000 - 190,000 Daltons based on viscosity. The second chitosan sample was obtained from Vanson Company with a (medium viscosity chitosan) viscosity average molecular weight of 1.0×10^6 was confirmed using intrinsic viscosity and the Mark Houwink Sakurada equation, $[\eta] = kM^a$ and deacetylation of 70% measured by acid base titration method [106].

The solvents used were acetic acid (obtained from VWR Internationals), formic acid (from Wako Pure chemicals) and Trifluoroacetic acid (TFA, from Sigma Aldrich). The deacetylation of chitosan was carried out by using 50% NaOH solution as described in Section 3.3. Methanol (99%) was used to wash the chitosan sample. Hydrochloric acid solution, 0.1N (N/10) (Certified) and sodium hydroxide solution 0.1 N (N/10) (Certified), both obtained from Fisher Chemical, were used in acid-base titration method to determine the

degree of deacetylation. Sodium Acetate Anhydrous (Fused Crystals/Certified ACS) was obtained from Fisher Chemical. All reagents and polymers were used as received.

3.2 Electrospinning Setup

To achieve the objectives of the research goal, a horizontal electrospinning system was used. Equipment used in the electrospinning setup include: a 10 mL syringe with luer-lock connection, a 4 inch 20 gauge blunt tip needle (Becton, Dickinson and Company), a NE-1000 programmable syringe pump (New Era Syringe Systems Inc.) and a FC Series 120 Watt regulated high voltage DC power supply with positive polarity (Gamma High Voltage Research). The feed rate was varied from 1 to15 µL/min, voltage from 10 to 35 kV, and needle tip to collector distance from 10-15 cm. The fibers were collected randomly on the aluminum foil which can be easily removed from the collector without damaging the nanofiber web.

A 20 gauge, 4 inch stainless steel needle was attached to the syringe and a feed rate of which ranges 1 to15µm/min was used. The syringe with needle was kept in such a position that the tip of the needle was directed at the center of the collector plate with the help of Garolite stand. The polymer solution was charged by applying a positive high voltage with the help of a high voltage power supply that provides up to 40 kV. The terminal wire from the high voltage supply was attached to the stainless steel needle with the help of crocodile clip.

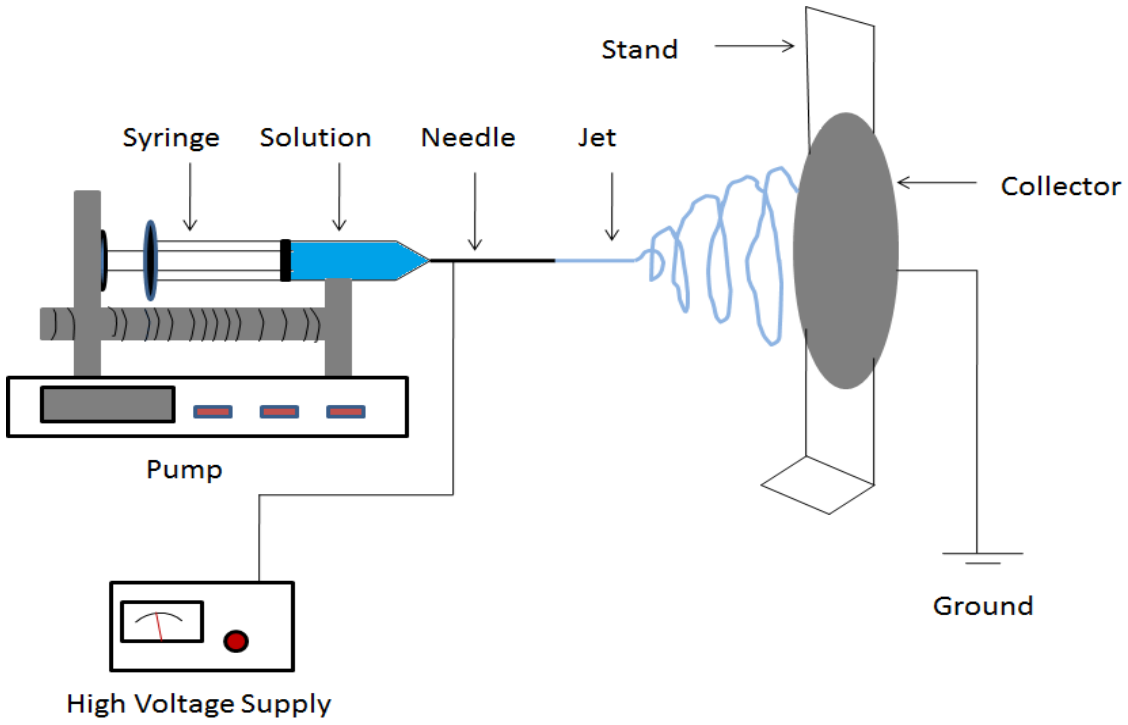

Figure 11 Electrospinning setup consists of a syringe pump, high voltage power supply syringe with needle, collector and the positive /negative voltage terminal wires.

The collecting device consisted of a circular plate which was covered with the aluminum foil on which the nanofibers get deposited. The collector was connected with a negative high voltage at the back of collector plate with the help of crocodile clip due to which a high electric field was generated in-between the tip of needle and the collector. The solution in the syringe gets charged and forms a Taylor cone at the tip of needle. When the charge of the solution exceeds the surface tension at the tip of the needle, the Taylor cone gets stretched and forms a jet travelling toward collector and in between that the solvent from the jet gets evaporated and only the fibers gets deposited on the collector as a nonwoven web.

3.3 Deacetylation of Chitosan to Form Chitosan of Different Degrees of Deacetylation

Chitosan (Vanson, DD-70) of viscosity average molecular weight of 1.0×10^6 and deacetylation of 70% was used as an initial product for deacetylation. Chitosan was deacetylated to different degrees using alkali treatment. For this, chitosan flakes (100 gm) were taken into three neck round bottom flask and 50% (w/w) aqueous NaOH solution (1.1 L) was poured into it. The mixture was stirred at 110° C for two hours to achieve certain degree of deacetylation. Nitrogen gas was continuously purged into the mixture to avoid degradation of sample. After completing the reaction, the mixture was allowed to cool to 80° C. The sample was then rinsed in water till the water showed a pH of 7 and then air dried for two days. Subsequently, it was washed with methanol to remove impurities. After this, the sample was again subjected to rinsing with water till the water shows neutral pH. Finally, the samples were air dried for two days for solution preparation and characterization. To achieve higher degree of deacetylation, the same process was repeated twice [107]. (see Table 3)

Table 3 Deacetylation of chitosan for different hours

Chitosan sample	As Received DD-70 (Vanson)	Deacetylated DD-81	Deacetylated DD-90
Reaction time (hours)	0	2	4+2
% Deacetylation	70	81	90

3.4 Methods and Solution Preparation in (Acetic Acid, Formic Acid, TFA)

3.4.1 Solution Preparation in Formic Acid

The chitosan solution was prepared by taking desired amount of chitosan, according to the required concentration in a container. Formic acid was poured slowly into the container as per the concentration. The solution was then sealed to avoid evaporation of solvent. The solution was stirred overnight using a magnetic stirrer. All the solutions were prepared at room temperature.

Table 4 Chitosan concentration in formic acid

CS-Sigma **Concentration Range**	**Solvent**
3-7 wt%	Formic acid

3.4.2 Solution Preparation in Acetic acid

Chitosan was taken into container with required concentration and acetic acid of known concentration was poured into the container. The solution was kept on stirring overnight for proper dissolution with the help of magnetic stirrer. After the complete dissolution of chitosan, it was used to measure the viscosity and to electrospin the solution.

Table 5 Concentration range of chitosan having different degree of deacetylation in acetic acid

Sample name	Concentration Range	Degree of Deacetylation	Acetic Acid Concentration
DD-81	0.5- 4.5 wt%	81 %	90 %
DD-90	0.5- 5 wt%	90 %	90 %

3.4.3 Solution Preparation in TFA (Trifluoroacetic acid)

Chitosan was taken into glass container with required concentration. Known volume of TFA was added into the glass container and it is kept for stirring which required some initial heating of solution.

Table 6 Concentration range of chitosan having different degree of deacetylation in TFA

Sample Name	Concentration Range	Degree of Deacetylation
DD-70	1- 7 wt%	70 %
DD-81	4-7 wt%	81 %
DD-90	4-7 wt%	90 %

3.5 Electrospinning of Chitosan Solutions

The electrospinning process was carried out at room temperature. The chitosan solution was drawn into the syringe and was attached with the stainless steel needle. While taking the

solution into the syringe, care was taken to avoid air bubbles. Air bubbles in the syringe were removed manually by pushing the polymer solution from the needle. Later the syringe with needle was attached to the syringe pump with the required flow rate of 10 μL/min. The electric field (10-30kV) and the distance between the needle tip and collector (5-20cm) were balanced according to the viscosity of the solution.

The needle and the collector were attached with the positive and negative electrode with the help of crocodile clip, respectively. All the connections were grounded to prevent any interference of external field. The syringe pump was covered with non-conducting material to prevent static generation. When the high electric field 10-30kV was applied, the solution in the syringe gets charged. The solution at the tip of the needle forms a Taylor cone because of charge repulsion. As the Taylor cone forms, the solution forms a very fine jet because of the attraction between the cathode and anode connection. The jet was being pulled towards the collector plate. The distance between the needle tip and collector plate was kept around 5-15cm depending upon the viscosity of solution. The electrospinning process was then carried out for 30 min to 2 hours until a white solid sample was being deposited on the aluminum foil. The sample was carefully taken out and stored for 24 hours before any characterization.

3.6 Characterization Techniques

Various methods have been used to characterize the samples. An acid-base conductometric titration method is used to determine the degree of deacetylation of chitosan. The intrinsic viscosity and the viscosity average molecular weight was determined using Mark-Houwink-

Sakurada equation. The rheological studies were used to determine the zero shear rate viscosity (η_o) of the chitosan solutions to see the effect of viscosity on fiber formation through electrospinning process. Scanning electron microscopy (SEM) was used to examine the quality of electrospun sample and determine the fiber diameter, fiber diameter distribution and to further inspect the morphology of chitosan nanofiber web with the polysaccharide film (SEPRA film).

3.6.1 Method to Determine the Degree of Deacetylation of Chitosan (Acid-Base Titration Method)

The degree of deacetylation of chitosan can be determined by the conductometric titration method [106]. Chitosan was dissolved in acidic medium which was titrated with the alkaline solution and the reading was noted using the conductometric instrument.

A known amount of chitosan was taken in a 250 ml beaker (see Table 7). The chitosan was then dissolved by adding 10 ml of 0.1 *N* hydrochloric acid. And then, 90 ml of distilled water was added to the beaker. A few drops of phenolphthalein were added as an indicator. The conductivity meter (Orion conductivity cell, model 013030) was immersed into the solution and the solution was kept for constant stirring. The solution was then titrated with 0.1 *N* NaOH solution with the help of 10 ml burette. The readings were noted after adding the NaOH solution. The readings were plotted as volume of NaOH solution verses conductivity. The graphs show two deflection points (see Figure 12).

The first deflection point corresponds to the neutralization of excess H^+ions of HCl by OH^- ions of NaOH added. The amount of NaOH between the two deflection points corresponds to the neutralization of the protonated amino groups of chitosan. The increase in conductivity after the second deflection point is due to the excess of NaOH addition [108].

According to *Khaled and Hudson* [106],

$$No.\ of\ Moles\ of\ amino\ groups = M_{NaOH}(mol/L) * V(mL)/1000 \qquad \textbf{Equation 3.1}$$

M_{NaOH} is the molarity and V is the difference in the volume between two inflection points.

Chitosan ($C_6H_{11}O_4N$) Molecular Weight = 161 g/mol

So,

$$\text{Degree of Deacetylation (\%)} = \frac{No.\ of\ Moles\ of\ amino\ groups\ (mol)}{(Amount\ of\ Chitosan\ in\ gm)/(Mw\ of\ repeat\ unit\ in\ g/mol)} \times 100$$

Equation 3.2

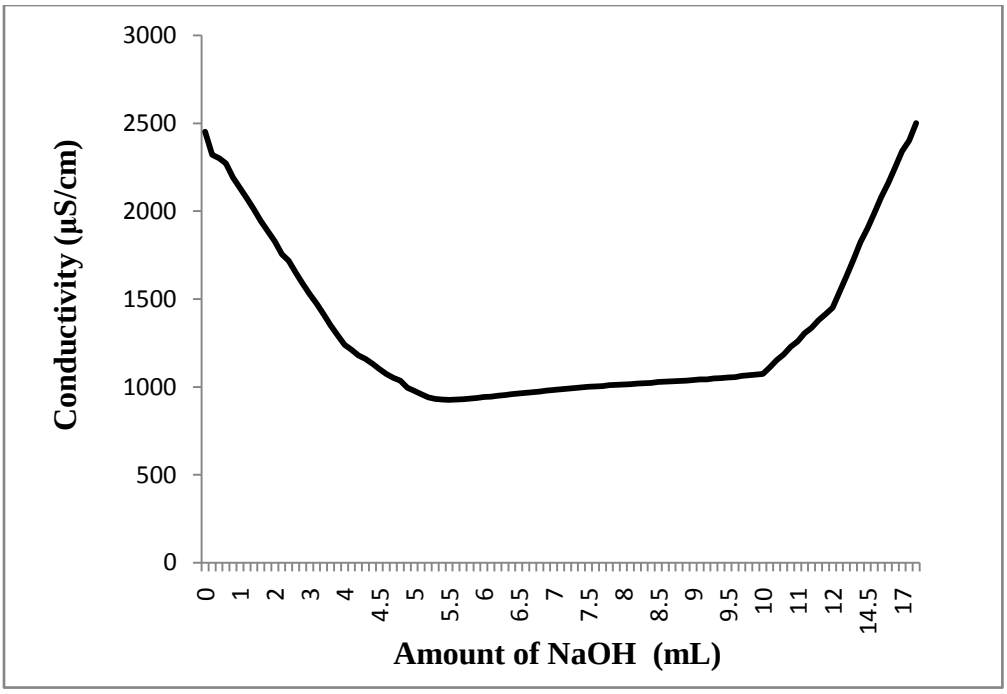

Figure 12 Conductometric titration curve for chitosan sample

Table 7 Chitosan having different degree of deacetylation calculated by conductometric titration method

Chitosan sample	Reaction time (hours)	Amount of chitosan (gm)	Difference in volume between two deflection point (ml)	No. of Moles of amino groups (mol)	Degree of Deacetylation-DD (%)
DD-70	0	0.0937	9.6-5.5=4.1	0.00041	70
DD-81	2	0.0927	10.1-5.4=4.7	0.00047	81
DD-90	4+2	0.0932	10.5-5.3=5.2	0.00052	90

3.6.2 Intrinsic Viscosity and Molecular Weight Determination by Ubbelohde viscometer

The intrinsic viscosity and the viscosity average molecular weight M_v can be determined according to the Mark-Houwink Sakurada equation.

$$[\eta] = kM^a \qquad \textbf{Equation 3.2}$$

Considerable research has been done on the viscometric constants, *k* and a for the Mark-Houwink equation, $[\eta] = kM^a$. According to Roberts and Maghami [109], the value of viscometric constant ($k = 1.81 \times 10^{-3}$ cm^3/gm) and (a = 0.93) remains constant for a range of degree of deacetylation 60-100 % by using 0.1 M acetic acid/0.2 M NaCl as solvent. However, Wang and coworkers [110] had found out that the values of viscometric constants changes as the degree of deacetylation changes when chitosan was dissolved in an aqueous solution of 0.2 M CH_3COOH/0.1 M CH_3COONa.

$$k = 1.64 \times 10^{-30} \times (\%DD)^{14} \qquad \textbf{Equation 3.3}$$

$$a = -1.02 \times 10^{-2} \times (\%DD) + 1.82 \qquad \textbf{Equation 3.4}$$

As the degree of deacetylation increases, the free amino group on the backbone of chitosan also increase which ultimately increases the dimension of coil which causes increase in intrinsic viscosity [111].

As the degrees of deacetylation of our samples were in the range of 70 % to 90 %, we followed Wang and coworkers method. A series of dilute chitosan solution were prepared in 0.2 M CH_3COOH/0.1 M CH_3COONa aqueous solution at 30°C. The solution of 10 ml was taken into a Cannon-Ubbelohde semi-micro viscometer (size 75 J- 134) and the instrument was immersed into the constant water bath having 30°C. It is kept for 20 min for equilibration before the readings were recorded. For each concentration, ten flow times were recorded for the polymer solution to flow from upper mark to lower mark on the viscometer and then the readings were averaged. These readings were then compared with the pure solvent flow time to give the relative viscosity and the specific viscosity.

$$\eta_{rel} = t_{solution} / t_{solvent} \qquad \textbf{Equation 3.5}$$

$$\eta_{sp} = (t_{solution} / t_{solvent}) - 1 \qquad \textbf{Equation 3.6}$$

where $t_{solution}$ and $t_{solvent}$ are the time required for the polymer solution and pure solvent to flow from the marking on the viscometer, respectively. The results of viscosity measurement are reported in Table 8, 9, and 10.

Table 8 Scheme of intrinsic viscosity measurement of the as received chitosan (DD-70)

c (gm/mL)	0 (solvent)	0.001	0.000714	0.0004	0.000266	0.000133
Time (sec)	98.52	196.076	152.954	123.762	113.66	105.214
η_{sp}		0.990215	0.552517	0.256212	0.153674	0.067946
η_{sp}/c		990.2152	773.617	640.5298	577.7232	510.8691
η_{rel}		1.990215	1.552517	1.256212	1.153674	1.067946
$\ln \eta_{rel}/c$		688.2428	615.9026	570.252	537.4134	494.2616

Table 9 Scheme of intrinsic viscosity measurement of the deacetylated chitosan (DD-81)

c (gm/mL)	0 (solvent)	0.0014	0.001	0.0007	0.0004	0.000266	0.000133
Time (sec)	98.52	284.29	213.224	178.202	141.962	126.518	112.018
η_{sp}		1.885607	1.164271	0.80879	0.440946	0.284186	0.137008
η_{sp}/c		1346.862	1164.271	1155.414	1102.365	1068.368	1030.133
η_{rel}		2.885607	2.164271	1.80879	1.440946	1.284186	1.137008
$\ln \eta_{rel}/c$		756.9538	772.0837	846.6545	913.2496	940.3196	965.4135

Table 10 Scheme of intrinsic viscosity measurement of the deacetylated chitosan (DD-90)

c (gm/mL)	0 (solvent)	0.0014	0.001	0.0007	0.0004	0.000266
Time (sec)	98.52	225.814	190.002	159.27	131.558	119.956
η_{sp}		1.292063	0.928563	0.616626	0.335343	0.21758
η_{sp}/c		922.9018	928.5627	880.8944	838.3577	817.9706
η_{rel}		2.292063	1.928563	1.616626	1.335343	1.21758
$\ln \eta_{rel}/c$		592.4658	656.775	686.2019	722.9706	740.0956

A graph of η_{sp}/c versus c and ln η_{rel} versus c was plotted based on Huggins's equation, and Kraemer's equation, respectively (see Figure 13, 14, and 15), where c is the concentration of chitosan solution. For measuring the intrinsic viscosity [η], the points were extrapolated to zero concentration. The point at which the linear line touches the η_{sp}/c (y-axis) is the intrinsic viscosity. The degree of deacetylation which was calculated with the help of acid base titration method was used to determine *k* and a values. Then the average viscosity molecular weight was calculated with the help of [η], *k* and a by the Mark-Houwink Sakurada equation. The properties of original chitosan and deacetylated chitosan are provided in Table 11.

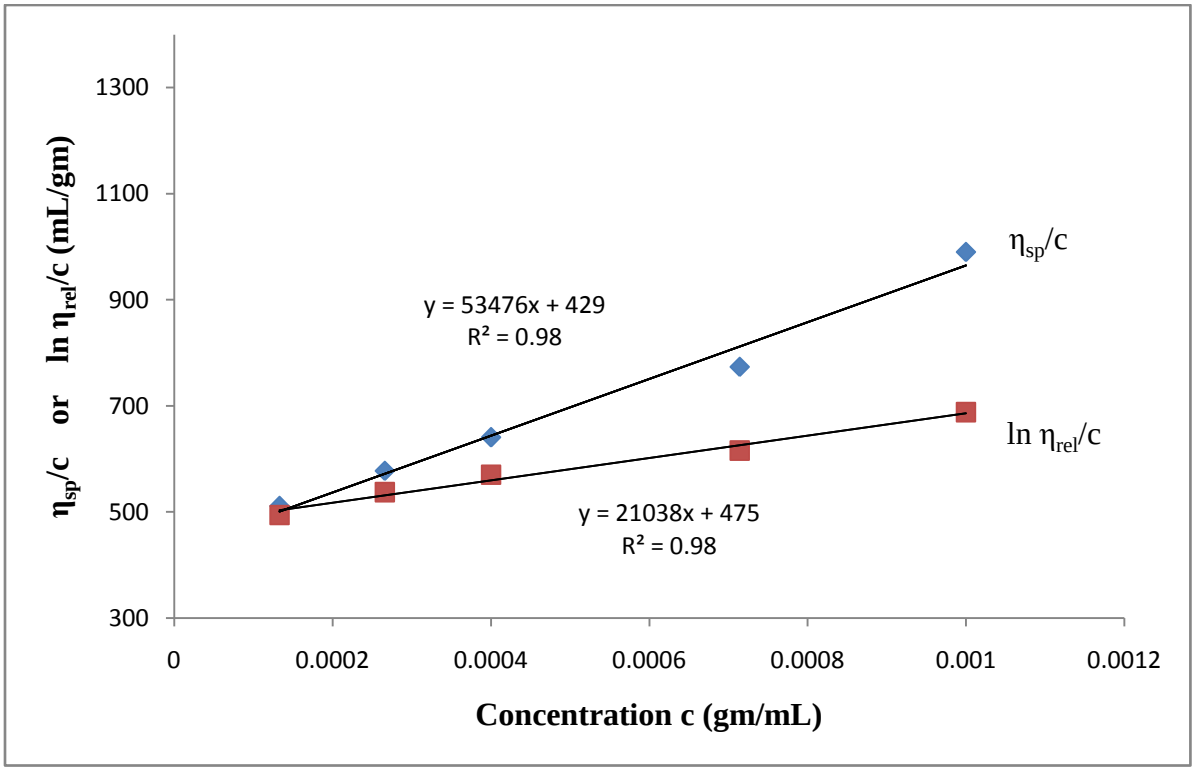

Figure 13 Huggin's and Kraemer plot of η_{sp}/c versus c and ln η_{rel}/c versus c for the as received chitosan (DD-70) in 0.2 M CH_3COOH/0.1 M CH_3COONa aqueous solution

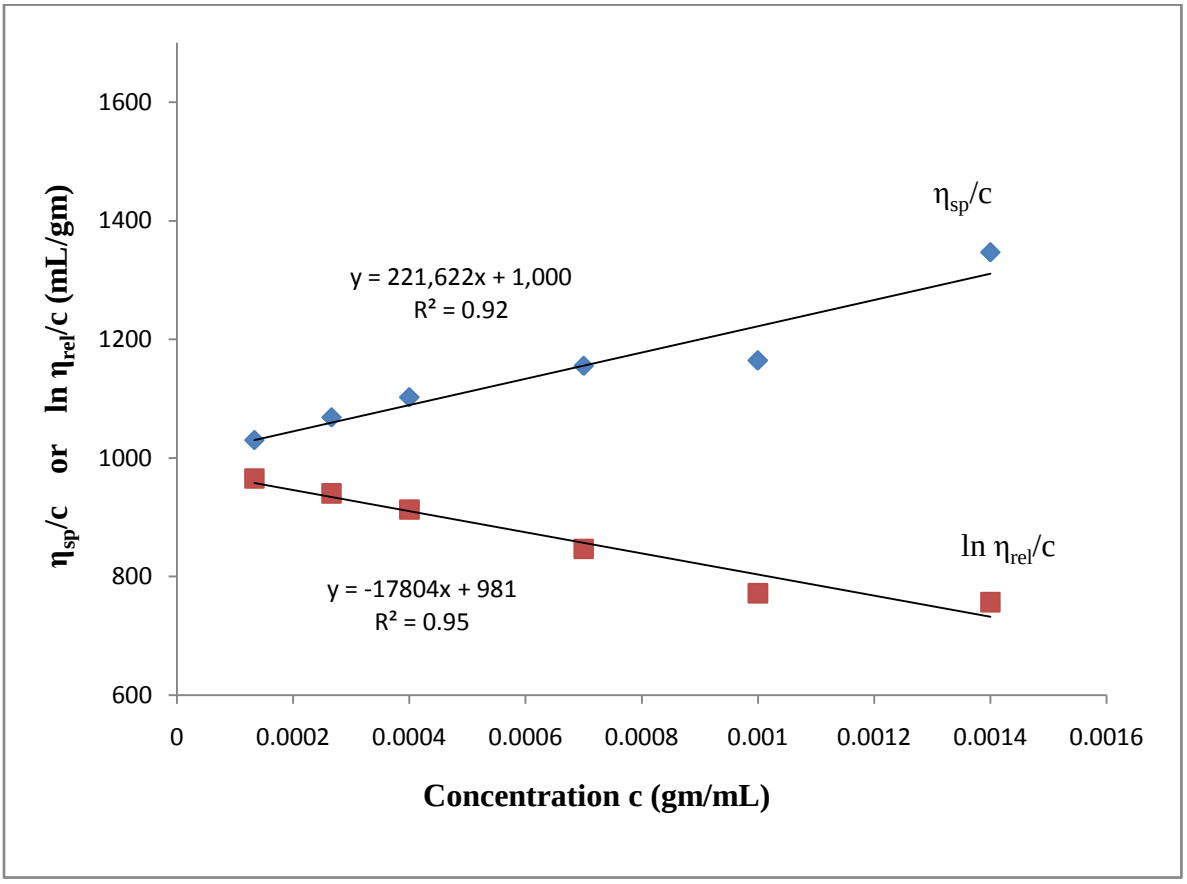

Figure 14 Huggin's and Kraemer plot of η_{sp}/c versus c and ln η_{rel}/c versus c for the deacetylated chitosan (DD-81) in 0.2 M CH_3COOH/0.1 M CH_3COONa aqueous solution

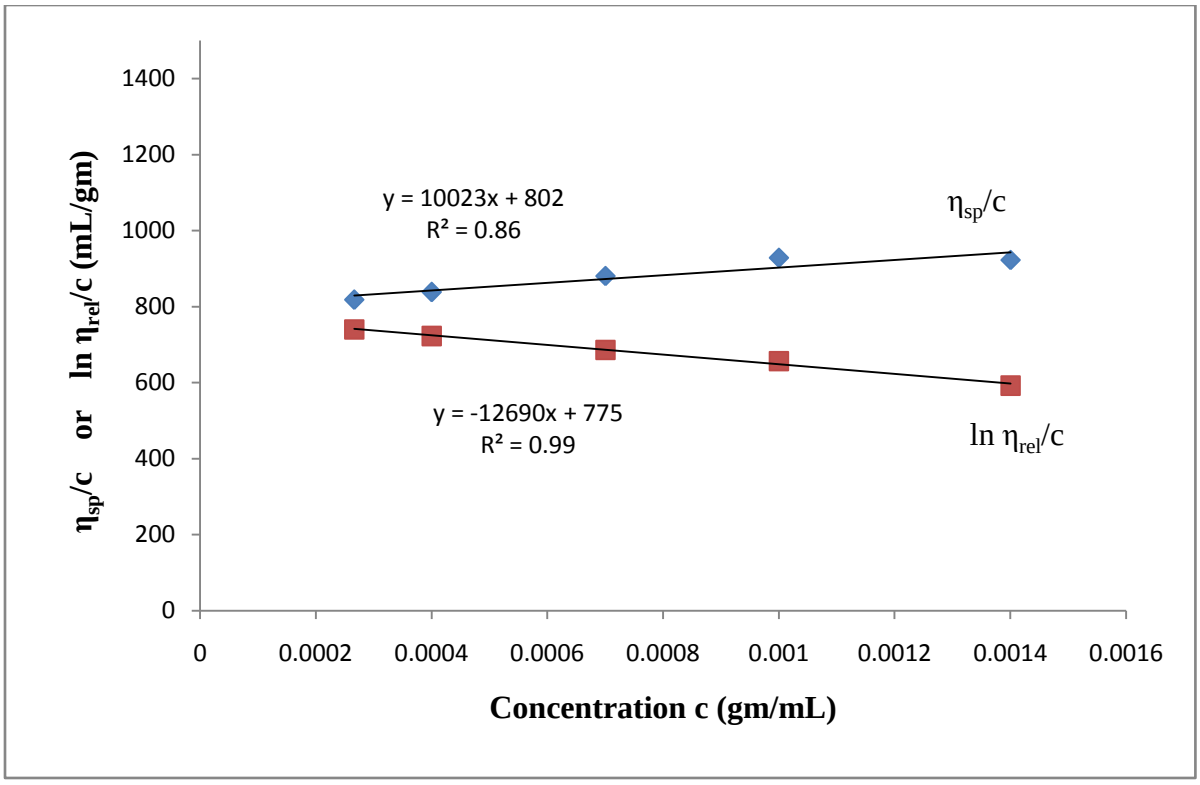

Figure 15 Huggin's and Kraemer plot of η_{sp}/c versus c and ln η_{rel}/c versus c for the deacetylated chitosan (DD-90) in 0.2 M CH_3COOH/0.1 M CH_3COONa aqueous solution

Table 11 Properties of medium viscosity and deacetylated chitosans

Chitosan sample	Reaction time (hours)	DD (%)	*k* (mL/gm)	a	Intrinsic viscosity [η]	Viscosity average molecular weight, M_v
Original	0	70	0.000122	1.10141	475.4	1.0×10^6
1	2	81	0.000957	0.987374	981.4	1.0×10^6
2	4+2	90	0.003653	0.9037	802.2	8.2×10^5

3.6.3 Rheological Measurement of Chitosan Solutions

The rheology can be defined as the study of polymer solution under flow and deformation. The viscosity and the elasticity of the polymer are used to determine the consistency of material. The viscosity is the measurement of fluid's resistance to the flow and the elasticity is the related to the degree of structure. The rheometer measure the rheological property of solution as a function of rate of formation. For example, by applying a shear flow on solution and measuring the resultant stress or by applying a shearing stress and determining the resultant shear rate. Different assemblies are available to measure the viscous flow like concentric cylinder, cone and plate, parallel plate, capillary and ball falling. A parallel plate rheometer is able to determine both high and low viscosity data because the sample is easy to load and the data can be obtained in few minutes.

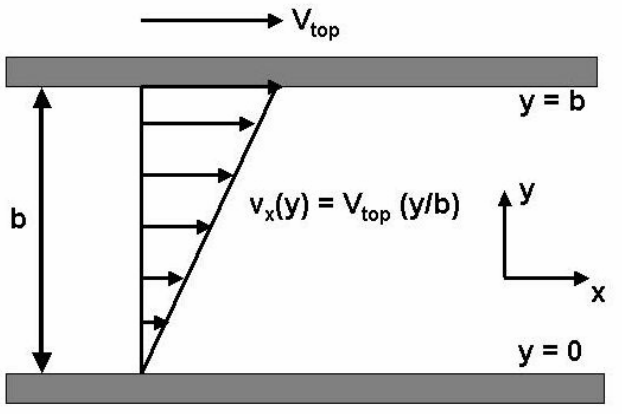

Figure 16 Parallel plate assembly of rheometer [112]

The viscosity can be measured when the fluid is sheared between the two flat plates which are parallel. Under the action of shear stress, the shape of the fluid between the plates changes. The stress can be defined as the force acting on the fluid on a surface per unit area of that surface, in the direction parallel to the flow. The shear viscosity can be defined as

$$\eta = \sigma / \dot{\gamma} \qquad \textbf{Equation 3.7}$$

where viscosity η is the ratio of the shear stress to the shear rate. Shear rate is defined as the rate of change of shear stress or the velocity gradient (see Figure 16) perpendicular to the direction of shear flow (dv/dx). Shear rate can be measured in 1/s or s^{-1} and the viscosity are usually measured in poise (P) or pascal-seconds (Pa.s).

In this study, the rheological property of the chitosan solution as a function of degree of deacetylation and concentration of polymer was determined by using ATS Rheosystem Stresstech HR Rheometer at 25°C to study and evaluate the electrospinnability of chitosan solution. A 50 mm parallel plate system with a gap of 0.4 mm was use for the all the samples. The viscosity of sample as a function of stress and or shear/rate is measured. The zero shear rate viscosity (η_o) was calculated from the Newtonian plateau region of each sample by using Rheologica Rheo-Explorer 5.0 software.

3.6.4. Scanning Electron Microscopy (SEM)

Scanning electron microscopy is used to see the morphology of the resulting fibers. The information provided by the SEM images includes fiber diameter, bead density, and fiber diameter distribution. This information will determine the effect of degree of deacetylation on fiber morphology which will be suitable as an extra cellular matrix on the polysaccharide film.

From the collection material (aluminum foil), samples of 1 × 1 cm were cut from two different section. The samples were then coated with a layer of gold approximately 100 Å thick using a gold sputter machine to reduce charge interruptions. Two types of SEM were used: JEOL 6400F Field Emission SEM and FEI Phenom. After the coating, the samples were mounted on the SEM and focused, and viewed at magnification between 5000-40000 times their original sizes. Those images were the used to evaluate the fiber diameter and consistency.

Revolution software was used to measure the diameter of fibers from the images obtained from JEOL 6400F Field Emission SEM. Two images were taken from different section of foil and fifty fiber diameters were measured from each sample. The readings were average to determine the mean fiber diameter and the distribution For some of the images, the small fibrous web within the nanofibers were excluded from the measurement in order to have consistency.

ImageJ software was used for the SEM images obtained from FEI Phenom to determine the fiber diameter by line length function. A scale bar was set according to the scale bar on the SEM image, and then the line length function gave the fiber diameter. Fifty readings were measured from two different SEM images and the readings were averaged to determine the mean fiber diameter and the distribution.

3.7 Initial Trials

Initial trials were carried out in formic acid and acetic acid by using commercial chitosan (CS-Sigma) to investigate the electrospinnability of chitosan solution. CS-Sigma was attempted to electrospin with 90% acetic acid at a concentration of 3 wt%, based on literature review work. In both the cases, SEM images revealed that only bead formation occurred during electrospinning process. Other chitosan sample (DD-70) having a viscosity average molecular weight of 1.0×10^6 and a DD of 70 % was used as an initial product to electrospin in acetic acid This chitosan was dissolved in 90% acetic acid, but even after 120 hours of dissolution, there were some small residue of un-dissolved chitosan flakes present in the solution. So therefore, deacetylation of chitosan was carried out to produce chitosan of different degrees of deacetylation (81% and 90%) having nearly same molecular weight.

Several trials were carried out to find out the upper limit and lower limit of chitosan concentration in acetic acid through the rheological studies. The rheological studies of chitosan solution in TFA were not recommended due to environmental concerns. For

electrospinning, the upper limit of chitosan concentration 5 wt% in acetic acid and 8 wt% in TFA was carried out. Due to the very viscous nature of solution at these concentrations, the solution does not come out from the needle even at very high feed rate. These concentrations were considered as the upper limit concentration. So it was decided to conduct the experiments through a concentration range of 1- 4.5 wt% in acetic acid and 1-7% wt% in TFA to evaluate the electrospinnablity and fiber formation. Different experiments were done to see the effect of concentration, voltage and needle tip to collector distance.

3.8 Design of Experiments

3.8.1 Experimental Design: Electrospinning of Chitosan in Acetic Acid

As the SEM images of commercial chitosan (CS-Sigma) revealed bead formation during electrospinning and DD-70 was not soluble in 90% acetic acid, the chitosan sample (DD-70) was deacetylated to a certain degree to increase its solubility. Experiments were carried out to find out the upper and lower limit of chitosan concentration. Results indicate that concentration from 2.5 wt% to 4 wt% showed some fiber formation with some beads. However, below 2 wt% only bead formations occurred. So to obtain the optimal conditions for electrospinning, a design of experiments were made which include different parameters (see Table 12). In these experiments, feed rate of 10 µL/min was kept constant, and voltage and tip to collector distance was changed according to the concentration of solution.

Table 12 Experimental Design: Electrospinning of chitosan in acetic acid

Degree of Deacetylation (%)	Concentration (wt%)	Voltage (kV)	Tip to ollector Distance (cm)	Number of Experiments
81	1,2,2.5,3,3.5,4	15, 20, 25,30	10,15	6×4×2 = 48
90	2,2.5,3,3.5,4,4.5	15,20,25,30	10,15	6×4×2 = 48

3.8.2 Experimental Design: Electrospinning of chitosan in TFA

These set of experiments was carried out to find out the effect of degree of deacetylation of chitosan on the fiber formation and the fiber diameter. Initial experiments were carried out to find out the upper and lower limits of concentration of chitosan for electrospinning. Results showed that from concentration 3 wt% -7 wt% of (DD 70%), fiber formation were possible. Below 3 wt% only bead formation resulted. So to optimize the electrospinning condition, an experimental design was made (see Table 13). For DD 81% and 90%, concentration range of 4-7 wt% was selected. In all the experiments, feed rate was kept constant (10 µL/min) and the voltage and tip-to-collector distance was changed according to the concentration of chitosan.

Table 13 Experimental design: electrospinning of chitosan in TFA

Degree of deacetylation (%)	Concentration (wt%)	Voltage (kV)	Tip to collector Distance(cm)	Number of Experiments
70	3,4,5,6,7	15,20	10,15	5×2×2=20
81	4,5,6,7	15,20	10,15	4×2×2=16
90	4,5,6,7	15,20	10,15	4×2×2=16

3.9 System Validation

A typical horizontal electrospinning system used in this project is illustrated in Figure 17. It consists of a NE-1000 programmable syringe pump which extrudes the polymer solution from the 10 ml syringe (luer-lock connection) at a definite flow rate. The syringe encapsulates a 4 inch 20 gauge blunt tip metal needle. Regulated DC voltage was provided by FC Series 120 Watt regulated high voltage DC power supply. The needle and the collector were connected with the positive and the negative terminal of the high voltage DC power supply, respectively. The height of the collector plate on the stand can also be varied by the sliding slot on the stand.

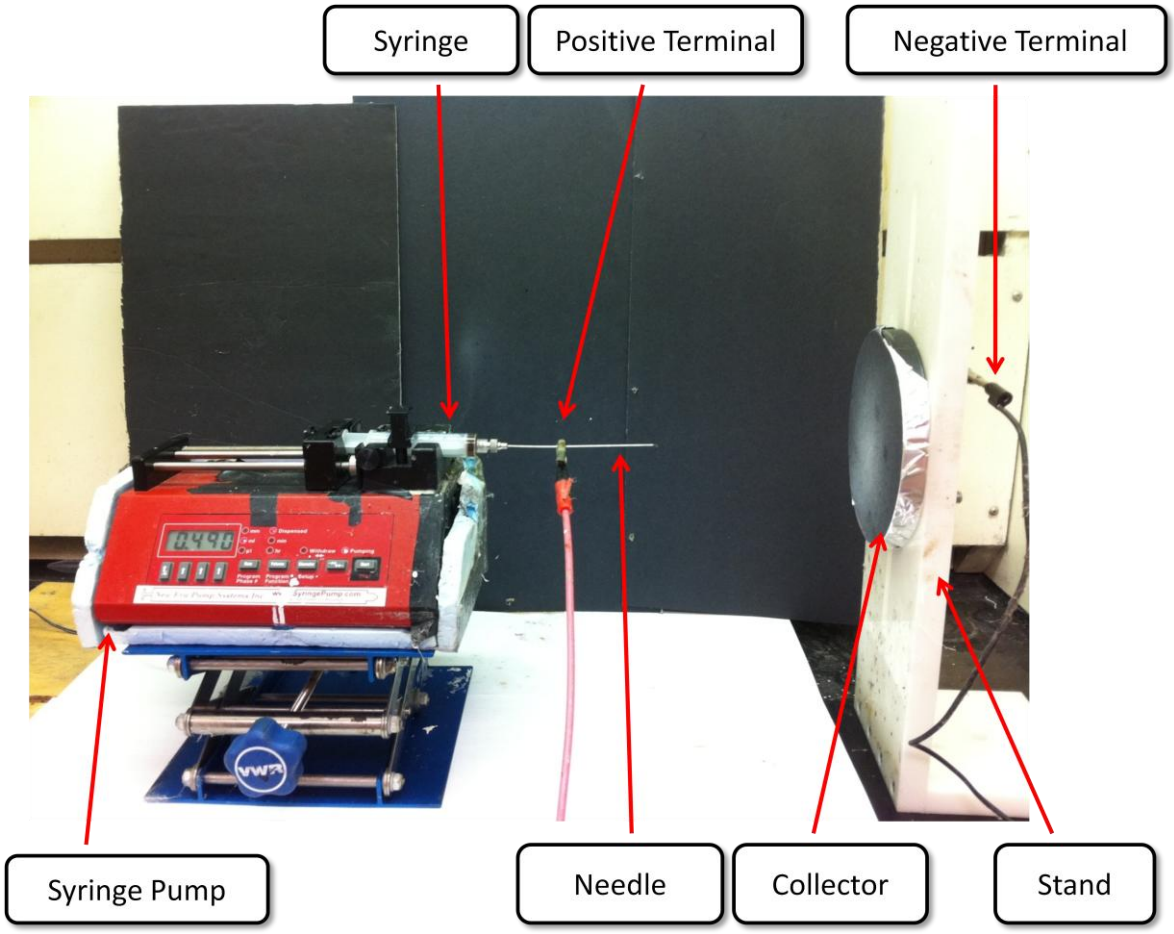

Figure 17 Electrospinning setup consists of a syringe pump, syringe with needle, collector and the positive /negative voltage terminal wires

In order to verify the functionality of electrospinning setup, PEO solution was electrospun into nanofibers mats as illustrated in Figure 18. A PEO solution of 6 wt% (400,000 MW) was used to see the functionality of the electrospinning setup. The sample was electrospun to find the threshold for successful electrospinning. The diameter of the nanofibers was then measured and compared with the reported PEO electrospun nanofibers to evaluate the fiber

morphology. The electrospinning system produced smooth bead-free nanofibers in the range of 100 nm to 250 nm.

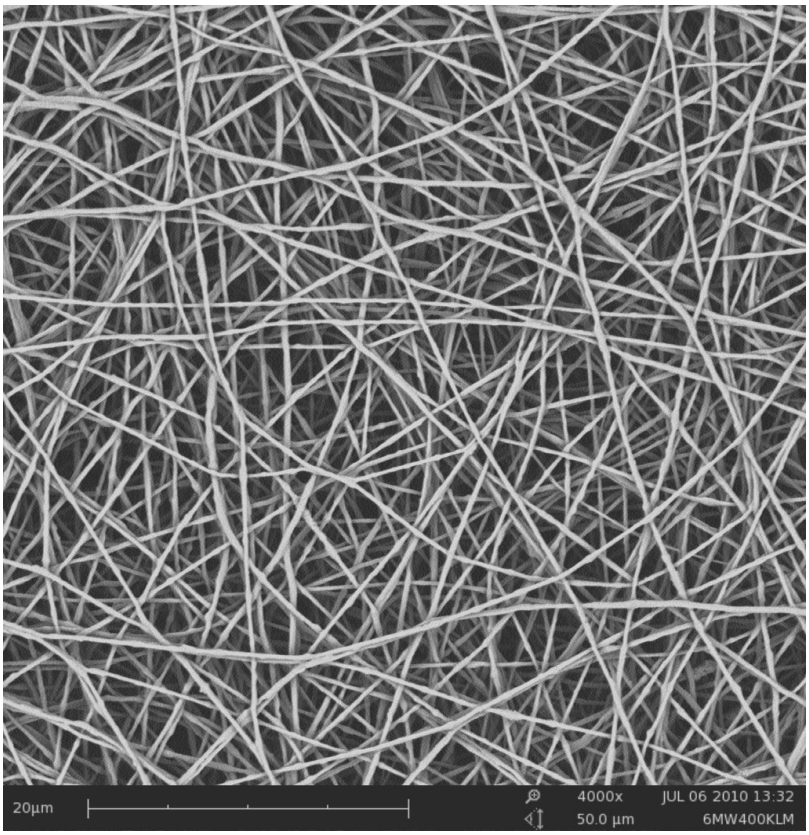

Figure 18 SEM image of PEO/deionized water (6 wt%, 400,000 gm/mol) electrospun at an applied voltage =11 kV, tip-to-collector distance =15 cm and feed rate =10 µm/min (Magnification-4000x)

4. RESULTS AND DISCUSSION

4.1 Initial Trails with Acetic acid and Formic acid.

Chitosan is found to be challenging to electrospin, although it has many beneficial biological properties which could be use as nanofibers mats for biomedical application like tissue engineering and for the prevention of post surgical adhesions. Initial attempts were made to electrospin pure chitosan for nanofiber production as reported in the literature review. Commercial chitosan, CS-Sigma ($1.9–3.1 \times 10^5$ g mol^{-1}, degree of deacetylation is 75–85%) was attempted to electrospin with 90% acetic acid at a concentration of 3 wt%, based on literature review work. A solvent system of 90% acetic acid was found to be appropriate, as it decreases the surface tension and increases the charge density of the jet at same time which resulted in using lower electric field for jet formation [101]. De Vrieze *et al*. was able to produce chitosan nanofibers of 3 wt% with a molecular weight ranging from 190,000 – 310,000 having a degree of deacetylation 75-85%, which was similar to our chitosan [102]. Also, the same chitosan was tried with 90% formic acid. All the electrospinning attempts were either unsuccessful or ended up with bead formation instead of nanofibers (see Figure 19 and 20). Similar results have been found when Rebecca *et al*. attempted to electrospun 3 wt% of CS-Sigma in 90% acetic acid. The entanglement concentration of the chitosan was found to be 2.9 wt% and having a concentration dependence of $\eta_{sp} \sim c^{6.0}$ in semidilute entangled regime, which was much stronger than the predicted relationship. This high scaling dependence was due to the associate formation of polymers chains [96].

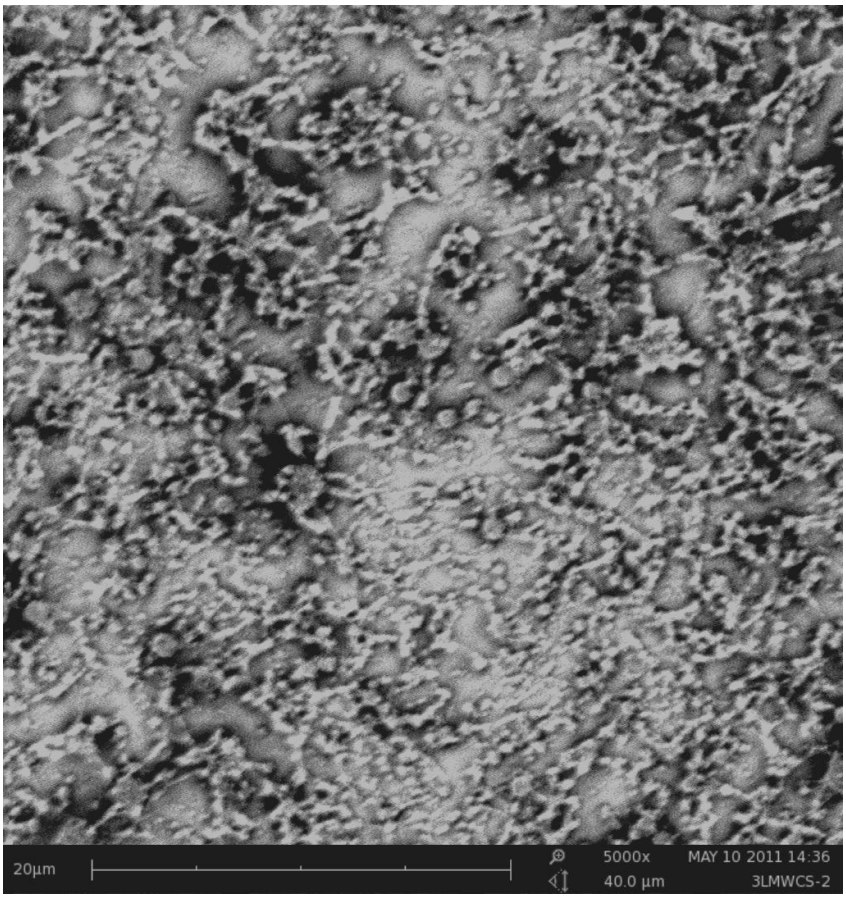

Figure 19 SEM image of electrospun chitosan in 90% acetic acid/water as solvent with the feed rate = 0.3 mL/Hr, applied voltage = 20kV and tip to collector distance = 10 cm (Mw=1.9–3.1 × 105 g mol-1, degree of deacetylation =75–85% and concentration =3wt%, 5000x)

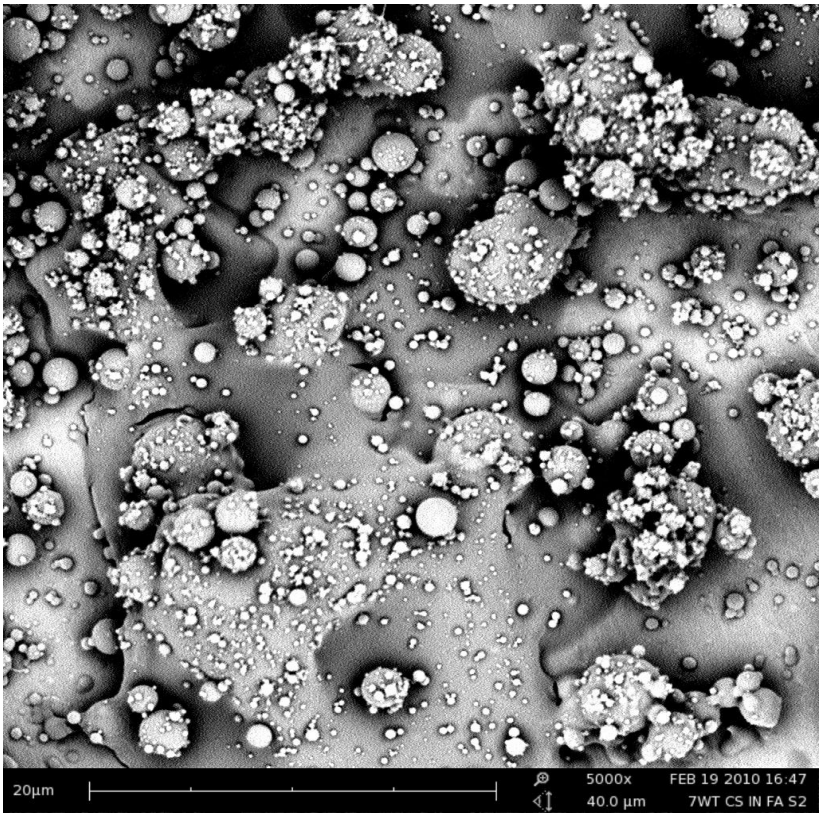

Figure 20 SEM image of electrospun chitosan in 90% formic acid/water as solvent at a concentration of 3wt%. (Feed rate = 0.3 mL/Hr, applied voltage = 20 kV and tip to collector distance =10 cm) showing bead formation. (Magnification-5000x)

Another batch of chitosan (DD-70, from Vanson) having a viscosity average molecular weight of 1.0×10^6 and a DD-70% was used as an initial product to electrospin with acetic acid. Because the chitosan didn't dissolve in 90% acetic acid, the deacetylation of chitosan was carried out to produce chitosan of different degrees of deacetylation (81% and 90%) of nearly same molecular weight by alkali treatment to increase the solubility and for further study.

4.2 Processing Effect on Electrospinning Process

4.2.1. Effect of Chitosan Concentration in Acetic acid with Different Degrees of Deacetylation

After deacetylating the chitosan and finding out its degree of deacetylation and molecular weight, initial trials were carried out to find out the upper and lower limit of chitosan concentration for electrospinning. Solutions of DD-81% and DD-90% chitosan were made in concentration from 0.5 to 4.5 wt% in increment from 0.5 wt%. Electrospinning were attempted on all the solutions by changing the electric field. The viscosities of all the solutions were measured using rheometer to find out the optimal viscosity and concentration of solution for successful electrospinning. Results indicate that the concentration from 2.5 wt% to 4 wt% showed some fiber formation with some beads (see Figure 21).

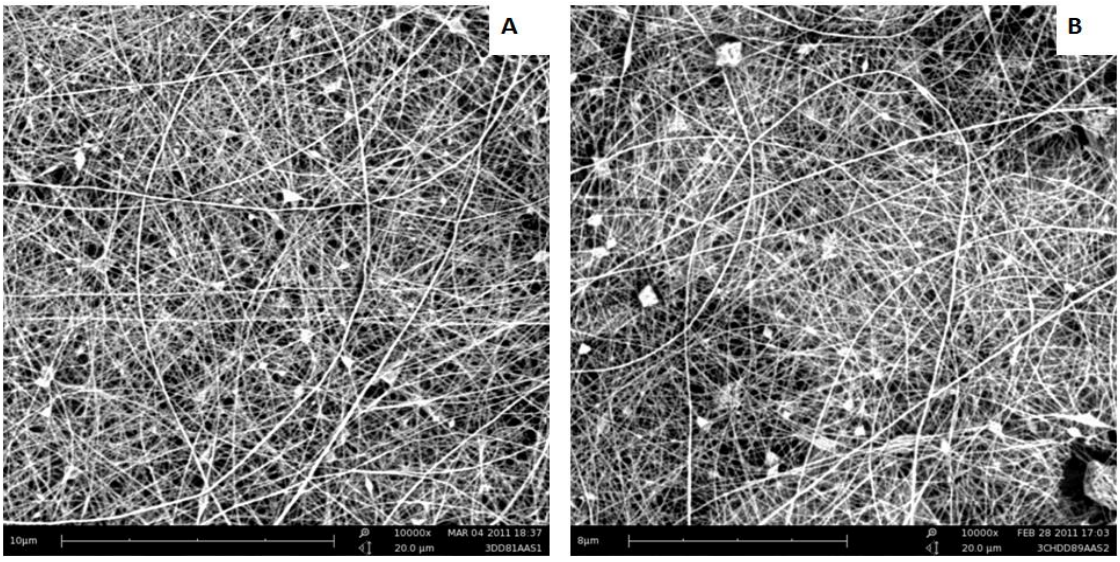

Figure 21. SEM image of electrospun chitosan of different degree of deacetylation (A-81% and B-90%) in 90% acetic acid/water as solvent at a concentration of 3 wt% (feed rate = 10 µL/min, applied voltage = 15kV and tip to collector distance = 10 cm), at 10,000x

Fiber formation occurs only when there is sufficient chain entanglement present in the polymer solution. When the concentration of a solution is increased to have sufficient chain entanglement, the viscosity of the polymer solution also increases. If the viscosity is too high it becomes difficult to electrospin. McKee *et al*. attributed that to successfully electrospin a polymer solution, the concentration should be 2-2.5 times its entanglement concentration (C_e), to form continuous beadless fibers [113]. The dilute and concentrated regime are defined by the overlap concentration (C^*), which is a concentration at which the polymer chains starts overlapping. In dilute regime, the polymer chains are isolated from each other in solvent and in concentrated regime, the polymer chains are entangled and C_e is the polymer concentration above which the chain dimensions forms entanglements. In other words, dilute solution is for $C < C_e$ and concentrated entangled solution is for $C > C_e$ [114].

In order to know the entanglement concentration for our chitosan samples, we measured the zero shear viscosities of all the chitosan solutions from low concentration to high concentration depending upon the solubility of chitosan. Figure 22 and 23 show the zero shear rate viscosities for DD-81% and DD-90%, respectively.

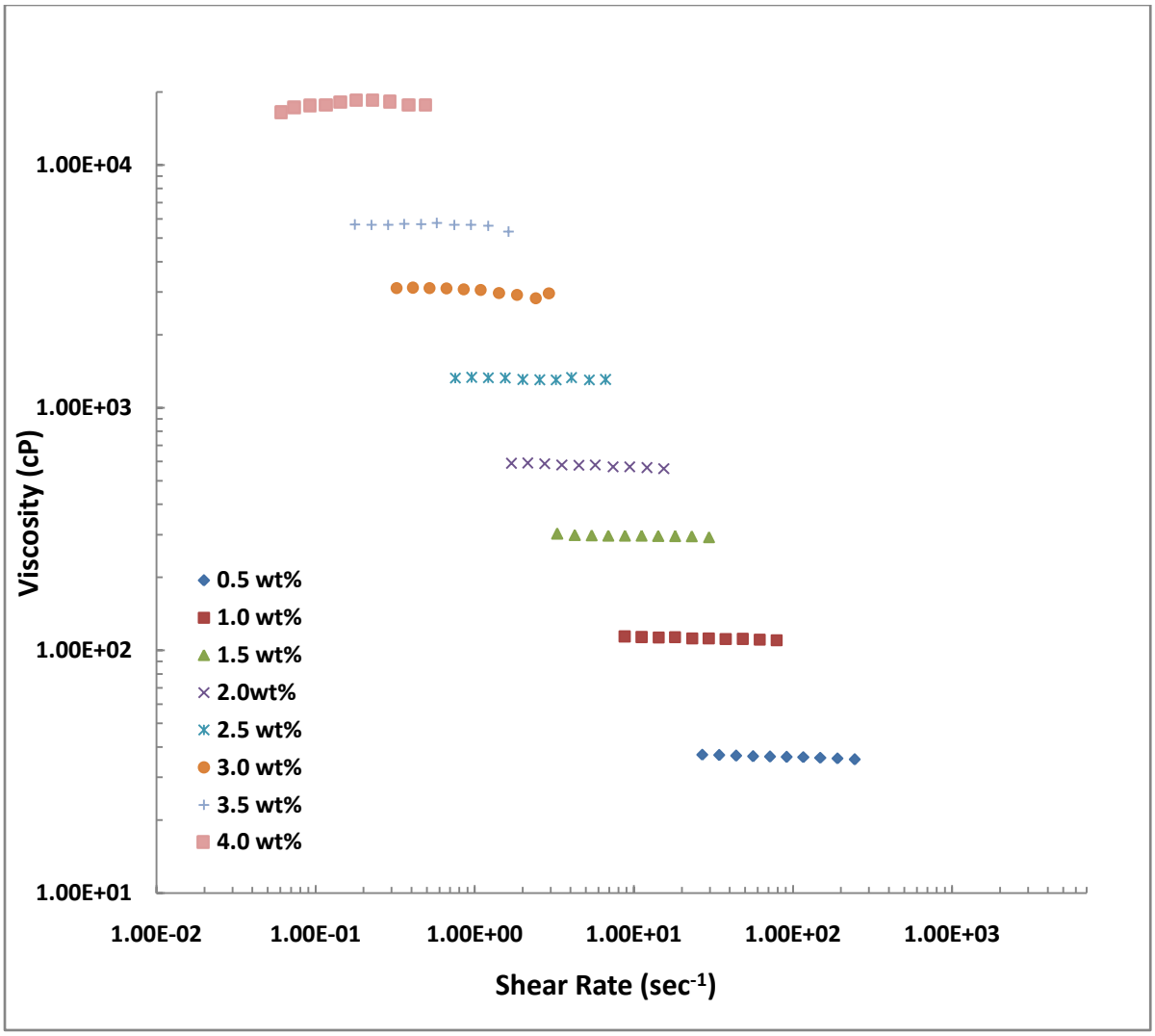

Figure 22 Effect of shear rate and concentration on the rheological property of chitosan solution in 90% acetic acid/water as solvent for DD-81%

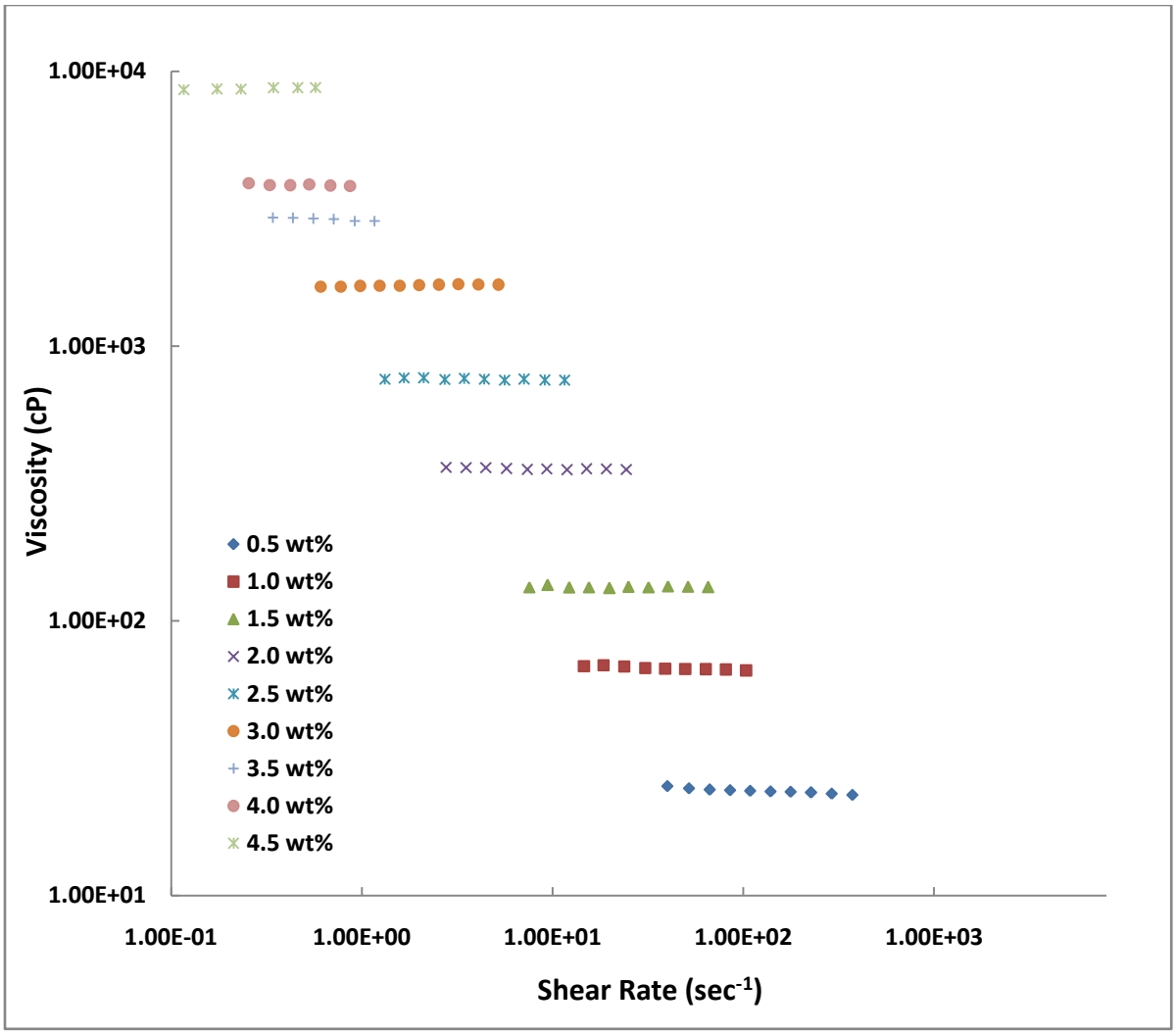

Figure 23 Effect of shear rate and concentration on the rheological property of chitosan in 90% acetic acid/water as solvent for DD-90%

From Figures 22 and 23, we can observed that the 1) the shear viscosity increases with increasing chitosan concentration, 2) the low concentrations, the solutions are Newtonian for entire range of shear rate measured 3) and at high concentrations, the solutions showed a Newtonian flow region, that is a constant zero-shear viscosity ($\eta_{\circ}$) at low shear rate and then showed a shear thinning behavior (non-Newtonian) at higher shear rate. (not shown in

figures because shear thinning viscosity is not a characteristic of steady shear rate for measuring zero-shear viscosity). Similar results have also been found in many articles [115-117]. At low shear rate, the ($\eta_{\circ}$) can be maintained because the rate of disentanglements exerted by shear force is same as that of entanglements newly formed. At higher concentration, there is an increase in the intermolecular entanglement and the motion of individual chains gets restricted. This requires more time to form new entanglement to replace the disrupted ones by external deformation [115]. Therefore, with increasing concentration, the Newtonian flow region moves towards lower values of shear rate.

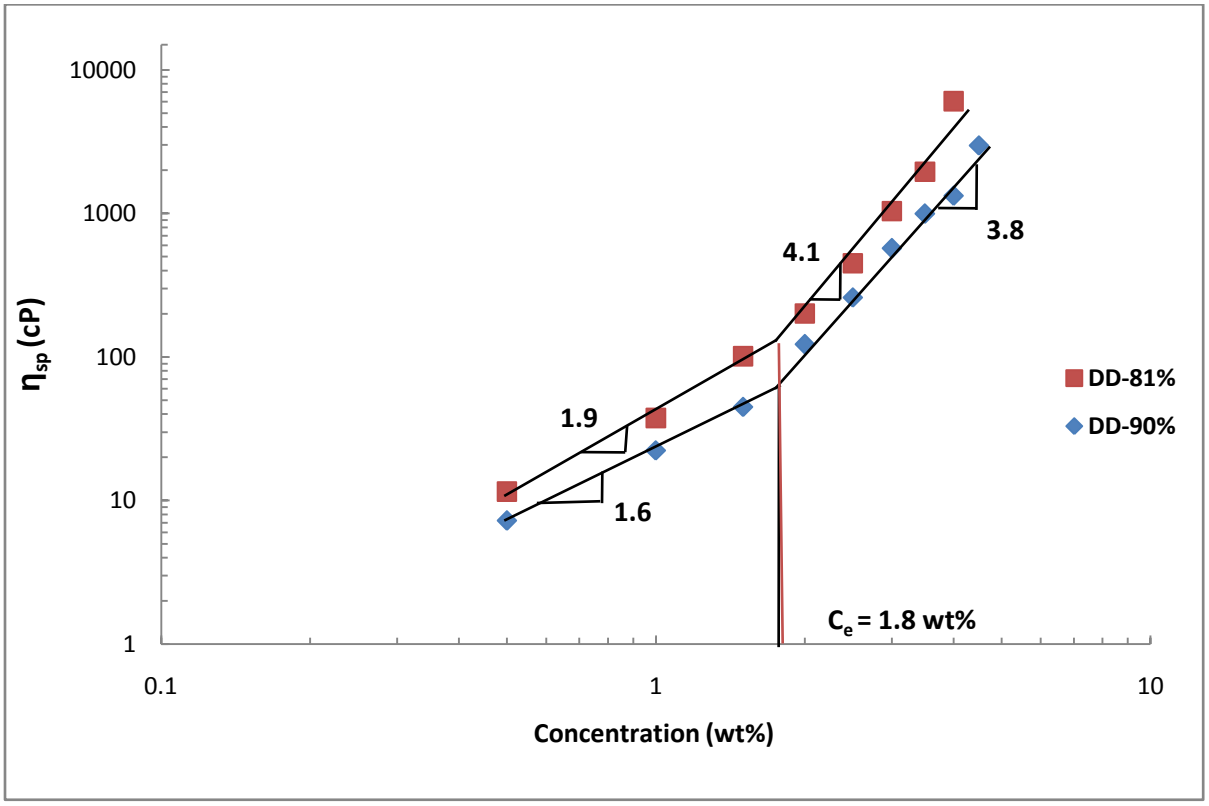

Figure 24 Plot of specific viscosity (η_{sp}) versus concentration for the chitosan of degrees of deacetylation (DD-81%) and (DD-90%) in 90% acetic acid as solvent. The entanglement concentration is 1.85 wt% and it is determined by the change in slopes

From the zero-shear rate viscosity, specific viscosity [$\eta_{sp}=(\eta_{\circ}-\eta_{s)/}\eta_s$] versus concentration of chitosan data was plotted for the samples DD-81% and DD-90% on a double logarithmic scale, where η_s is the solvent viscosity. From the plot, a crossover from the semidilute unentangled regime to the semidilute entangled regime can be observed as a change in slope. The entanglement concentration for both the samples was determined to be 1.8 wt% by the change in slopes. In the semidilute unentangled regime the specific viscosities with concentration were ($\eta_{sp} \sim c^{1.9}$) and ($\eta_{sp} \sim c^{1.6}$) for DD-81% and DD-90%, respectively. In semidilute entangled regime, the specific viscosities with concentration were found to be ($\eta_{sp} \sim c^{4.1}$) and ($\eta_{sp} \sim c^{3.8}$) for DD-81% and DD-90%, respectively. The concentration dependence in both the regimes for the DD-90% is in good agreement with the predicted relationship ($\eta_{sp} \sim c^{1.5}$) [113] and ($\eta_{sp} \sim c^{3.75}$) [113,115,118]. This scaling relationship is similar to that of neutral polymers [119] where the polymer chain adopts a flexible, coil-like conformation above C_e. This is also because of the decrease in molecular weight for DD-81 to DD-90 due to deacetylation process, which hydrolyses the polymer chain resulting in reduction of polymer chain length So, the coil occupies a smaller volume in solution than extended rod like chains. This ultimately increases the solubility of chitosan [113].

For DD-81%, both the slopes and zero-shear viscosities are higher than the DD-90%. This is because the DD-81% has a slightly higher molecular weight than DD-90%; and the low DD are less soluble than high DD; as they form associates and aggregates in acidic solution. In the Figure 24, the viscosities were much higher even at low concentration of chitosan

solution. This is caused by the above mention reason and due to the increased interaction of chitosan macromolecules leading to their entanglement [117]. The concentration dependence in both the regimes ($\eta_{sp} \sim c^{1.9}$) and ($\eta_{sp} \sim c^{4.1}$) for the DD-81% were found to be in good agreement ($\eta_{sp} \sim c^{2.0}$) [120] and ($\eta_{sp} \sim c^{4.1}$) with literature [114][120]. Cho *et al*. demonstrated that for chitosan with a molecular weight of 850,000 g/mol and a degree of deacetylation 93%, the η_{sp} scales with an exponent of 4.1 in the concentrated regime, which agrees with our result ($\eta_{sp} \sim c^{4.1}$). This is because of the higher number of interaction such as hydrogen bonding and hydrophobic interactions which causes associates formation in acidic solution [114].

4.2.1.1 Electrospinning of Chitosan in Acetic Acid with Different Degree of Deacetylation

In order to produce fibers from electrospinning process, the concentration should be 2-2.5 times its entanglement concentration (C_e). Then the minimum concentration for the DD-81% and DD-90% should be 3.7 wt% to 4.6 wt%. However, the resulting viscosities of these samples were very high. Table 14 provides the values of $\eta_\circ$ and η_{sp} of both the samples. For the DD-81%, the concentration above 4 wt% was difficult to dissolve. Solution above 3 wt% were attempted to electrospin, however the electric field was insufficient to overcome the combined effect of resulting viscosity (3.5 wt%= 5680 cP and 4 wt%= 17600 cP) and the surface tension of chitosan solution. At these concentrations ($2C_e$), the Taylor cone did not form. However, at 3 wt% (3020 cP) which is above C_e but less than 2 C_e, the Taylor cone

formed which resulted in fibers with some beads (see Figure 25). Below the C_e (i.e. $C < C_e$), Taylor cone formation take place which resulted in beads rather than fibers because there were no chain entanglements or topological constraints present in the solution and the Taylor cone cannot withhold the electric field and surface tension of the solution. This results in bursting of Taylor cone into fine droplets which gets deposited on the collector.

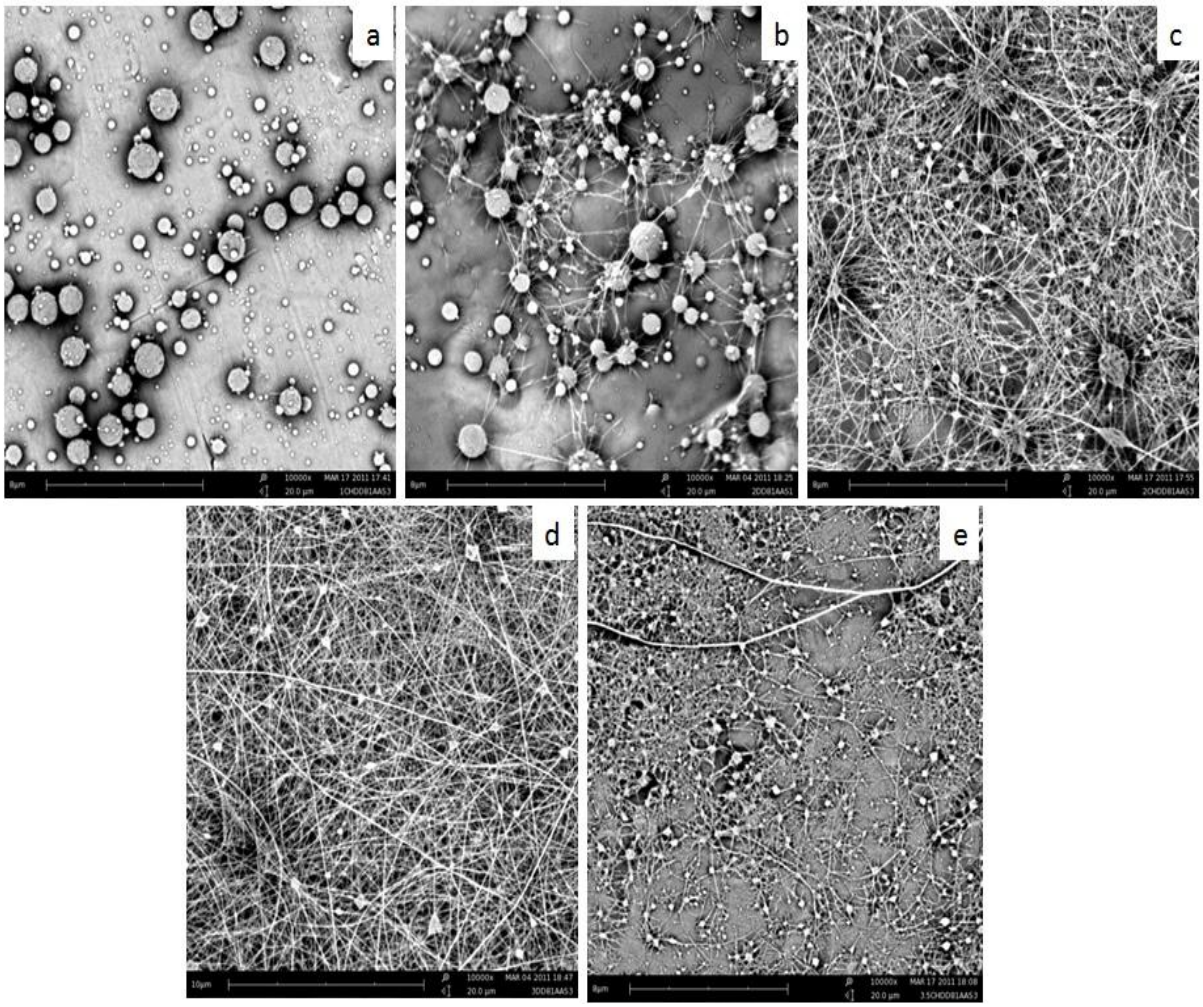

Figure 25 SEM images of electrospun chitosan (DD-81%) in 90% acetic acid/water produced at an electric field of 1 kV/cm with concentrations: (a) 1 wt%, (b) 2 wt%, (c) 2.5 wt%, (d) 3 wt% and (e) 3.5 wt%. (Magnification 10,000x)

Table 14 Zero-shear rate viscosity and specific viscosity for DD-81% and DD-90%

Concentration (wt%)	For DD-81%		For DD-90%	
	$\eta_{\circ}$(cP)	η_{sp}	$\eta_{\circ}$(cP)	η_{sp}
0.5	36.4	11.5517	23.9	7.24138
1	112	37.6207	67.7	22.3448
1.5	297	101.414	133	44.8621
2	586	201.069	358	122.448
2.5	1310	450.724	757	260.035
3	3020	1040.38	1660	571.414
3.5	5680	1957.62	2890	995.552
4	17600	6067.97	3860	1330.03
4.5	-	-	8660	2985.21

For the DD-90%, concentration above 4 wt% was difficult to electrospin, because of the high viscosity (4.5 wt%= 8600 cP) and surface tension of the chitosan solution, which results in unstable jet. However, at concentrations of 3 wt%, 3.5 wt% and 4 wt% which are the above C_e showed fiber formation with some beads (see Figure 26). Such concentrations result in the optimal viscosity for electrospinning and also for the degree of entanglements. The degree of entanglements is necessary for Taylor cone and jet formation. The strong acidic medium of

chitosan solution aligned the polymer chains in the electric field because of protonation (charged) of amine group, which promotes the entanglements of polymer chains [102].

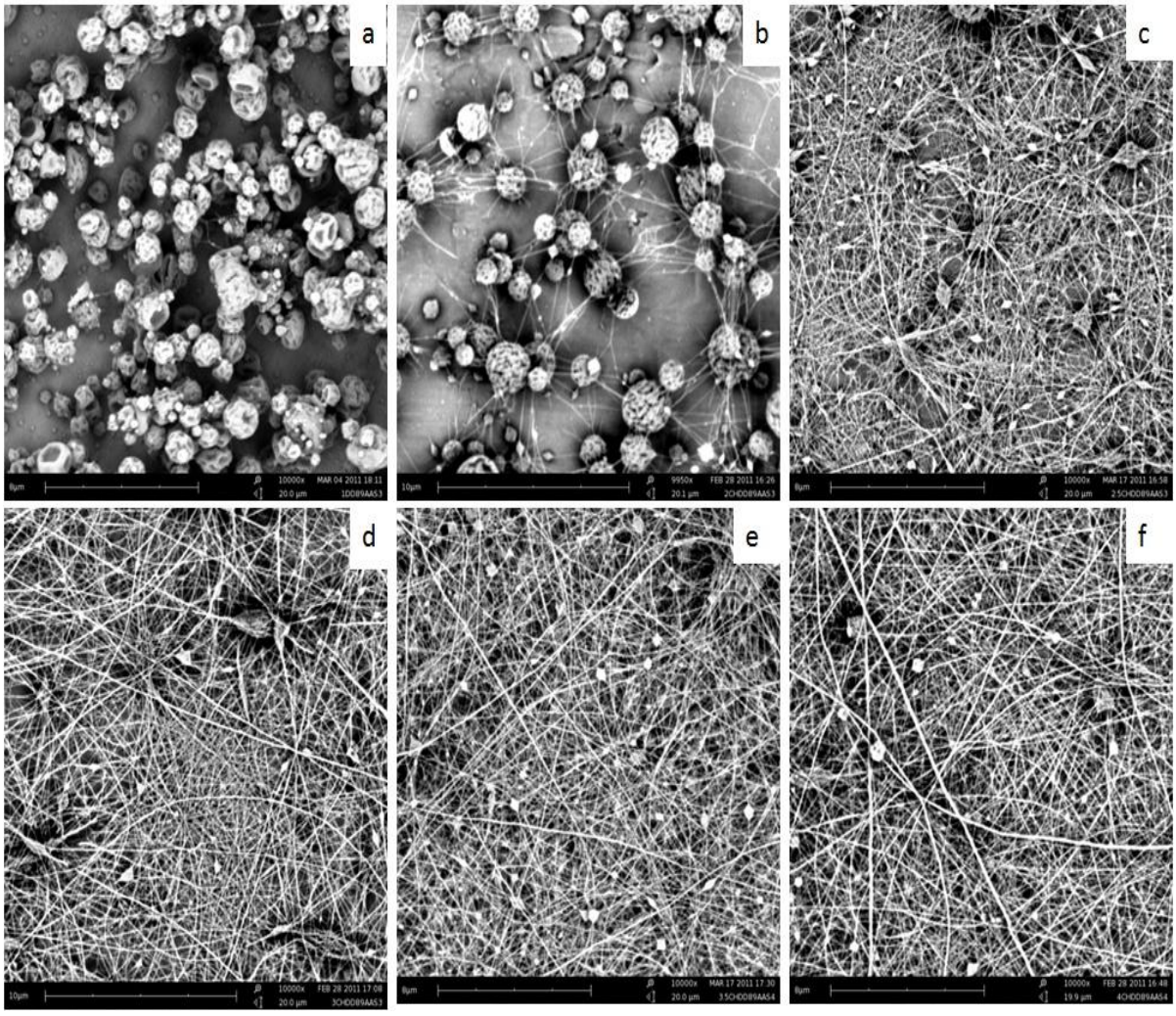

Figure 26 SEM images of electrospun chitosan (DD-90%) in 90% acetic acid/water produced at an electric field of 1 kV/cm with concentrations: (a) 1 wt%, (b) 2 wt%, (c) 2.5 wt%, and (d) 3 wt%, (e) 3.5 wt% and (f) 4 wt%. (Magnification 10,000x)

In contrast to our results, Geng *et al*. were able to electrospin the chitosan at 7 wt%; however their molecular weight (106,000 g/mol) and degree of deacetylation (54%) were lower than

our sample. Also at 5 wt%, the viscosity of their chitosan solution was 600 cP, where the viscosity of our sample at 4 wt% is 3860 cP (molecular weight 8.2×10^5 and degree of deacetylation 90%) [101]. Homayoni *et al*. used an alkali treatment which hydrolyzes the chitosan chain and reduces the molecular weight to produce chitosan nanofibers. The molecular weight (1,095,000 g/mol) and degree of deacetylation (75-85%) of their original sample is similar to our samples (M_v = 1.0×10^6, DD-81%; and M_v = 8.2×10^5, DD-90%) [103]. However, they were unable to electrospin the chitosan solution to produce nanofibers. Increasing the time of alkali treatment to 48 hours, they were able to decrease the molecular weight to 294,000 g/mol, but they didn't mention its degree of deacetylation value. The NaOH in alkali treatment deacetylated the chitosan and also depolymerizes it, which increased the amine groups on the chitosan backbone. This amine groups gets protonated under acidic medium which ultimately increases the hydrodynamic volume of polymer chain, thus compensating for the decrease in molecular weight. By lowering the molecular weight by 73%, they were able to electrospin chitosan from 5 wt% instead of 2.5 wt% [103]. Similar to our results, we were able to able to electrospin from 3 wt% (DD-81%, M_v=1.0×10^6) to 4 wt% (M_v=8.2×10^5, DD-90%) by the deacetylation process. So by increasing the degree of deacetylation and lowering the molecular weight, the deacetylation process increases the amine groups which in turn increase the positive charge on chitosan backbone under acidic conditions. Also, lowering molecular weight of chitosan increases the alignment of polymer chains in the electromagnetic field of electrospinning unit [103].

Further investigation was required to see the effect of concentration at different electric field on fiber diameter. As the fiber formation starts from 3 wt%, which was above the entanglement concentration, the chitosan solution of 3.5 wt% and 4 wt% was electrospun at 2 kV/cm to see the effect of concentration at higher electric field. Figure 27 shows the SEM images of electrospun chitosan mats and Figure 28 shows the effect of concentration on average fiber diameter. As the concentration of chitosan was increased, the average fiber diameter also increased. This may be due to the increase in solution viscosity as concentration increased which lead to resistance to stretching of jet during whipping action, producing thicker fibers [47]. From the Figure 27, we can observe that at lower concentration (a) and (b), more beads were formed with smaller diameter fibers as compared to higher concentration (c), which was more than $2C_e$. The fibers with more beads may be due to the insufficient chain entanglement in the polymer solution, while at higher concentration, the chain entanglement favors the formation of larger diameter fibers with some beads [77,101]. The average fiber diameter and their distribution are shown in Figure 29. The fiber diameter distribution becomes large as the concentration of chitosan increased from 3 wt% to 4 wt%, indicating the formation of both thicker and thinner fibers. This may be due to the resistance to stretching of Taylor cone at the tip of needle which results in splaying of jet.

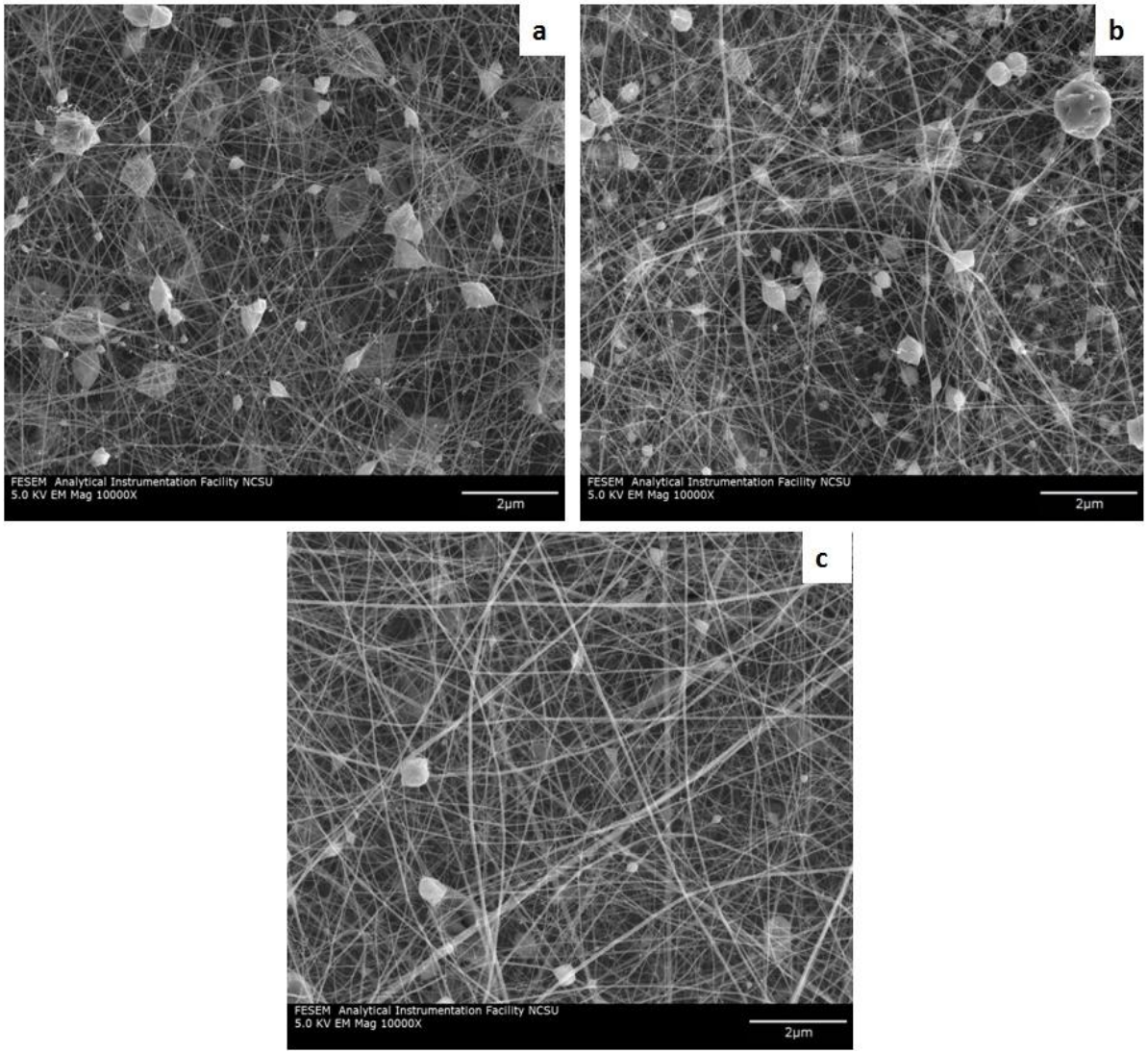

Figure 27 SEM images of electrospun chitosan (DD-90%) in 90% acetic acid/water as solvent produced at an electric field of 2 kV/cm with concentrations: (a) 3 wt%, (b) 3.5 wt%, and (c) 4 wt%

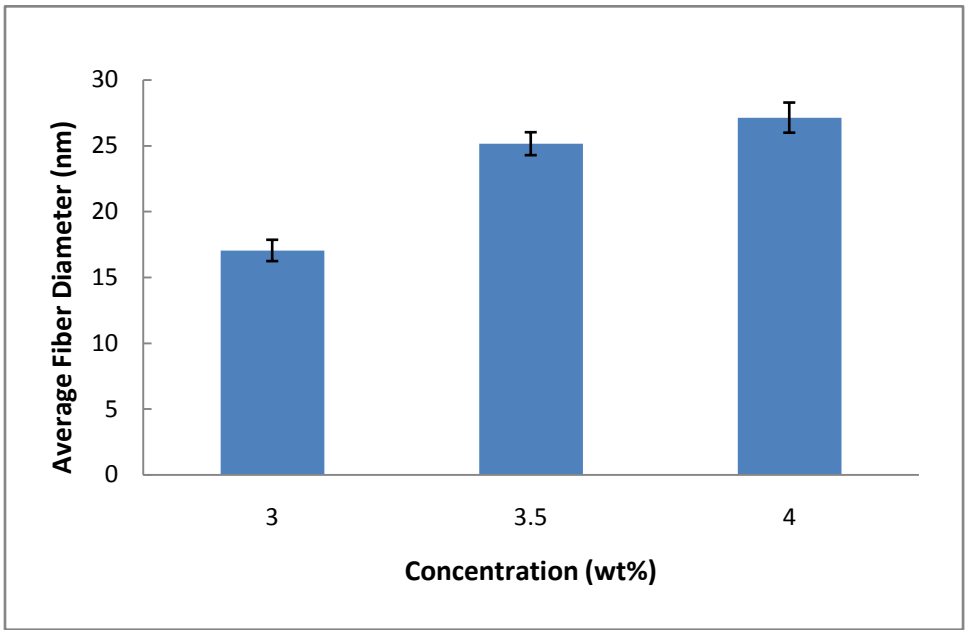

Figure 28 Effect of chitosan concentration on average fiber diameter. (DD-90%, electric field-2 kV/cm)

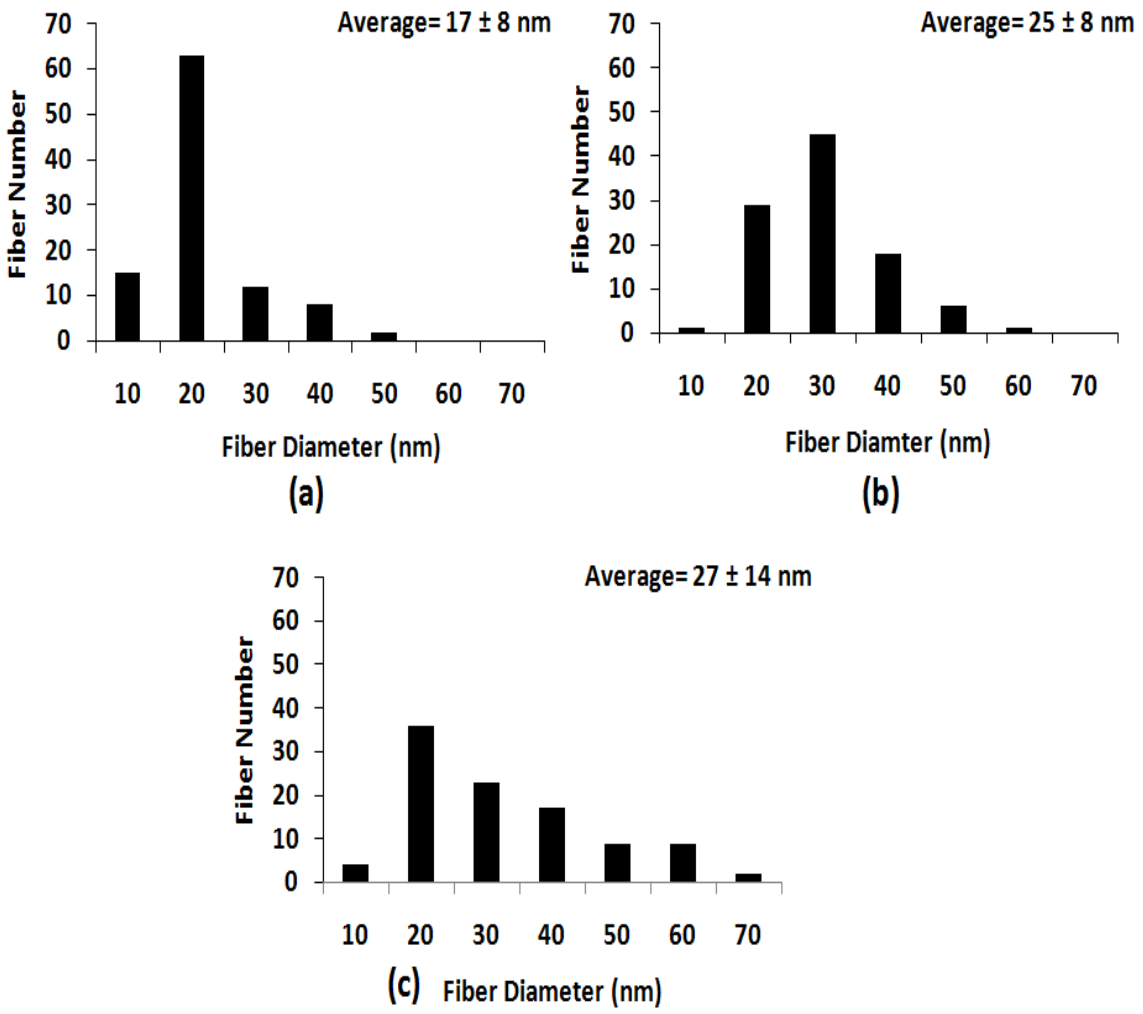

Figure 29 Fiber diameter distribution of electropsun chitosan (DD-90%) in 90% acetic acid/water as solvent produced with different concentrations: (a) 3 wt%, (b) 3.5 wt%, and (c) 4 wt%

4.2.1.2 Effect of Electric Field on Fiber Formation

The electrospinning of chitosan solution is challenging due its low solubility in most of the organic solvents. In acidic condition, their amine group gets protonated and becomes a polyacationic in nature which contributes to its high solution viscosity even below its entanglement concentration. Therefore, control and optimization of the process parameters

such as feed rate, applied voltage and tip to collector distance is needed for successful electrospinning.

The electrospinning process gets initiated and when the electrostatic force overcomes the combined effect of solution viscosity and surface tension, a fine continuous jet emerges out from the Taylor cone producing nanofibers. The viscosities of our chitosan solutions were high as compared to neutral polymers at same concentration. Therefore, higher viscosity solution required a higher voltage. A strong electric field is necessary to accelerate the jet and also to stretch it. The electric field can aligned the polymers chains which helps in jet stretching due to which larger amount of polymer solution was drawn out. But at higher electric field, more stretching of polymer solution occurs which result in instability of jet and affecting the fiber morphology producing fibers with more beads [103].

In this section, a concentration of 3 wt%, feed rate of 10 μL/min and different electric fields (varied from 1 to 2 kV/cm) for two chitosan samples was used for electrospinning. A complete design of experiments for different tip to collector distance and voltages is shown in Table 15. Below 1 kV/cm, the electric field was insufficient to overcome the viscous nature of chitosan solution. When the electric field was high enough to overcome the viscosity and surface tension of solution (in the range of 1-2 kV/cm), fibers with some beads were formed. At 2 kV/cm, mostly thinner fibers were produced with an increase in bead number also. This may be due to the uneven charged distribution and uneven elongation of jet causing instability [103]. From the Figures 30 and 31, as the electric field increased from

1 to 1.5 kV/cm, the fiber diameter also increased for DD-81%. Similar results have also been found in another article [122,123]. This was probably due to the higher viscosity of polymer solution and more polymer ejection causing less stretching and elongation of jet resulting in higher fiber diameter [122,123]. However, at 2 kV/cm (10 cm and 20 kV), the voltage was too high to stretch the polymer jets causing instability which resulted in more beaded structure with small diameter fibers [77,123]. For the DD-90%, as the electric field increased, the average fiber diameter decreased, except for the electric field 1.33 kV/cm (tip to collector distance 15 cm and applied voltage 20 kV). The decrease in fiber diameter was due to the increase in electrostatic repulsive force on the fluid jet and also due to the greater stretching of the solution which leads to rapid evaporation of solvent from the fiber [47]. The increase in fiber diameter at 1.33 kV/cm was due to rapid discharge of solution from the needle as jet was ejected from the Taylor cone and the reduce flight time for the evaporation of solvent [122,123].

Table 15 Set of experiments for the electrospinning of chitosan with different electric field and their resulting average fiber diameters

Concentration (wt%)	**Applied Voltage (kV)**	**Needle tip to Collector Distance (cm)**	**Electric Field (kV/cm)**	**Average Fiber Diameter (nm) (DD-81%)**	**Average Fiber Diameter (nm) (DD-90%)**
3	15	15	1	20 ± 8	29 ± 15
	20	15	1.33	21 ± 9	23 ± 11
	15	10	1.5	25 ± 8	26 ± 8
	20	10	2	18 ± 8	17 ± 8

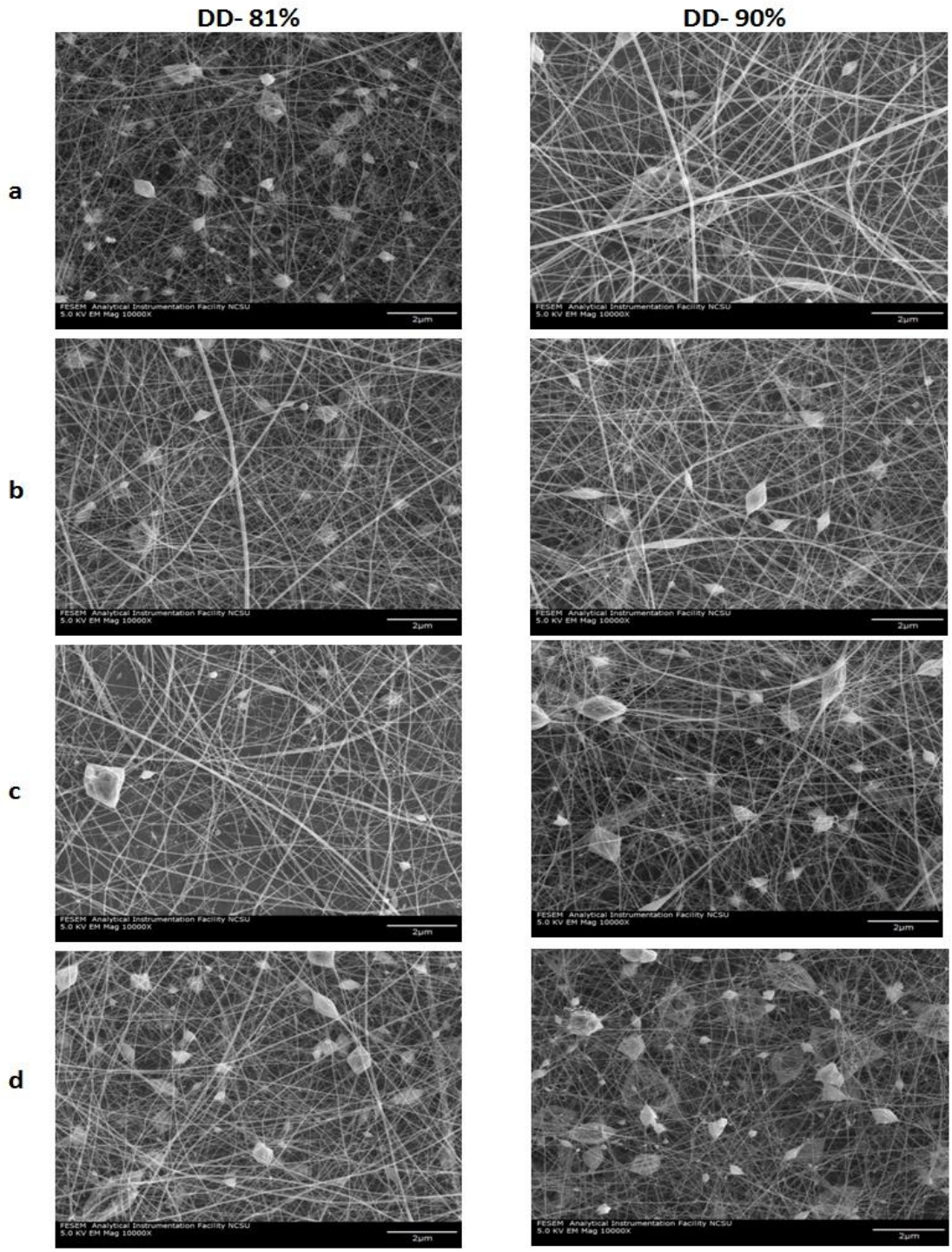

Figure 30 SEM images of electrospun chitosan of 3 wt% with the DD-81% and DD-90% produced at different electric field – kV/cm (a) 1 (b) 1.33 (c) 1.5 and (d) 2 (Magnification-10,000x)

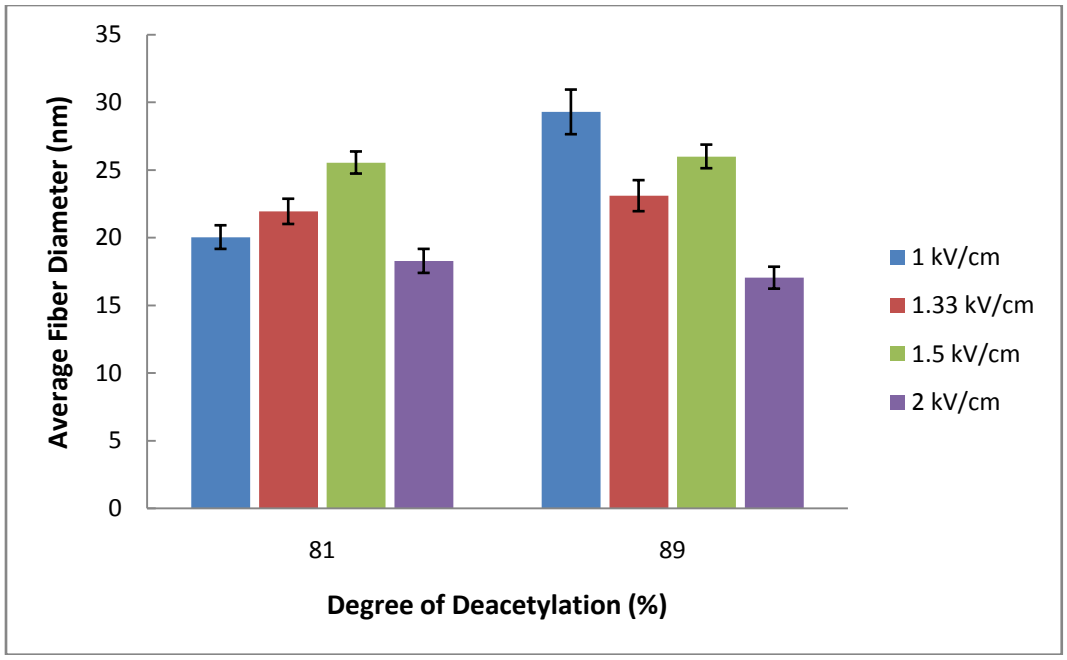

Figure 31 Effect of electric field and degree of deacetylation on average fiber diameter of chitosan electrospun at 3 wt% in 90% acetic acid/water as solvent

4.2.1.3 Effect of Degree of Deacetylation on Average Fiber Diameter

Form the Table 15 and Figure 31, the average fiber diameter increased with an increase in degree of deacetylation at low applied voltage. At 1 and 1.33 kV/cm, the average fiber diameter for DD-81% was found to be 20 ± 8 nm and 21 ± 9 nm, respectively. However, for DD-90%, it was found to be 29 ± 15 nm and 23 ± 11 nm. And at 1 kV/cm, the electrospun mat of DD-81% showed more beads and less uniform fibers as compared to DD-90%. This increase in fiber diameter with the degree of deacetylation was due to the deacetylation of chitosan, which increases the solubility of chitosan by the reduction in molecular weight to some extent and mostly due to increase in degree of deacetylation. The deacetylation process hydrolyses the polymer chains and when chitosan chain dissolved in acidic medium, it

became a polyelectrolyte. If the chitosan has high degree of deacetylation, then the chitosan will have more -NH_2 group on the polymer backbone Due to this, the chitosan becomes a charged polyelectrolyte under acidic medium and its linear chain gets extended by the electrostatic repulsion between the charges. Also the charge density along the chitosan backbone increases with an increase in degree of deacetylation [103,124]. This helps the polymer chains to align more effectively in the presence of electromagnetic field during electrospinning. Similar results have been obtained with the chitosan/PEO and chitosan/PVA blends in which increasing the degree of deacetylation leads to more uniform nanofibers with increased fiber diameter [97,99]. However, the effect of degree of deacetylation at high electric field is not significant as compared to lower electric field because is a very complex interplay of solution conductivity, applied voltage and net charge density. Figure 32 shows the fiber diameter distribution graphs for different degree of deacetylation and electric field for a concentration of 3 wt%.

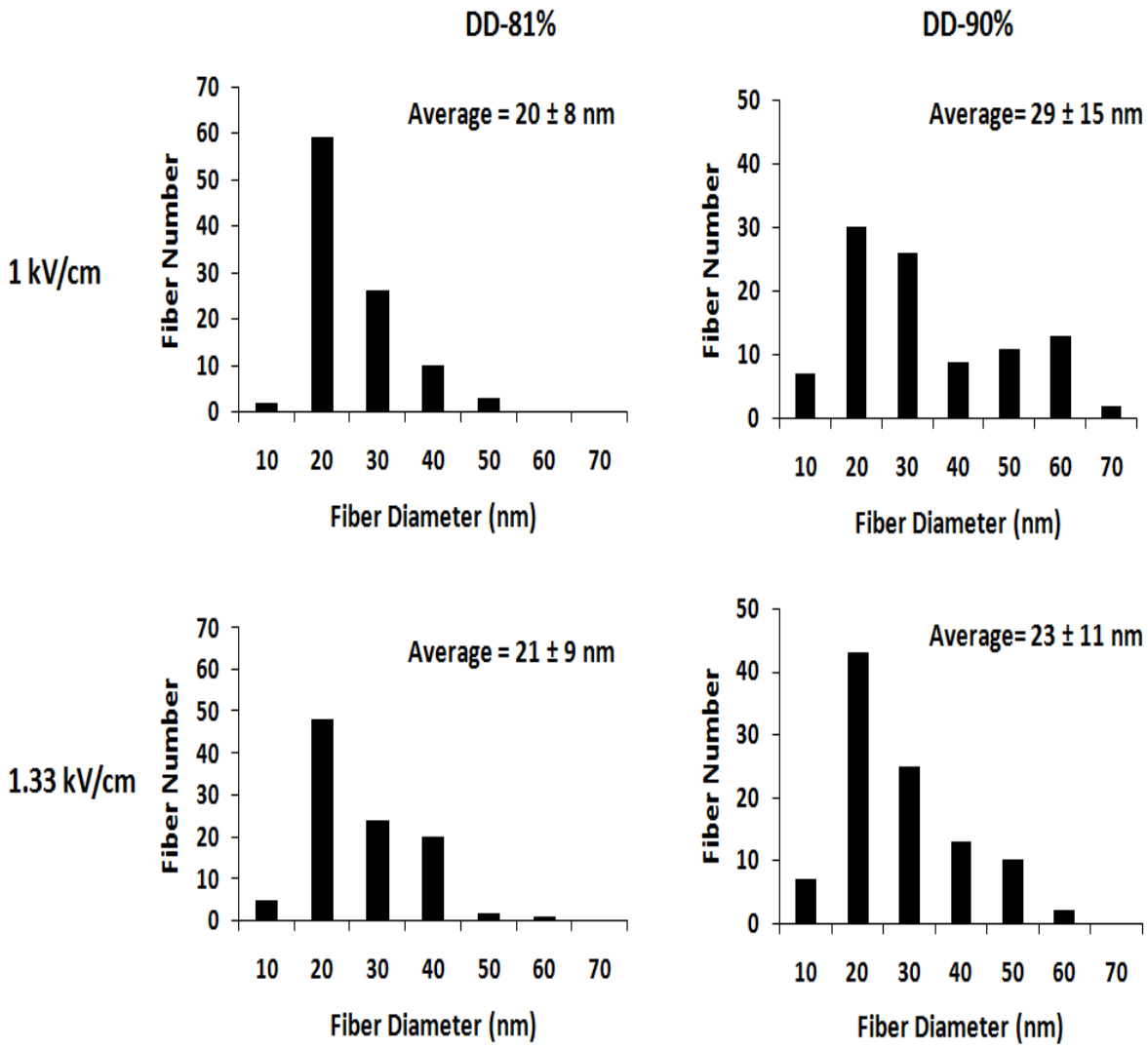

Figure 32 Fiber diameter distribution of electropsun chitosan at concentration of 3 wt% in 90% acetic acid/water as solvent with different degree of deacetylation and electric field

4.2.2 Electrospinning of Chitosan with TFA (Initial Trails)

Trifluoroacetic acid (TFA) is another solvent system used to study the effect of degree of deacetylation on electrospinning process. Successful electrospinning of chitosan with TFA has already been done by many researchers [104,105,125-127]. Ohkawa, *et al*.. used

TFA/dichloromethane (70/30) to electrospin chitosan having a viscosity average molecular weight of 210,000 g/mol and degree of deacetylation 78% at 8 wt%. The mean diameter of fibers was found to be 330nm [104]. In a later article of Ohkawa, *et al.* they used four different kind of commercial chitosan with a viscosity average molecular weight ranging from 210,000 – 1,80,0000 g/mol. They have studied the effect of molecular weight and the concentration depending upon the molecular weight (means lower concentration of chitosan was used for high molecular weight chitosan for electrospinning). They have found out that the fiber diameter decreased with decrease in concentration and increased molecular weight [105]. However, Schiffman, *et al.* had some contradictory results. They have used four types of chitosan of same concentration (2.7% w/v) and degrees of deacetylation with different molecular weights, namely, low (70 kDa), medium (190-310 kDa), and high (500 kDa) molecular weight, as well as a commercial chitosan (190-375 kDa) for electrospinning. They have found out that the average fiber diameter increased with the increase in molecular weight except for the practical grade chitosan which showed smaller average diameter though its molecular weight was similar to the medium molecular weight chitosan [125].

In the above mention articles, all focus was on the molecular weight and concentration of chitosan. None of the articles discussed the effect the degree of deacetylation on electrospinning, which is the most important property of chitosan as mention in the above literature review. To study the effect of degree of deacetylation, chitosan (DD-70, Vanson) sample having a viscosity average molecular weight of 1.0×10^6 and degree of deacetylation

(DD-70%) was used, it was deacetylated by alkaline treatment to produce chitosan of (DD-81%, $M_v = 1.0 \times 10^6$ and DD-90%, $M_v = 8.2 \times 10^5$).

Initial trails were carried out to find out the upper and lower limits of chitosan concentration in TFA for successful electrospinning. The rheological studies of chitosan solution with TFA were not recommended due to environmental concerns. For electrospinning, the upper limit of chitosan concentration 8 wt% in TFA was carried out. Due to very viscous nature of chitosan solution at this concentration, the solution was not extruded from the needle even at very high feed rate preventing the electrospinning process. So, a set of experiments was carried out through a concentration range of 1-7 wt% (DD-70%) to evaluate the electrospinnability and fiber formation. Different experiments were also carried out to see the effect of electric field and degree of deacetylation. To find out the lower limit of chitosan concentration for electrospinning, different solutions were prepared with the range of concentration of 1-3 wt%. Electrospinning trials were conducted from these solutions with different electric field. Table 16 shows the details of the parameters that were used to carried out the initial trials and Figure 33 shows the corresponding SEM images.

Table 16 Set of experiments for the electrospinning of chitosan (DD-70%) with different concentration and electric field

Concentration (wt%)	**Applied Voltage (kV)**	**Tip to collector distance (cm)**	**Electric field (kV/cm)**
1,2,3	15	10	1.5
	20	10	2
	15	15	1
	20	15	1.33

At very low polymer concentration (1 wt% and 2 wt%), only beads and discontinuous films were formed (see Figure 33). This was because the solution did not contain sufficient chain entanglement for fiber formation [113]. When the polymer concentration was increased to 3 wt%, drastic morphological changes were observed. With the increase in polymer concentration, morphology seemed to change from beads to mixture of fibers and beads. This was because the polymer chains were overlapping and the concentration was above the entanglement concentration (C_e). The entanglements or the topological constraints present in the solution helps in the Taylor cone formation. A jet from Taylor cone emerges on the application of electric field, which stretches the jet due to electrostatic repulsion and formed a smooth fiber more likely due to the stronger whipping instability of the jet.

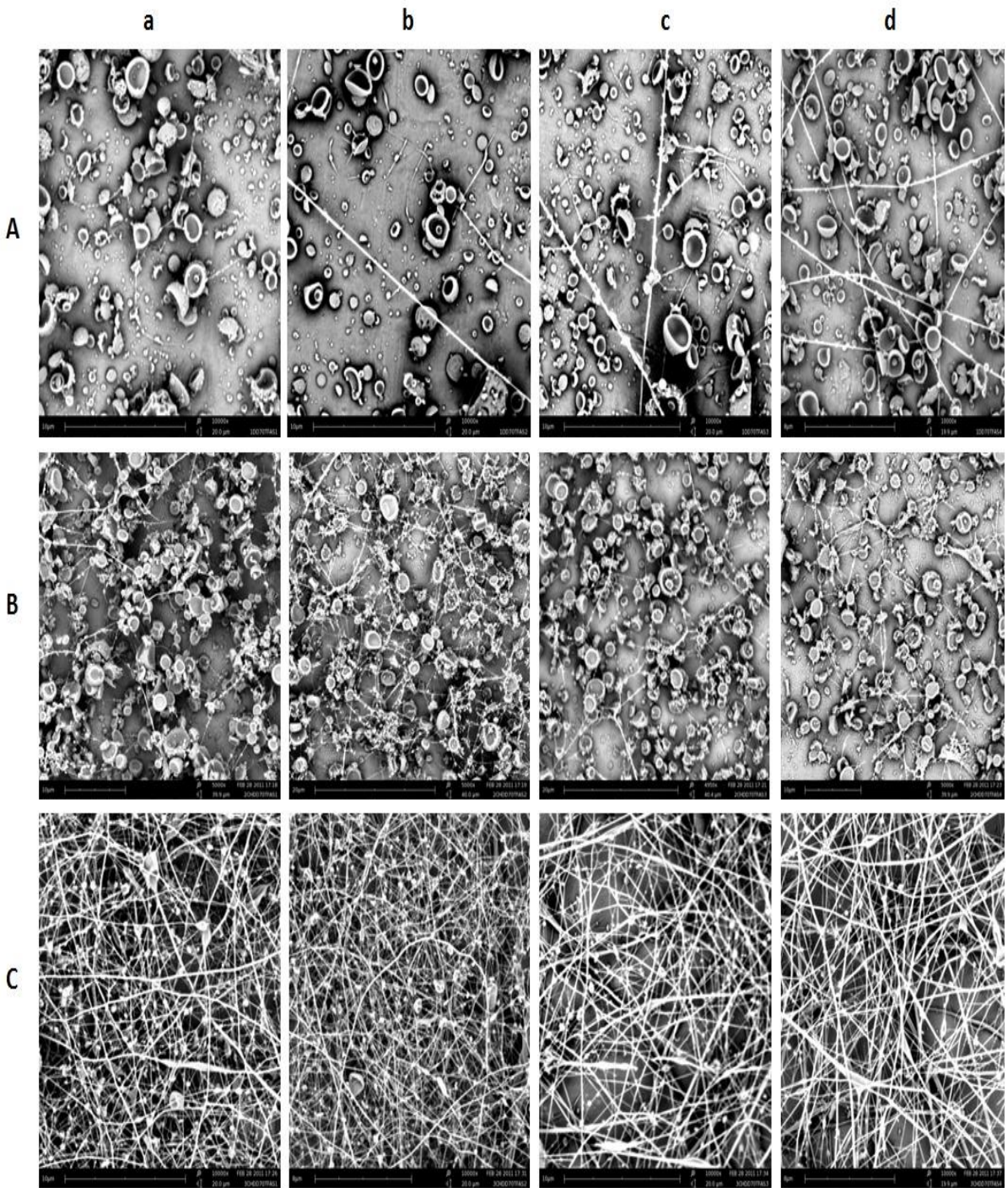

Figure 33 SEM images of electrospun chitosan/TFA solutions having DD-70% with different concentrations. (A) 1 wt%, (B) 2 wt%, (C) 3 wt% and with different electric field (a) 1.5 kV/cm,(b) 2 kV/cm,(c) 1 kV/cm and (d) 1.33 kV/cm. (Magnification-10,000x)

4.2.2.1. Effect of Concentration on Fiber Diameter Produced with Chitosan-TFA Solution of Different Degree of Deacetylation

As the 3 wt% solution yielded fibers with some beads, solutions with higher concentrations were attempted to electrospin with different degrees of deacetylation. A series of polymer solutions were made in the concentration range of 4-7 wt% for the DD-70%, DD-81%, and DD-90%. These polymer solutions were electrospun at a constant electric field of 1.33 kV/cm (tip-to-collector distance = 15 cm and applied voltage = 20 kV) and a feed rate of 10 μL/min. Figure 34 shows the SEM images of electrospun chitosan in TFA with different concentration and degrees of deacetylation. As the polymer concentration increased, the average fiber diameter also increased. This was a result of increased solution viscosity and resistance to jet stretching during the whipping motion, which resulted in increased fiber diameter. Also, as the polymer concentration increased from 6 wt% to 7 wt%, solution viscosity and the chain entanglement increased, which favors the formation of smooth fibers without beads. Table 17 shows the average fiber diameter of electrospun fibers produced at an electric field of 1.33 kV/cm and a feed rate of 10 μL/min with different degree of deacetylation.

Table 17 Average fiber diameter of electrospun chitosan fibers with different concentration and degree of deacetylation at 1.33 kV/cm

Concentration (wt%)	**Average Fiber Diameter (nm) (DD-70%)**	**Average Fiber Diameter (nm) (DD-81%)**	**Average Fiber Diameter (nm) (DD-90%)**
4	79 ± 3	87 ± 3	121 ± 3
5	83 ± 2	92 ± 3	128 ± 4
6	126 ± 5	128 ± 4	136 ± 5
7	128 ± 5	401 ± 7	290 ± 8

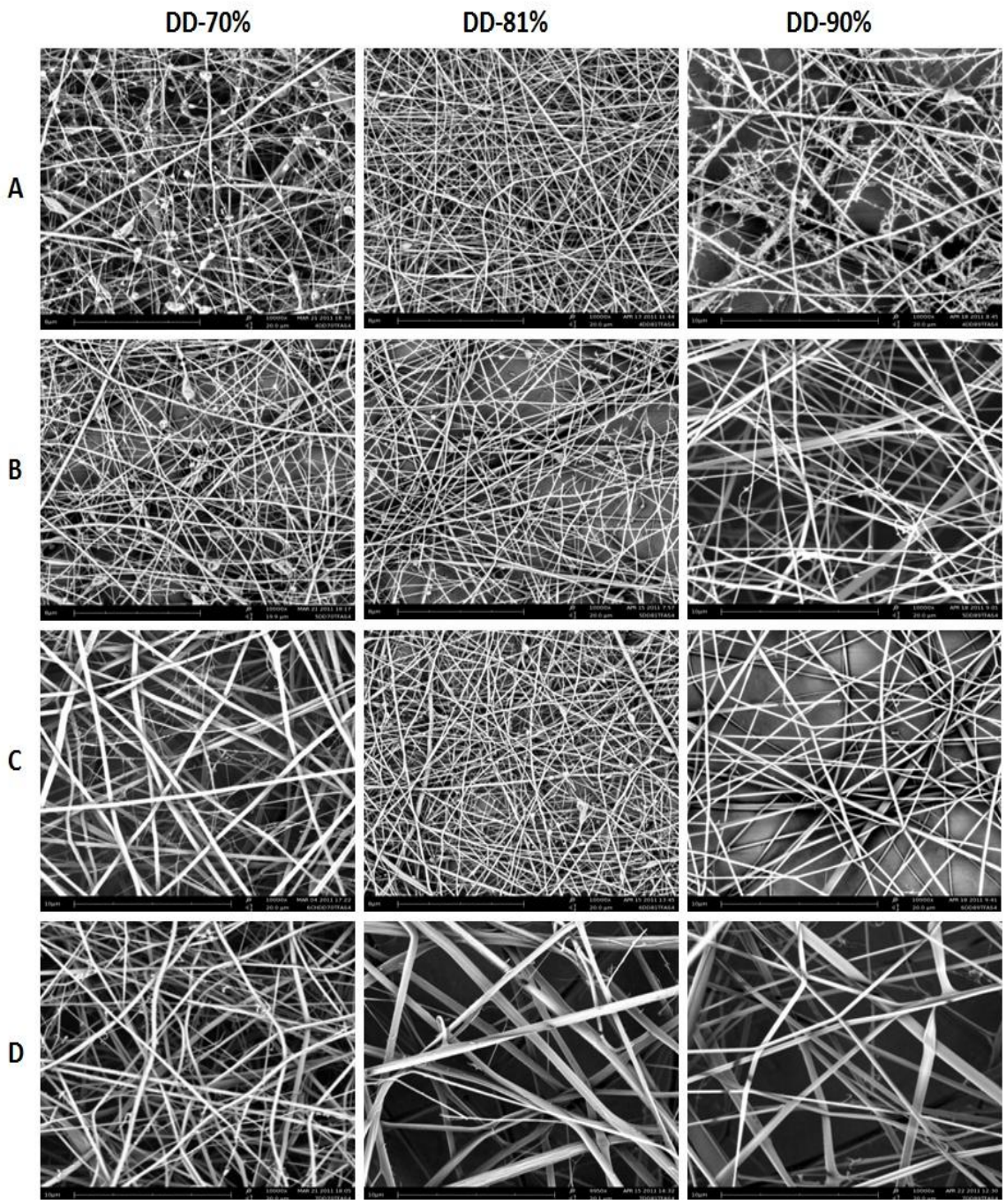

Figure 34 SEM images of electrospun chitosan in TFA with different degree of deacetylation (DD-70%), (DD-81%) and (DD-90%) at a constant electric field of 1.33 kV/cm produced with different concentrations: (A) 4 wt%, (B) 5 wt%, (C) 6 wt% and (D) 7 wt% (Magnification-10,000x)

As mentioned by the Ohkawa *et al*., the successful electrospinning of chitosan with TFA was possible because the TFA forms salts with the amino groups of chitosan and this salt formation destroys the rigid interchain between the chitosan molecules which can be easily electrospun. During the salt formation, protonation of the amino ($-NH_2$) groups along the chitosan chain occurs and these protonated amine ($-NH_3^+$) groups interact with trifluroacetate anions ionically [104,127,128]. The high volatility of TFA was also advantageous for the rapid evaporation of solvent during whipping of jet.

4.2.2.2 Effect of Electric Field on Fiber Diameter Produced with Chitosan-TFA Solution of Different Degree of Deacetylation

The electric field (controlled by the applied voltage) is one of the most important parameters that govern the fiber formation in electrospinning. The fiber diameter of the chitosan nanofibers can be controlled by applying the optimum voltage and tip to collector distance. The average fiber diameter can be reduced without the formation of beads by applying proper electric field. Typically at low electrical field, the solution at the tip of needle will drop under the influence of gravitational field; however, as the applied electric field increases, the volume at the tip of needle decreases until the Taylor cone forms. An optimal range of electric field for the fiber formation exists because too weak or too high electric field increases the chances of beaded fibers.

In this section, polymer solutions of chitosan-TFA with increasing concentration (4 wt%-7 wt%) were made with different degrees of deacetylation. All the solutions were electrospun

with different electric field (1-2 kV/cm). Constant feed rate of 10 µL/min was used for the all the polymer solutions. A complete design of experiments with different applied voltage and tip-to-collector distance is shown in Table 18 with the resulting average fiber diameter. Figure 35 shows the SEM images of the electrospun chitosan (7 wt%) with different electric field and degree of deacetylation.

Below 1 kV/cm, the electric field was insufficient to overcome the viscous nature and surface tension of polymer solution. From the Figures 36 to 38, as the electric field increased, the average fiber diameter decreased, except at an electric of 1.33 kV/cm (20 kV/15 cm) for DD-81% and DD-90%. The decrease in fiber diameter with respect to increase in electric field was due to the increase in the electrostatic repulsion force on the fluid jet and also due to the greater stretching of the solution which lead to rapid evaporation of the solvent from the fiber [47].The increase in fiber diameter at 1.33 kV/cm (applied voltage 20 kV and tip to collector 15 cm) for DD-81% (401 ± 7 nm) and DD-90% (290 ± 8 nm), was due to the increased mass flow rate relative to the increase in the electrostatic force. The higher flow of polymer solution causes less stretching and elongation of jet resulting in increased fiber diameter [122,123]. Also the SEM images include some small fibrous web with the nanofibers which we excluded from measurement because of splaying of nanofibers. The SEM images includes flat and fused fibers instead of round ones, which might be the reason in increased fiber diameter. The average fiber diameter for 7 wt% (DD-70%) at an electric field of 1, 1.33, 1.5, and 2 kV/cm was found to be 138, 128, 121 and 94 nm, respectively. The fiber diameter distribution of these chitosan nanofibers is shown in Figure 39. The ranges of diameter

distribution become narrower at higher electric field (2 kV/cm). This result indicates that even at high polymer concentration, chitosan can be successfully electrospin into thinner fibers.

Table 18 Mean fiber diameter of electrospun chitosan in TFA with different electric field, concentration and DD

Concentration (wt%)	Applied Voltage (kV)	Needle tip to Collector Distance (cm)	Electric Field (kV/cm)	Average Fiber Diameter (nm) (DD-70%)	Average Fiber Diameter (nm) (DD-81%)	Average Fiber Diameter (nm) (DD-90%)	Standard Error (nm) (DD-70%)	Standard Error (nm) (DD-81%)	Standard Error (nm) (DD-90%)
4	15	15	1	90 ± 3	95 ± 3	162 ± 4	3.3	3.59	4.51
	20	15	1.33	79 ± 3	87 ± 3	121 ± 3	3.39	3.34	3.26
	15	10	1.5	80 ± 3	84 ± 3	120 ± 5	3.29	3.51	4.74
	20	10	2	73 ± 2	75 ± 2	83 ± 2	2.19	2.57	2.55
5	15	15	1	106 ± 3	110 ± 4	169 ± 6	3.15	3.64	5.68
	20	15	1.33	83 ± 2	92 ± 3	128 ± 4	2.49	3.15	4.24
	15	10	1.5	83 ± 3	90 ± 4	119 ± 4	2.81	4.19	3.69
	20	10	2	59 ± 2	78 ± 4	87 ± 3	1.38	3.73	3.08
6	15	15	1	140 ± 5	146 ± 5	175 ± 7	4.65	5.52	7.11
	20	15	1.33	126 ± 5	128 ± 4	136 ± 5	4.82	4.44	4.63
	15	10	1.5	120 ± 6	125 ± 4	130 ± 5	5.55	4.27	5.3
	20	10	2	78 ± 2	84 ± 3	100 ± 5	2.33	3.15	4.68
7	15	15	1	137 ± 7	237 ± 6	272 ± 8	7.2	5.62	8.33
	20	15	1.33	128 ± 5	401 ± 7	290 ± 8	5.37	6.79	8.12
	15	10	1.5	121 ± 7	224 ± 8	245 ± 9	6.79	7.56	8.87
	20	10	2	93 ± 5	188 ± 8	202 ± 7	5.05	7.65	7.15

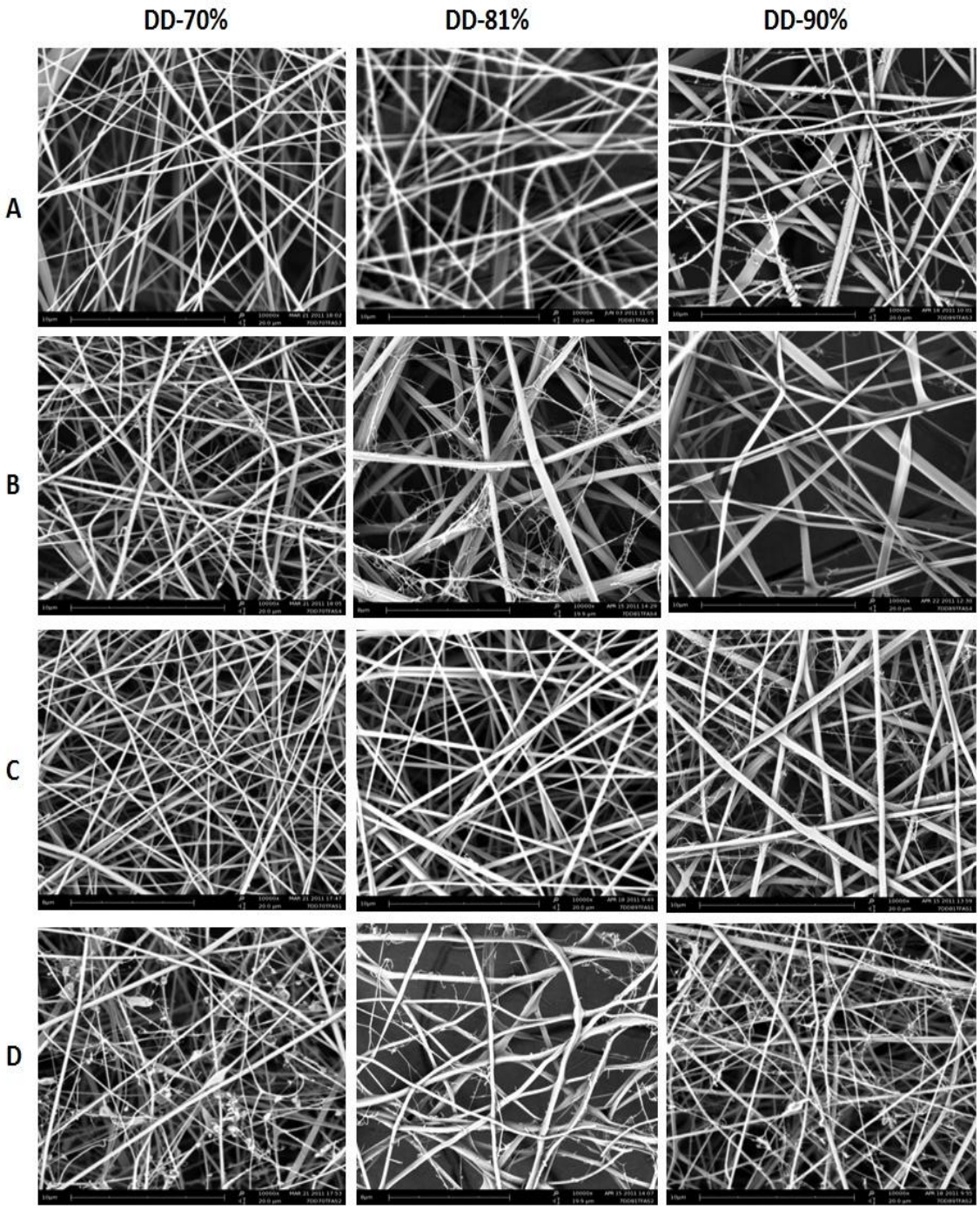

Figure 35 SEM images of electrospun chitosan in TFA with different degrees of deacetylation (DD-70%), (DD-81%) and (DD-90%) at a concentration of 7 wt% with different electric field: (A) 1 kV/cm (B) 1.33 kV/cm, (C) 1.5 kV/cm and (D) 2 kV/cm (Magnification-10,000x)

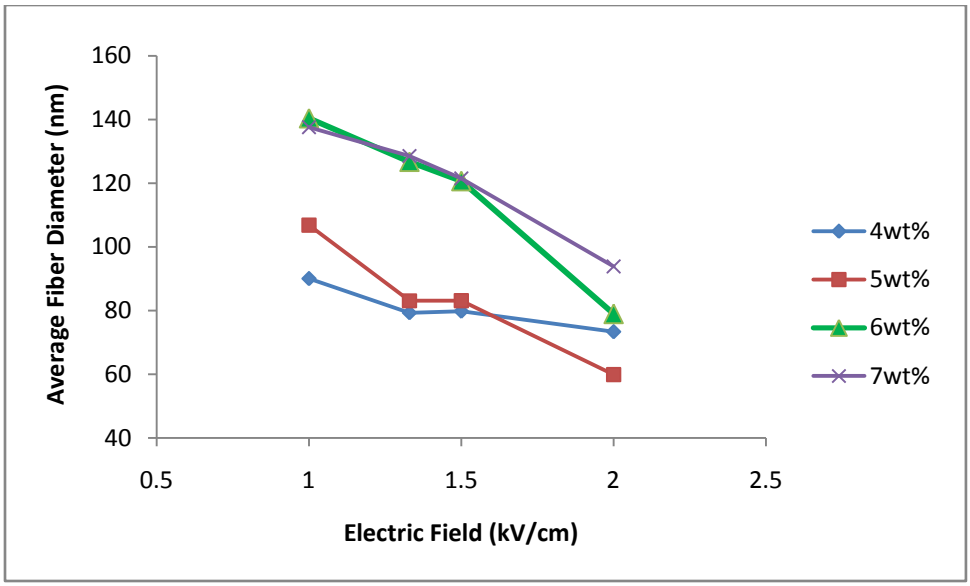

Figure 36 Effect of electric field on average fiber diameter of chitosan (DD-70%) electrospun in TFA with different concentrations

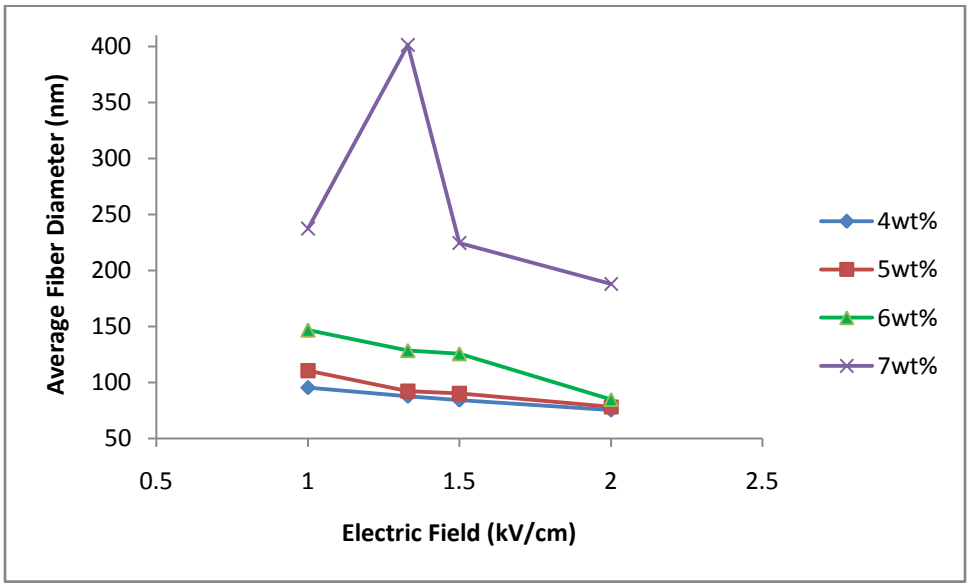

Figure 37 Effect of electric field on average fiber diameter of chitosan (DD-81%) electrospun in TFA with different concentrations

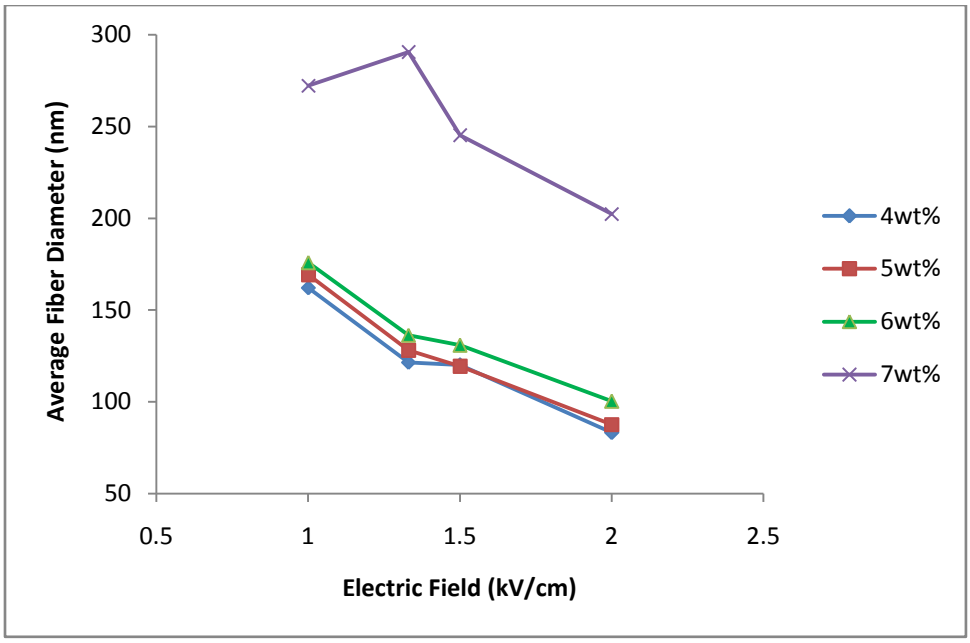

Figure 38 Effect of electric field on average fiber diameter of chitosan (DD-90%) electrospun in TFA with different concentrations

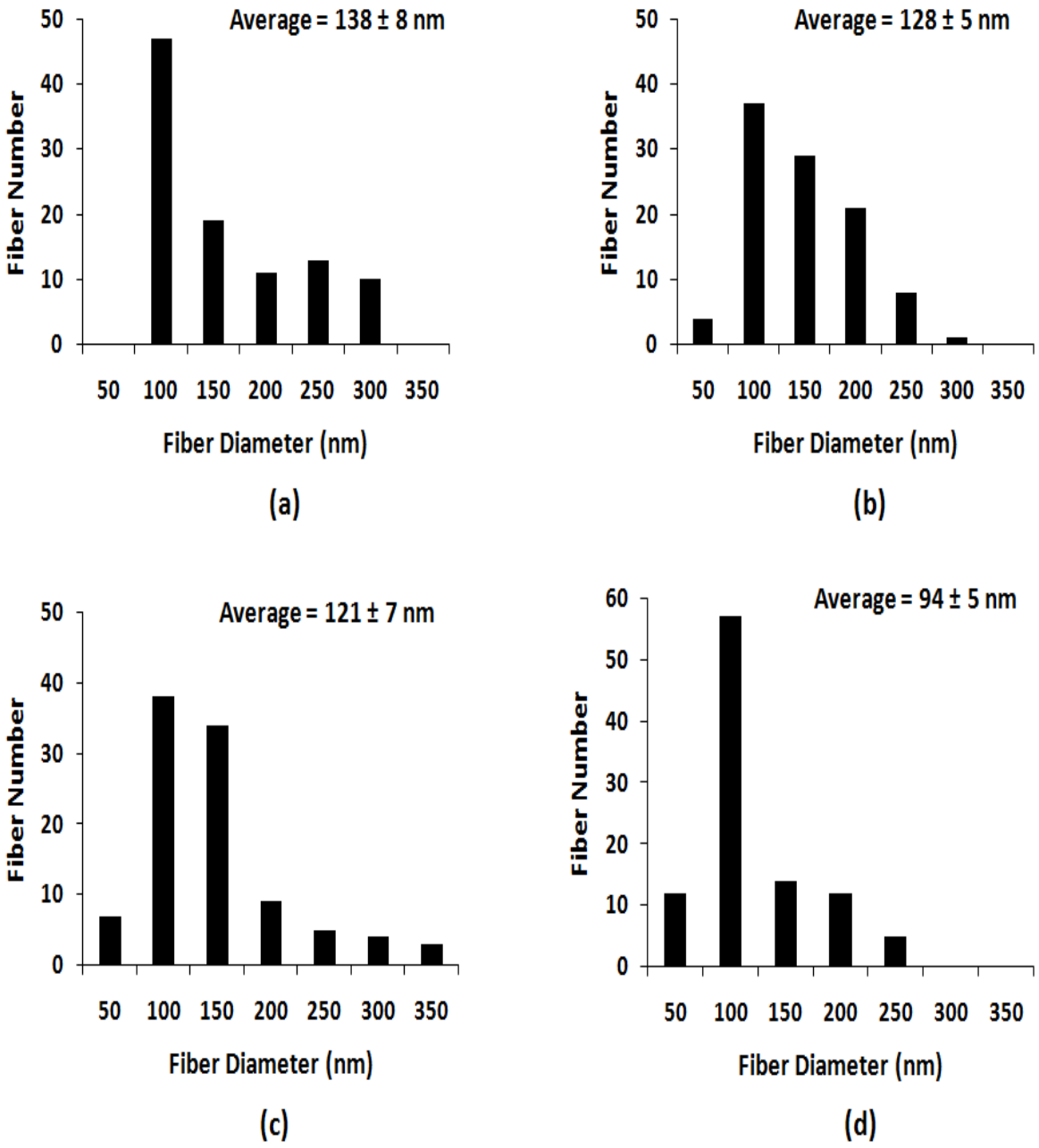

Figure 39 Fiber diameter distribution of electropsun chitosan (DD-70%) at concentration of 7 wt% in TFA with different electric fields – kV/cm: (a) 1, (b) 1.33, (c) 1.5, and (d) 2

4.2.2.3 Effect of Degree of Deacetylation on Fiber Diameter Produced with Chitosan-TFA Solution of Different Concentration and Electric Field

Chitosan when deacetylated to certain degree, it becomes soluble in acidic medium if the pH of the solution is less than 6.5. The protonation of the amine ($-NH_2$) group along the chitosan backbone happens and because of this the polymer becomes a polyelectrolyte. Since, the deacetylated amine groups can gains or lose protons, the charge density on the chitosan backbone depends upon the degree of deacetylation to the ratio of the two monomers in the chain. Therefore, if the chitosan has high degree of deacetylation (means high number of amino groups on chitosan backbone), then the chitosan will have a higher number of protonated amino groups in acidic medium which makes the chitosan a highly charged polycation with increased viscosity.

In this section, polymer solutions of different degree of deacetylation (DD-70%, DD-81%, and DD-90%) were made with different concentration (4 wt%-7 wt%) and they were electrospun with different electric field (1-2 kV/cm). A constant feed rate of 10 µL/min was used for all the polymer solutions. A complete set of experiments is represented in Table 18 with different electric field and concentration and their resulting average fiber diameters. Figure 40 shows the SEM images of electrospun chitosan in TFA at a concentration of 7 wt% and 1.5 kV/cm with different degrees of deacetylation. Figures 41 to 44, shows the effect of degree of deacetylation on average fiber diameter with increasing concentration at specific electric field.

From the SEM images and Figures 41 to 44, the average fiber diameter increased with the degree of deacetylation at same concentration and electric field. The average fiber diameters for DD-70%, DD-81% and DD-90% at 7 wt% concentration and 1.5 kV/cm were found to be 121, 224, and 245 nm, respectively. The ranges of the fiber diameter distribution (see Figure 45) become broader as the degree of deacetylation increased indicating that the higher degree of deacetylated chitosan gave thicker fiber as compared to lower degree of deacetylated chitosan. This was due to the deacetylation of chitosan, by which there was an increase of amino ($-NH_2$) group on the chitosan backbone which gets protonated in TFA. The solubility of chitosan also increased as the degree of deacetylation increased as it is seen that, the chitosan of DD-70% was not soluble in 90% acidic acid/water solvent system against DD-81%. However, the protonation caused some extent of increase in viscosity of polymer solution which is compensated with decrease in molecular weight from ($M_v = 1.0 \times 10^6$, DD-81%) to ($M_v = 8.2 \times 10^5$, DD-90%). The deacetylation process hydrolyses the chitosan chains which become more expanded by electrostatic repulsion between the charges. Therefore, the chitosan solution behaved like a cationic polyelectrolyte under acidic medium having high charge density depending upon the degree of deacetylation. The polymer solution containing high degree of deacetylation will have high net charge density on the surface of ejected jet in the electrospinning field and the higher charge density carried by the jet formed a smooth fibers due to the stronger whipping instability of the jet [101].

From the Table 18, it was also found out that as the concentration increased, the average fiber diameter increased. While as the electric field increased the average fiber diameter decreased.

The average fiber diameters for DD-70%, DD-81% and DD-90% at 7 wt% concentration and 1.33 kV/cm (see Figure 42) were found to be 128 ± 5, 401 ± 7, and 290 ± 8 nm, respectively. The increase in average fiber diameter for DD-81% (401 ± 7 nm) as against DD-90% (290 ± 8) was due to the increased mass flow rate relative to the increase in the electrostatic force. The higher ejaculation of polymer solution causes less stretching and elongation of jet resulting in increased fiber diameter [122,123].

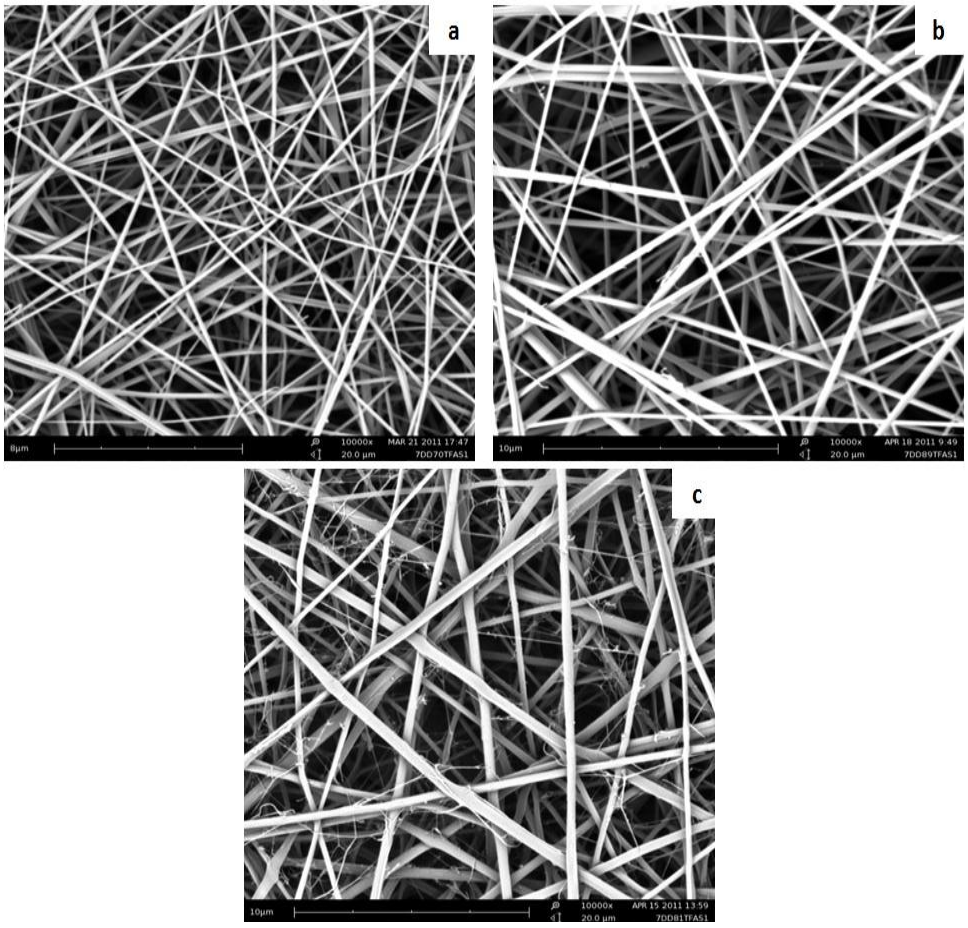

Figure 40 SEM images of electrospun chitosan produced at a concentration of 7 wt% and an electric field of 1.5 kV/cm with different degrees of deacetylation: (a) DD-70%, (b) DD-81% and (c) DD-90% (Magnification-10,000x)

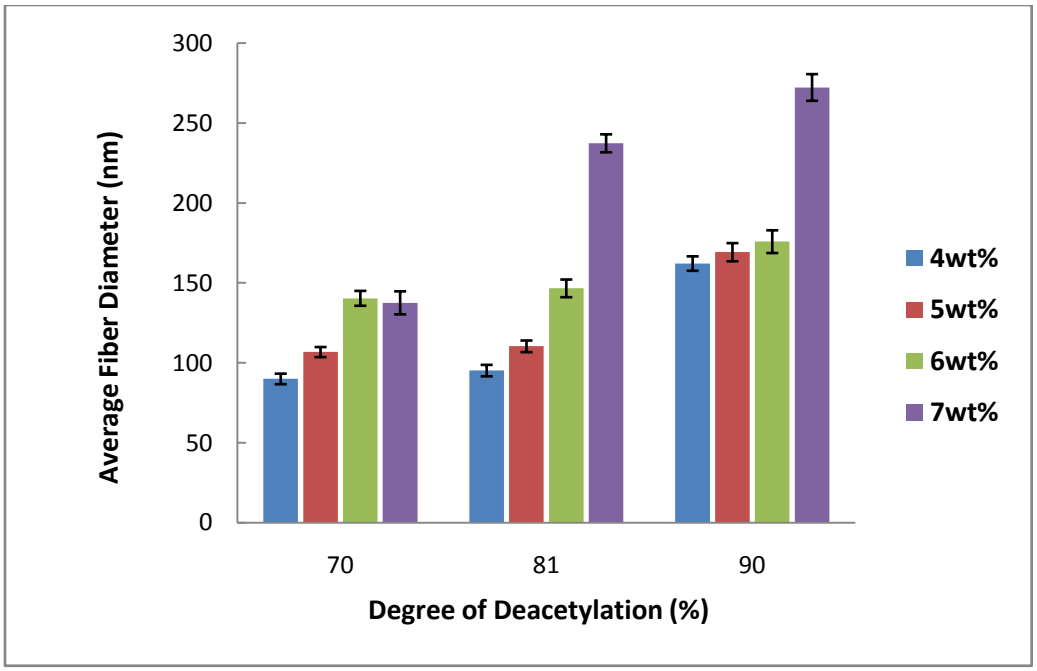

Figure 41 Effect of degree of deacetylation on average fiber diameter of chitosan electrospun in TFA at an electric field of 1 kV/cm with different concentrations

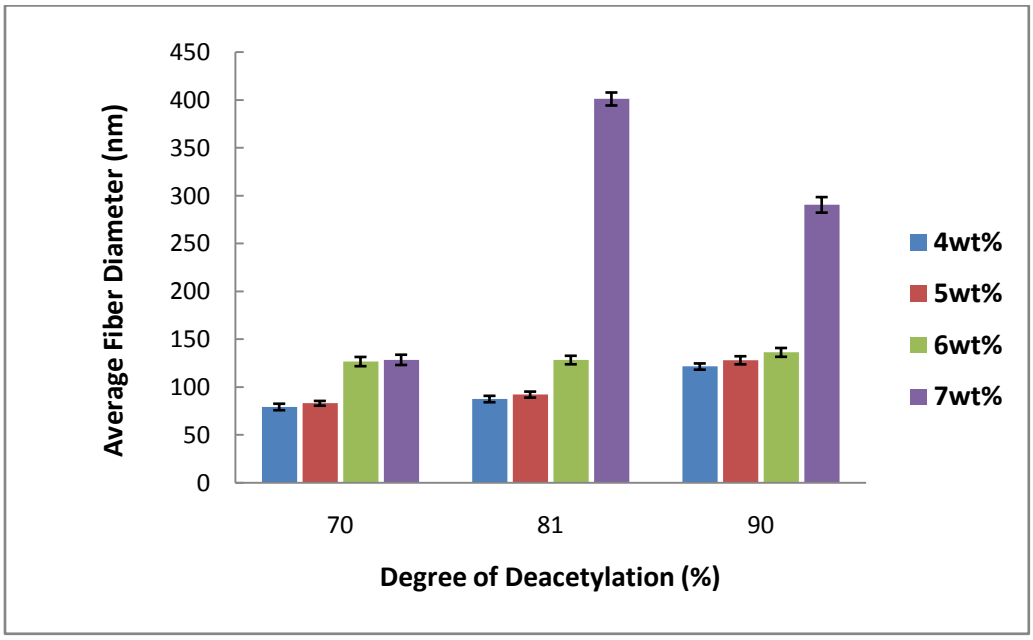

Figure 42 Effect of degree of deacetylation on average fiber diameter of chitosan electrospun in TFA at an electric field of 1.33 kV/cm with different concentrations

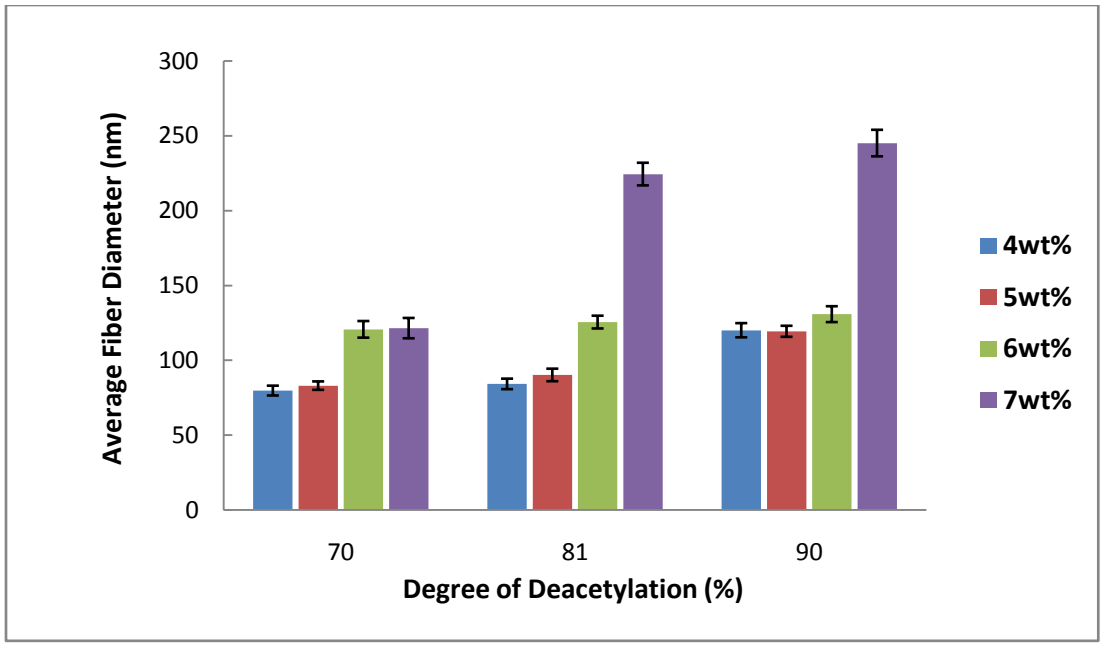

Figure 43 Effect of degree of deacetylation on average fiber diameter of chitosan electrospun in TFA at an electric field of 1.5 kV/cm with different concentrations

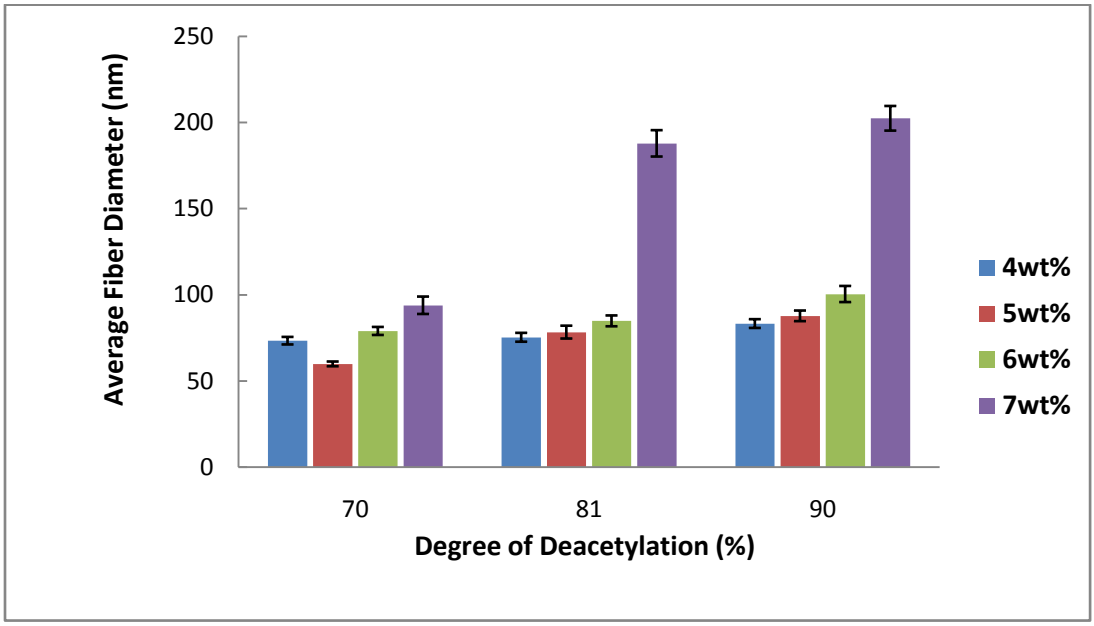

Figure 44 Effect of degree of deacetylation on average fiber diameter of chitosan electrospun in TFA at an electric field of 2 kV/cm with different concentrations

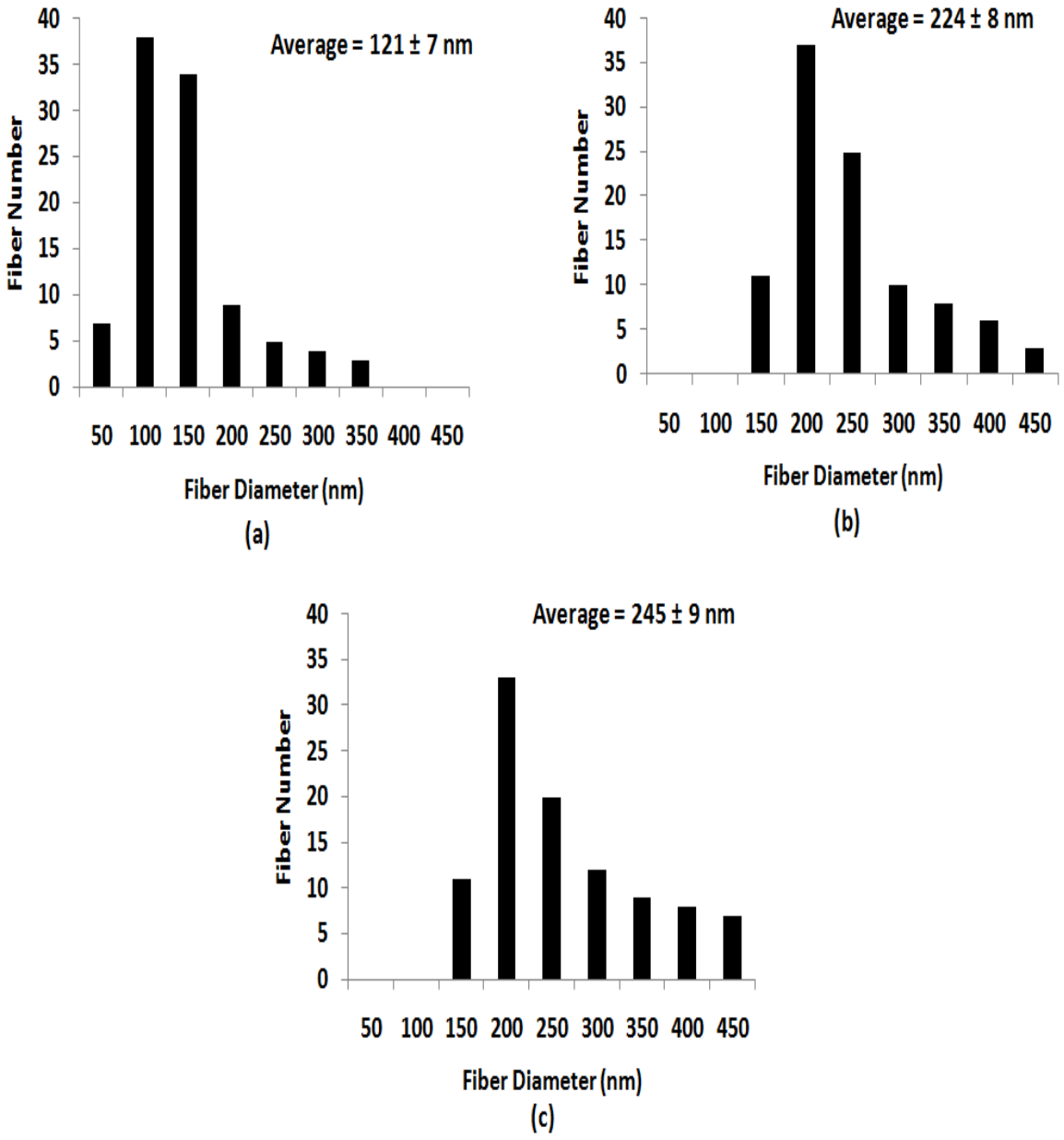

Figure 45 Fiber diameter distribution of electropsun chitosan at a concentration of 7 wt% in TFA and an electric field of 1.5 kV/cm produced with different degrees of deacetylation: (a) 70%, (b) 81%, and (c) 90%

4.3 Electrospinning on Seprafilm™

The final step of this research project was to electrospin pure chitosan nanofibers onto Seprafilm™ that would be biocompatible, bioresorbable, and bioactive on which cells can grow and multiply. This will help in cell proliferation and tissue growth for wound healing applications. The Seprafilm™ in conjunction with a chitosan nanofibrous mesh (artificial ECM) would be beneficial as adhesion barrier films. The biomedial company, Genzyme, manufactures a polysaccharide film called Seprafilm™ for use as a surgical adhesion barrier. This barrier film has shown significant reduction in adhesion formation after abdominal and pelvic surgery. However, 49% of the patients who use Seprafilm™ still showed some degree of post-surgical adhesion (see section 1.1). The incorporation chitosan nanofibers onto Seprafilm™ may reduce the wound healing time and would likely decrease the chance of post-surgical adhesion as chitosan itself has biological properties such as biocompability, biodegradability, antibacterial, haemostatic and wound healing properties. High surface area of nanofibers may help reduce the slippage of film from the wound site until the seprafilm-chitosan nanofibers film absorb into the body.

Electrospinning on Seprafilm™ has been previously reported by a member of our group.[129]. Queen, *et al.* have successfully electrospin PEO and PEO-chitosan blend bead-less nanofibers on Seprafilm™ instead of aluminum foil.

To evaluate the feasibility of electrospinning the 100 % chitosan nanofibers on Seprafilm™, the surface characteristics of Seprafilm were observed using SEM.

Figure 46 SEM image of SeprafilmTM (Magnification-1200x)

The SEM image revealed no visual surface defect that would interfere with the electrospinning process or the addition of another material layer. The average fiber diameter for chitosan DD-70%, DD-81% and DD-90% at 6 wt% concentration and 1.33 kV/cm were found to be 127, 128, and 136 nm, respectively. After successfully electrospinning the chitosan solution of 6 wt% from TFA on aluminum foil, the next series of experiments was to successfully electrospin a chitosan-TFA based solution onto Seprafilm^{TM}. Chitosan with different degrees of deacetylation 70%, 81% and 90% of same concentration (6 wt%) was electrospun at an electric field of 1.33 kV/cm (i.e. 20 kV-15 cm) onto Seprafilm^{TM} to see the effect of degree of deacetylation. The results showed nearly defect free chitosan nanofibers electrospun onto Seprafilm^{TM}. (see Figure 47)

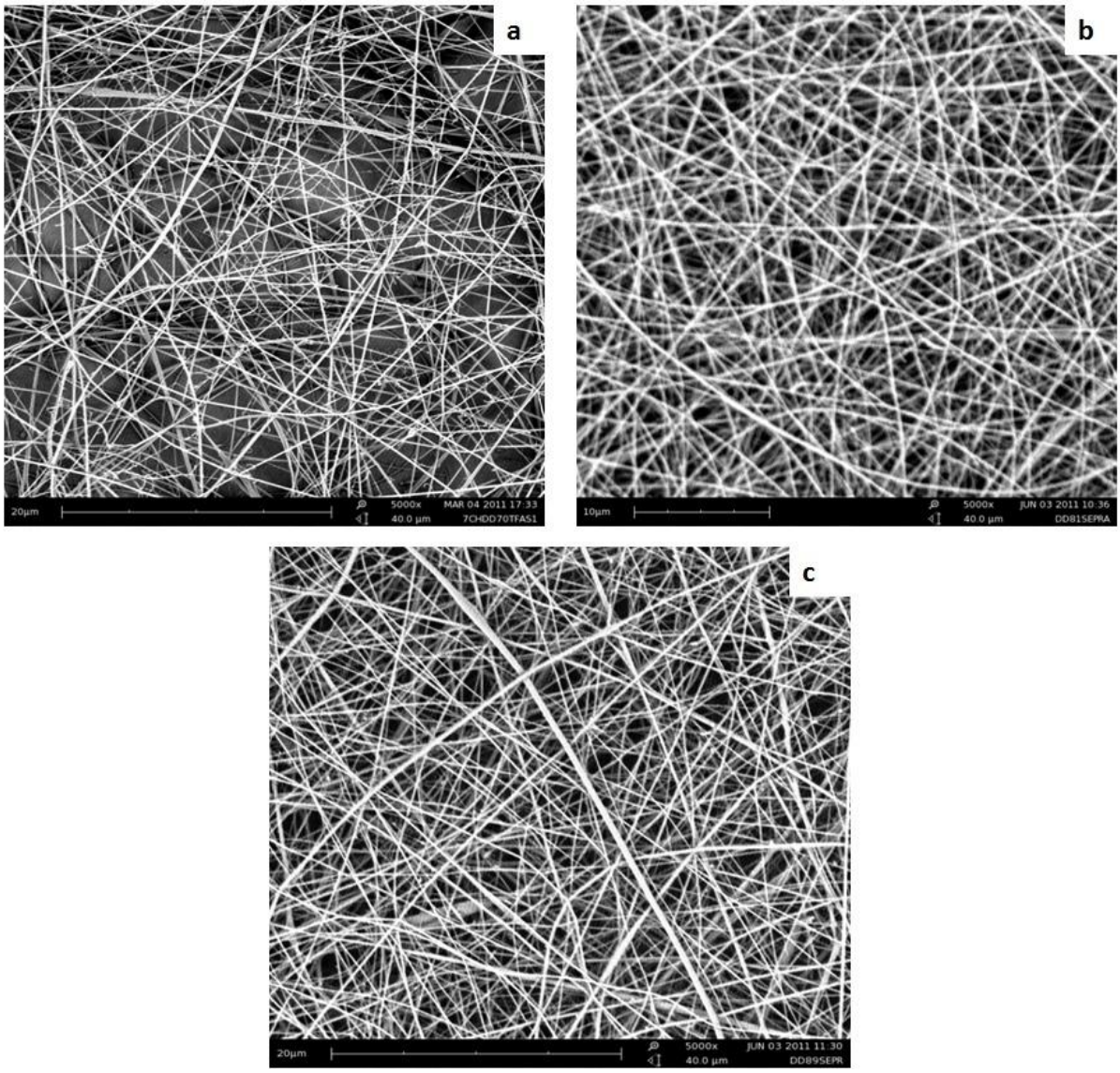

Figure 47 SEM images of electrospun chitosan-TFA produced at a concentration of 6 wt% and an electric field of 1.33 kV/cm onto Seprafilm^{TM} with different degrees of deacetylation: (a) DD-70%, (b) DD-81% and (c) DD-90% (Magnification-5,000x)

5. CONCLUSIONS

Chitosan from two different companies were used in this study to electrospin in different solvents (acetic acid, formic acid, and TFA). The commercial chitosan (CS-Sigma) could not be electrospun in 90% acetic acid/water and formic acid at different electric field due to its low molecular weight. Another chitosan (DD-70, from Vanson) having viscosity average molecular weight of 1.0×10^6 and DD-70% was used for electrospinning the chitosan in 90% acetic acid. However, the chitosan could not be fully dissolved due to its low degree of deacetylation. The chitosan sample was deacetylated in aqueous alkaline NaOH solution to produce chitosan of different degrees of deacetylation (DD-81% and DD-90%). The degree of deacetylation and the viscosity average molecular weight was measured by the acid-base titration and Ubbelohde viscometer, respectively. Chitosan solution of 3 wt% with DD-81% and DD-90% in 90% acetic acid were electrospun and the initial trials showed some fiber formation with beads. The electrospinning of chitosan solution is possible with acetic acid as solvent. Chitosan solutions were made with increasing concentration of 0.5 wt% to 4.5 wt%. Several parameters including polymer concentration and electric field were investigated in the electrospinning of chitosan dissolved in 90% acetic acid. The zero-shear rate viscosities of all the solutions were measured using rheometer to find out the optimal viscosity and concentration of solution for successful electrospinning.

From the log-log plot of [$\eta_{sp} = (\eta_{\circ}\text{-}\eta_{s)}/\eta_s$] versus concentration, the entanglement concentration for the both the chitosan samples (DD-81% and DD-90%) was found to be 1.8 wt%. In the semidilute unentangled regime the specific viscosities with concentration were

found to be ($\eta_{sp} \sim c^{1.9}$) and ($\eta_{sp} \sim c^{1.6}$) for DD-81% and DD-90%, respectively. And In semidilute entangled regime, the specific viscosities with concentration were found to be ($\eta_{sp} \sim c^{4.1}$) and ($\eta_{sp} \sim c^{3.8}$) for DD-81% and DD-90%, respectively. The scaling relationship for DD-90% was found similar to the neutral polymers because the polymer chains adopt a flexible coil like conformation and also because of the decreased molecular weight by the deacetylation process. For DD-81%, both the slopes and zero-shear viscosities were higher than DD-90%. The scaling of ($\eta_{sp} \sim c^{4.1}$) in the concentrated regime was due to the higher number of interactions such as hydrogen bonding and hydrophobic interactions which forms associates in acidic medium.

From the SEM results, below the entanglement concentration (1.8 wt%), only beads had formed. Results indicate that the concentration from 2.5 wt% to 3.5 wt% with viscosities in the range of 1310-5680 cP for the DD-81% showed fiber formation with some beads. For the DD-90%, the trails showed some fiber formation within a concentration range of 2.5 wt% to 4 wt% with viscosities in the range of 260-1330 cP. From the SEM results, below the entanglement concentration (1.8 wt%), only beads had formed and above this concentration, the electrospinning was not possible because of the viscous nature of solution. The average fiber diameter increased with the increased in chitosan concentration for DD-90% and also it showed larger distribution of fibers. The electric field had profound effect on the average fiber diameter. For the DD-81%, the average fiber diameter increased with increase in electric field and for DD-90%, the average fiber diameter decreased with the increase in

electric field. Also, the average fiber diameter increased with degree of deacetylation at low electric field.

Another solvent system used for electrospinning the chitosan was the TFA. Different degrees of deacetylated chitosan were used to study the effect of concentration, electric field, and degree of deacetylation. Concentration of 1 wt% and 2 wt% could not be able to produce nanofibers; only beads were formed due to insufficient chain entanglements in the polymer solution and concentration of 3 wt% showed drastic morphological changes from beads to mixture of fibers and beads. Concentrations of 3 wt% to 7 wt% were studied to see the effect of above mention parameters. The results showed that as the concentration and the degree of deacetylation increased the average fiber diameters also increased at certain electric field. Below 1 kV/cm, the electric field was insufficient to overcome the viscous nature of polymer solution and as the electric field increased from 1 to 2 kV/cm, the average fiber diameter decreased for all the concentration ranges and different degrees of deacetylated chitosan. The ranges of diameter distribution become narrower at higher electric field indicating the formation of thinner fibers.

Seprafilm^{TM} is a barrier film which has unique biological properties that had used for the prevention of post surgical adhesions. Chitosan-TFA solutions of 6 wt% was been successfully electrospun onto the Seprafilm^{TM} showing nearly defect free chitosan nanofibers with different degrees of deacetylation. This could be an excellent example of biomedical

product that could be use as a barrier film with chitosan nanofiber layer on it for the treatment of post surgical adhesion with fast wound healing rates.

6. FUTURE WORK

Considering the successful electrospinning of chitosan nanofibers from this series of experiments, the next series of experiments will include a detailed evaluation of the material distribution of nanofibers such as covering power, basis weight, and fiber diameter that determine the surface area of the structure which is related to the antimicrobial property. Further investigation for potential applications in wound dressings, such as gauzes, tissue engineering scaffolds, and drug delivery would require the antibacterial, cytotoxity assessment as well as *in vitro* tests to determine the cell attachment, proliferation of cells and growth. Only chitosan nanofibers and in conjunction with another material can also be evaluated *in vitro* to study the killing and prevention efficiency from bacteria.

In addition, different degree of deacetylated chitosan nanofibers electrospun onto Seprafilm^{TM} can be tested to study the delamination between two materials and as well as investigating the biodegradation rate to study the effect of degree of deacetylation.

One of the original goals of this study was to study the effect of solvent on electrospinning of chitosan. The successful electrospinning of chitosan was possible only with TFA giving larger nanofibers. However, with the acetic acid, the electrospinning process produced chitosan nanofibers in the range of 20 nm to 30nm with some beads. Since, TFA is more harmful and hazardous to health as compared to acetic acid; therefore, it is recommend to optimize the solution property of chitosan solution containing acetic acid. There are many ways to address this concern such as adding different salts in the polymer solution to screen

out the charges from polymer chains which reduces the viscosity of solution and facilitates in electrospinning. In addition to this, more amount of polymer can be electrospun with little impact on viscosity.

Other focuses for future studies include the investigation of align chitosan nanofibers for the application of tissue engineering scaffolds and wound healing. For this kind of application, the mechanical stability of the scaffolds is required and this can be tested by analyzing the mechanical properties, and the stability of nanofibers in aqueous solutions.

REFERENCES

[1] Subbiah, T.; Bhat, G.S.; Tock, R.W.; Parameswaran, S.; Ramkumar, S.S. Electrospinning of Nanofibers. J Appl Polym Sci 2005, *96*, 557-569.

[2] Qin, X.; Wang, S. Filtration Properties of Electrospinning Nanofibers. J Appl Polym Sci 2006, *102*, 1285-1290.

[3] Podgórski, A.; Bałazy, A.; Gradoń, L. Application of Nanofibers to Improve the Filtration Efficiency of the most Penetrating Aerosol Particles in Fibrous Filters. Chemical Engineering Science 2006, *61*, 6804-6815.

[4] Gibson, P.; Schreuder-Gibson, H.; Rivin, D. Transport Properties of Porous Membranes Based on Electrospun Nanofibers. Colloids Surf. Physicochem. Eng. Aspects 2001, *187-188*, 469-481.

[5] Schreuder-Gibson, H.; Gibson, P.; Senecal, K.; Sennett, M.; Walker, J.; Yeomans, W.; Ziegler, D.; Tsai, P.P. Protective Textile Materials Based on Electrospun Nanofibers. J. Adv. Mater. 2002, *34*, 44-55.

[6] Xu, C.Y.; Inai, R.; Kotaki, M.; Ramakrishna, S. Electrospun Nanofiber Fabrication as Synthetic Extracellular Matrix and its Potential for Vascular Tissue Engineering. Tissue Eng. 2004, *10*, 1160-1168.

[7] Lim, S.H.; Mao, H. Electrospun Scaffolds for Stem Cell Engineering. Adv. Drug Deliv. Rev. 2009, *61*, 1084-1096.

[8] Li, W.; Laurencin, C.T.; Caterson, E.J.; Tuan, R.S.; Ko, F.K. Electrospun Nanofibrous Structure: A Novel Scaffold for Tissue Engineering. J. Biomed. Mater. Res. 2002, *60*, 613-621.

[9] Bhattarai, S.R.; Bhattarai, N.; Yi, H.K.; Hwang, P.H.; Cha, D.I.; Kim, H.Y. Novel Biodegradable Electrospun Membrane: Scaffold for Tissue Engineering. Biomaterials 2004, *25*, 2595-2602.

[10] Bhattarai, N.; Edmondson, D.; Veiseh, O.; Matsen, F.A.; Zhang, M. Electrospun Chitosan-Based Nanofibers and their Cellular Compatibility. Biomaterials 2005, *26*, 6176-6184.

[11] Thakur, R.A.; Florek, C.A.; Kohn, J.; Michniak, B.B. Electrospun Nanofibrous Polymeric Scaffold with Targeted Drug Release Profiles for Potential Application as Wound Dressing. Int. J. Pharm. 2008, *364*, 87-93.

[12] Chen, J.; Chang, G.; Chen, J. Electrospun collagen/chitosan Nanofibrous Membrane as Wound Dressing. Colloids Surf. Physicochem. Eng. Aspects 2008, *313-314*, 183-188.

[13] Khil, M.S.; Cha, D.I.; Kim, H.Y.; Kim, I.S.; Bhattarai, N. Electrospun Nanofibrous Polyurethane Membrane as Wound Dressing. Journal of Biomedical Materials Research Part B-Applied Biomaterials 2003, *67B*, 675-679.

[14] Kenawy, E.; Abdel-Hay, F.I.; El-Newehy, M.H.; Wnek, G.E. Controlled Release of Ketoprofen from Electrospun Poly(Vinyl Alcohol) Nanofibers. Materials Science and Engineering: A 2007, *459*, 390-396.

[15] Katti, D.S.; Robinson, K.W.; Ko, F.K.; Laurencin, C.T. Bioresorbable Nanofiber-Based Systems for Wound Healing and Drug Delivery: Optimization of Fabrication Parameters. Journal of Biomedical Materials Research Part B-Applied Biomaterials 2004, *70B*, 286-296.

[16] Zeleny, J. The Electrical Discharge from Liquid Points, and a Hydrostatic Method of Measuring the Electric Intensity at their Surfaces. Physical Review 1914, *3*, 69-91.

[17] Laurencin, C.T.; Ambrosio, A.M.A.; Borden, M.D.; Cooper, J.A. Tissue Engineering: Orthopedic Applications. Annu. Rev. Biomed. Eng. 1999, *1*, 19-46.

[18] Agarwal, S.; Wendorff, J.H.; Greiner, A. Progress in the Field of Electrospinning for Tissue Engineering Applications. Adv Mater 2009, *21*, 3343-3351.

[19] Dvir, T.; Tsur-Gang, O.; Cohen, S. "Designer" Scaffolds for Tissue Engineering and Regeneration. Isr. J. Chem. 2005, *45*, 487-494.

[20] Khor, E.; Lim, L.Y. Implantable Applications of Chitin and Chitosan. Biomaterials 2003, *24*, 2339-2349.

[21] Ravi Kumar, M.N.V. A Review of Chitin and Chitosan Applications. React Funct Polym 2000, *46*, 1-27.

[22] Hudson, S.M.; Jenkins, D.W. Chitin and Chitosan. 2002.

[23] *Applications of Chitin and Chitosan*.; Technomic Pub: Lancaster, PA, 1997.

[24] Chatelet, C.; Damour, O.; Domard, A. Influence of the Degree of Acetylation on some Biological Properties of Chitosan Films. Biomaterials 2001, *22*, 261-268.

[25] Cohn, D.; Pines, E. Methods for Reducing Or Eliminating Post-Surgical Adhesion Formation. 01/27/1998, *678762*, 1.

[26] Zeng, Q.; Yu, Z.; You, J.; Zhang, Q. Efficacy and Safety of Seprafilm for Preventing Postoperative Abdominal Adhesion: Systematic Review and Meta-Analysis. World J. Surg. 2007, *31*, 2125-2131.

[27] Mohri, Y.; Uchida, K.; Araki, T.; Inoue, Y.; Tonouchi, H.; Miki, C.; Kusunoki, M. Hyaluronic Acid-Carboxycellulose Membrane (Seprafilm) Reduces Early Postoperative Small Bowel Obstruction in Gastrointestinal Surgery. Am. Surg. 2005, *71*, 861-863.

[28] Nappi, C.; Di Spiezio Sardo, A.; Greco, E.; Guida, M.; Bettocchi, S.; Bifulco, G. Prevention of Adhesions in Gynaecological Endoscopy. Hum. Reprod. Update 2007, *13*, 379-394.

[29] Hellebrekers, B.W.J.; Trimbos-Kemper, G.C.M.; van Blitterswijk, C.A.; Bakkum, E.A.; Trimbos, J.B.M.Z. Effects of Five Different Barrier Materials on Postsurgical Adhesion Formation in the Rat. Human Reproduction 2000, *15*, 1358-1363.

[30] Arnold, P.B.; Green, C.W.; Foresman, P.A.; Rodeheaver, G.T. Evaluation of Resorbable Barriers for Preventing Surgical Adhesions. Fertil. Steril. 2000, *73*, 157-161.

[31] Becker, J.M.; Dayton, M.T.; Fazio, V.W.; Beck, D.E.; Stryker, S.J.; Wexner, S.D.; Wolff, B.G.; Roberts, P.L.; Smith, L.E.; Sweeney, S.A. *et al.* Prevention of Postoperative: Abdominal Adhesions by a Sodium Hyaluronate-Based Bioresorbable Membrane: A Prospective, Randomized, Double-Blind Multicenter Study. J. Am. Coll. Surg. 1996, *183*, 297-306.

[32] Di Martino, A.; Sittinger, M.; Risbud, M.V. Chitosan: A Versatile Biopolymer for Orthopaedic Tissue-Engineering. Biomaterials 2005, *26*, 5983-5990.

[33] Formhals A. Process and Apparatus for Preparing Artificial Threads. 08/02/1934.

[34] Formhals, A. Artificial Thread and Method of Producing Same. 01/16/1940.

[35] Formhals, A. Producing of Artificial Fibers from Fiber Forming Liquids. 06/29/1943.

[36] Formhals, A. Method and Apparatus for Spinning. 05/30/1944.

[37] Vonnegut, B.; Neubauer, R.L. Production of Monodisperse Liquid Particles by Electrical Atomization. J. Colloid Sci. 1952, *7*, 616-622.

[38] Taylor, G. Electrically Driven Jets. 12/2/1969, 453.

[39] Baumgarten, P.K. Electrostatic Spinning of Acrylic Microfibers. J. Colloid Interface Sci. 1971, *36*, 71-79.

[40] Larrondo, L.; St. John Manley, R. Electrostatic Fiber Spinning from Polymer Melts. I. Experimental Observations on Fiber Formation and Properties. Journal of Polymer Science: Polymer Physics Edition 1981, *19*, 909-920.

[41] Larrondo, L.; St. John Manley, R. Electrostatic Fiber Spinning from Polymer Melts. II. Examination of the Flow Field in an Electrically Driven Jet. Journal of Polymer Science: Polymer Physics Edition 1981, *19*, 921-932.

[42] Hayati, I.; Bailey, A.I.; Tadros, T.F. Mechanism of Stable Jet Formation in Electrohydrodynamic Atomization. Nature 1986, *319*, 41-43.

[43] Doshi, J.; Reneker, D.H. Electrospinning Process and Applications of Electrospun Fibers. J. Electrostatics 1995, *35*, 151-160.

[44] Reneker, D.H.; Chun, I. Nanometre Diameter Fibres of Polymer, Produced by Electrospinning. Nanotechnology 1996, *7*, 216-223.

[45] Fong, H.; Chun, I.; Reneker, D.H. Beaded Nanofibers Formed during Electrospinning. Polymer 1999, *40*, 4585-4592.

[46] Srinivasan, G.; Reneker, D.H. Structure and Morphology of Small Diameter Electrospun Aramid Fibers. Polym. Int. 1995, *36*, 195-201.

[47] Bhardwaj, N.; Kundu, S.C. Electrospinning: A Fascinating Fiber Fabrication Technique. Biotechnol. Adv. 2010, *28*, 325-347.

[48] Rutledge, G.C.; Fridrikh, S.V. Formation of Fibers by Electrospinning. Adv. Drug Deliv. Rev. 2007, *59*, 1384-1391.

[49] Reneker, D.H.; Yarin, A.L.; Fong, H.; Koombhongse, S. Bending Instability of Electrically Charged Liquid Jets of Polymer Solutions in Electrospinning. J. Appl. Phys. 2000, *87*, 4531-4547.

[50] Sill, T.J.; von Recum, H.A. Electrospinning: Applications in Drug Delivery and Tissue Engineering. Biomaterials 2008, *29*, 1989-2006.

[51] Andrady, A.L.(. *Science and Technology of Polymer Nanofibers*.; Wiley: Hoboken, N.J., 2008.

[52] Yarin, A.L.; Koombhongse, S.; Reneker, D.H. Taylor Cone and Jetting from Liquid Droplets in Electrospinning of Nanofibers. J. Appl. Phys. 2001, *90*, 4836-4846.

[53] Rangupan, R.; Reneker, D. Electrospinning Process of Molten Polypropylene in Vacuum. 2003, 81-87.

[54] Wang, Z.; Xu, Z.; Wan, L.; Wu, J.; Innocent, C.; Seta, P. Nanofibrous Membranes Containing Carbon Nanotubes: Electrospun for Redox Enzyme Immobilization. Macromolecular Rapid Communications 2006, *27*, 516-521.

[55] Demir, M.M.; Yilgor, I.; Yilgor, E.; Erman, B. Electrospinning of Polyurethane Fibers. Polymer 2002, *43*, 3303-3309.

[56] Yu, J.H.; Fridrikh, S.V.; Rutledge, G.C. The Role of Elasticity in the Formation of Electrospun Fibers. Polymer 2006, *47*, 4789-4797.

[57] Shin, Y.M.; Hohman, M.M.; Brenner, M.P.; Rutledge, G.C. Electrospinning: A Whipping Fluid Jet Generates Submicron Polymer Fibers. Appl. Phys. Lett. 2001, *78*, 1149-1151.

[58] Fridrikh, S.V.; Yu, J.H.; Brenner, M.P.; Rutledge, G.C. Controlling the Fiber Diameter during Electrospinning. Phys. Rev. Lett. 2003, *90*, 144502.

[59] Deitzel, J.M.; Kleinmeyer, J.; Harris, D.; Tan, N.C.B. The Effect of Processing Variables on the Morphology of Electrospun Nanofibers and Textiles. Polymer 2001, *42*, 261-272.

[60] Theron, S.A.; Zussman, E.; Yarin, A.L. Experimental Investigation of the Governing Parameters in the Electrospinning of Polymer Solutions. Polymer 2004, *45*, 2017-2030.

[61] McKee, M.G.; Wilkes, G.L.; Colby, R.H.; Long, T.E. Correlations of Solution Rheology with Electrospun Fiber Formation of Linear and Branched Polyesters. Macromolecules 2004, *37*, 1760-1767.

[62] Jarusuwannapoom, T.; Hongroijanawiwat, W.; Jitjaicham, S.; Wannatong, L.; Nithitanakul, M.; Pattamaprom, C.; Koombhongse, P.; Rangkupan, R.; Supaphol, P. Effect of Solvents on Electro-Spinnability of Polystyrene Solutions and Morphological Appearance of Resulting Electrospun Polystyrene Fibers. European Polymer Journal 2005, *41*, 409-421.

[63] Koski, A.; Yim, K.; Shivkumar, S. Effect of Molecular Weight on Fibrous PVA Produced by Electrospinning. Mater Lett 2004, *58*, 493-497.

[64] Zuo, W.W.; Zhu, M.F.; Yang, W.; Yu, H.; Chen, Y.M.; Zhang, Y. Experimental Study on Relationship between Jet Instability and Formation of Beaded Fibers during Electrospinning. Polym. Eng. Sci. 2005, *45*, 704-709.

[65] You, Y.; Lee, S.J.; Min, B.M.; Park, W.H. Effect of Solution Properties on Nanofibrous Structure of Electrospun Poly(Lactic-Co-Glycolic Acid). J Appl Polym Sci 2006, *99*, 1214-1221.

[66] Thompson, C.J.; Chase, G.G.; Yarin, A.L.; Reneker, D.H. Effects of Parameters on Nanofiber Diameter Determined from Electrospinning Model. Polymer 2007, *48*, 6913-6922.

[67] Lin, T.; Wang, H.X.; Wang, H.M.; Wang, X.G. The Charge Effect of Cationic Surfactants on the Elimination of Fibre Beads in the Electrospinning of Polystyrene. Nanotechnology 2004, *15*, 1375-1381.

[68] Hohman, M.M.; Shin, M.; Rutledge, G.; Brenner, M.P. Electrospinning and Electrically Forced Jets. II. Applications. Phys. Fluids 2001, *13*, 2221-2236.

[69] Megelski, S.; Stephens, J.S.; Chase, D.B.; Rabolt, J.F. Micro- and Nanostructured Surface Morphology on Electrospun Polymer Fibers. Macromolecules 2002, *35*, 8456-8466.

[70] Tan, S.; Inai, R.; Kotaki, M.; Ramakrishna, S. Systematic Parameter Study for Ultra-Fine Fiber Fabrication Via Electrospinning Process. Polymer 2005, *46*, 6128-6134.

[71] Heikkilä, P.; Harlin, A. Parameter Study of Electrospinning of Polyamide-6. European Polymer Journal 2008, *44*, 3067-3079.

[72] Ki, C.S.; Baek, D.H.; Gang, K.D.; Lee, K.H.; Um, I.C.; Park, Y.H. Characterization of Gelatin Nanofiber Prepared from Gelatin-Formic Acid Solution. Polymer 2005, *46*, 5094-5102.

[73] Buchko, C.J.; Chen, L.C.; Shen, Y.; Martin, D.C. Processing and Microstructural Characterization of Porous Biocompatible Protein Polymer Thin Films. Polymer 1999, *40*, 7397-7407.

[74] De Vrieze, S.; Van Camp, T.; Nelvig, A.; Hagstrom, B.; Westbroek, P.; De Clerck, K. The Effect of Temperature and Humidity on Electrospinning. J. Mater. Sci. 2009, *44*, 1357-1362.

[75] Zong, X.H.; Kim, K.; Fang, D.F.; Ran, S.F.; Hsiao, B.S.; Chu, B. Structure and Process Relationship of Electrospun Bioabsorbable Nanofiber Membranes. Polymer 2002, *43*, 4403-4412.

[76] Huang, Z.; Zhang, Y.-.; Kotaki, M.; Ramakrishna, S. A Review on Polymer Nanofibers by Electrospinning and their Applications in Nanocomposites. Composites Sci. Technol. 2003, *63*, 2223-2253.

[77] Pham, Q.P.; Sharma, U.; Mikos, A.G. Electrospinning of Polymeric Nanofibers for Tissue Engineering Applications: A Review. Tissue Eng. 2006, *12*, 1197-1211.

[78] Ma, Z.W.; Kotaki, M.; Inai, R.; Ramakrishna, S. Potential of Nanofiber Matrix as Tissue-Engineering Scaffolds. Tissue Eng. 2005, *11*, 101-109.

[79] Venugopal, J.; Ramakrishna, S. Applications of Polymer Nanofibers in Biomedicine and Biotechnology. Appl. Biochem. Biotechnol. 2005, *125*, 147-157.

[80] Schiffman, J.D.; Schauer, C.L. A Review: Electrospinning of Biopolymer Nanofibers and their Applications. Polymer Reviews 2008, *48*, 317-352.

[81] Pillai, C.K.S.; Paul, W.; Sharma, C.P. Chitin and Chitosan Polymers: Chemistry, Solubility and Fiber Formation. Progress in Polymer Science 2009, *34*, 641-678.

[82] Rinaudo, M. Chitin and Chitosan: Properties and Applications. Progress in Polymer Science 2006, *31*, 603-632.

[83] Shahidi, F.; Arachchi, J.K.V.; Jeon, Y. Food Applications of Chitin and Chitosans. Trends Food Sci. Technol. 1999, *10*, 37-51.

[84] Kim, I.; Seo, S.; Moon, H.; Yoo, M.; Park, I.; Kim, B.; Cho, C. Chitosan and its Derivatives for Tissue Engineering Applications. Biotechnol. Adv. 2008, *26*, 1-21.

[85] Jayakumar, R.; Prabaharan, M.; Nair, S.V.; Tamura, H. Novel Chitin and Chitosan Nanofibers in Biomedical Applications. Biotechnol. Adv. 2010, *28*, 142-150.

[86] Ueno, H.; Mori, T.; Fujinaga, T. Topical Formulations and Wound Healing Applications of Chitosan. Adv. Drug Deliv. Rev. 2001, *52*, 105-115.

[87] Jayakumar, R.; Prabaharan, M.; Reis, R.L.; Mano, J.F. Graft Copolymerized Chitosan - Present Status and Applications. Carbohydr. Polym. 2005, *62*, 142-158.

[88] Prabaharan, M.; Mano, J.F. Chitosan-Based Particles as Controlled Drug Delivery Systems. Drug Deliv. 2005, *12*, 41-57.

[89] Ray, N.F.; Denton, W.G.; Thamer, M.; Henderson, S.C.; Perry, S. Abdominal Adhesiolysis: Inpatient Care and Expenditures in the United States in 1994. J. Am. Coll. Surg. 1998, *186*, 1-9.

[90] Beck, D.E.; Cohen, Z.; Fleshman, J.W.; Kaufman, H.S.; van Goor, H.; Wolff, B.G.; Adhesion Study Grp Steering Comm. A Prospective, Randomized, Multicenter, Controlled

Study of the Safety of Seprafilm (R) Adhesion Barrier in Abdominopelvic Surgery of the Intestine. Diseases of the Colon & Rectum 2003, *46*, 1310-1319.

[91] Duan, B.; Dong, C.H.; Yuan, X.Y.; Yao, K.D. Electrospinning of Chitosan Solutions in Acetic Acid with Poly(Ethylene Oxide). Journal of Biomaterials Science-Polymer Edition 2004, *15*, 797-811.

[92] Subramanian, A.; Vu, D.; Larsen, G.F.; Lin, H.Y. Preparation and Evaluation of the Electrospun chitosan/PEO Fibers for Potential Applications in Cartilage Tissue Engineering. Journal of Biomaterials Science-Polymer Edition 2005, *16*, 861-873.

[93] Lou, C.; Lin, J.; Yen, K.; Lu, C.; Lee, C. Preparation of Polyethylene oxide/chitosan Fiber Membranes by Electrospinning and the Evaluation of Biocompatibility. Text. Res. J. 2008, *78*, 254-257.

[94] Kriegel, C.; Kit, K.M.; McClements, D.J.; Weiss, J. Electrospinning of Chitosan-Poly(Ethylene Oxide) Blend Nanofibers in the Presence of Micellar Surfactant Solutions. Polymer 2009, *50*, 189-200.

[95] Kossovich, L.; Salkovskiy, Y.; Kirillova, I. Electrospun Chitosan Nanofiber Materials as Burn Dressing. 2010, 1212-1214.

[96] Klossner, R.R.; Queen, H.A.; Coughlin, A.J.; Krause, W.E. Correlation of Chitosan's Rheological Properties and its Ability to Electrospin. Biomacromolecules 2008, *9*, 2947-2953.

[97] Li, L.; Hsieh, Y. Chitosan Bicomponent Nanofibers and Nanoporous Fibers. Carbohydr. Res. 2006, *341*, 374-381.

[98] Lin, T.; Fang, J.; Wang, H.; Cheng, T.; Wang, X. Using Chitosan as a Thickener for Electrospinning Dilute PVA Solutions to Improve Fibre Uniformity. Nanotechnology 2006, *17*, 3718-3723.

[99] Desai, K.; Kit, K.; Li, J.; Zivanovic, S. Morphological and Surface Properties of Electrospun Chitosan Nanofibers. Biomacromolecules 2008, *9*, 1000-1006.

[100] Desai, K.; Kit, K.; Li, J.; Davidson, P.M.; Zivanovic, S.; Meyer, H. Nanofibrous Chitosan Non-Wovens for Filtration Applications. Polymer 2009, *50*, 3661-3669.

[101] Geng, X.Y.; Kwon, O.H.; Jang, J.H. Electrospinning of Chitosan Dissolved in Concentrated Acetic Acid Solution. Biomaterials 2005, *26*, 5427-5432.

[102] De Vrieze, S.; Westbroek, P.; Van Camp, T.; Van Langenhove, L. Electrospinning of Chitosan Nanofibrous Structures: Feasibility Study. J. Mater. Sci. 2007, *42*, 8029-8034.

[103] Homayoni, H.; Ravandi, S.A.H.; Valizadeh, M. Electrospinning of Chitosan Nanofibers: Processing Optimization. Carbohydr. Polym. 2009, *77*, 656-661.

[104] Ohkawa, K.; Cha, D.; Kim, H.; Nishida, A.; Yamamoto, H. Electrospinning of Chitosan. Macromolecular Rapid Communications 2004, *25*, 1600-1605.

[105] Ohkawa, K.; Minato, K.; Kumagai, G.; Hayashi, S.; Yamamoto, H. Chitosan Nanofiber. Biomacromolecules 2006, *7*, 3291-3294.

[106] El-Tahlawy, K.; Hudson, S.M. Chitosan: Aspects of Fiber Spinnability. J Appl Polym Sci 2006, *100*, 1162-1168.

[107] Mima, S.; Miya, M.; Iwamoto, R.; Yoshikawa, S. Highly Deacetylated Chitosan and its Properties. J Appl Polym Sci 1983, *28*, 1909-1917.

[108] Lim, S., 1971-. Synthesis of a Fiber-Reactive Chitosan Derivative and its Application to Cotton Fabric as an Antimicrobial Finish and a Dyeing-Improving Agent [Electronic Resource]. 2002.

[109] Maghami, G.G.; Roberts, G.A.F. Evaluation of the Viscometric Constants for Chitosan. Die Makromolekulare Chemie 1988, *189*, 195-200.

[110] Wang, W.; Bo, S.; Li, S.; Qin, W. Determination of the Mark-Houwink Equation for Chitosans with Different Degrees of Deacetylation. Int. J. Biol. Macromol. 1991, *13*, 281-285.

[111] Wang, W.; Qin, W.; Bo, S. Influence of the Degree of Deacetylation of Chitosan on its Mark-Houwink Equation Parameters. Die Makromolekulare Chemie, Rapid Communications 1991, *12*, 559-561.

[112] YOUNG, D. Hyaluronic Acid-Based Nanofibers viaElectrospinning. 2006.

[113] McKee, M.G.; Hunley, M.T.; Layman, J.M.; Long, T.E. Solution Rheological Behavior and Electrospinning of Cationic Polyelectrolytes. Macromolecules 2006, *39*, 575-583.

[114] Cho, J.Y.; Heuzey, M.C.; Begin, A.; Carreau, P.J. Viscoelastic Properties of Chitosan Solutions: Effect of Concentration and Ionic Strength. J. Food Eng. 2006, *74*, 500-515.

[115] Hwang, J.; Shin, H. Rheological Properties of Chitosan Solutions. 2001, *12 No. 3/4*, 175-179.

[116] Kienzlesterzer, C.A.; Rodriguezsanchez, D.; Rha, C.K. Flow Behavior of a Cationic Bio-Polymer - Chitosan. Polymer Bulletin 1985, *13*, 1-6.

[117] Mucha, M. Rheological Characteristics of Semi-Dilute Chitosan Solutions. Macromolecular Chemistry and Physics 1997, *198*, 471-484.

[118] Dobrynin, A.V.; Colby, R.H.; Rubinstein, M. Scaling Theory of Polyelectrolyte Solutions. Macromolecules 1995, *28*, 1859-1871.

[119] Takahashi, Y.; Isono, Y.; Noda, I.; Nagasawa, M. Zero-Shear Viscosity of Linear Polymer-Solutions Over a Wide-Range of Concentration. Macromolecules 1985, *18*, 1002-1008.

[120] Krause, W.E.; Bellomo, E.G.; Colby, R.H. Rheology of Sodium Hyaluronate Under Physiological Conditions. Biomacromolecules 2001, *2*, 65-69.

[121] Geng, X.; Kwon, O.; Jang, J. Electrospinning of Chitosan Dissolved in Concentrated Acetic Acid Solution. Biomaterials 2005, *26*, 5427-5432.

[122] Baker, S.C.; Atkin, N.; Gunning, P.A.; Granville, N.; Wilson, K.; Wilson, D.; Southgate, J. Characterisation of Electrospun Polystyrene Scaffolds for Three-Dimensional in Vitro Biological Studies. Biomaterials 2006, *27*, 3136-3146.

[123] Zhang, C.; Yuan, X.; Wu, L.; Han, Y.; Sheng, J. Study on Morphology of Electrospun Poly(Vinyl Alcohol) Mats. European Polymer Journal 2005, *41*, 423-432.

[124] Del Blanco, L.F.; Rodriguez, M.S.; Schulz, P.C.; Agullo, E. Influence of the Deacetylation Degree on Chitosan Emulsification Properties. Colloid Polym. Sci. 1999, *277*, 1087-1092.

[125] Schiffman, J.D.; Schauer, C.L. Cross-Linking Chitosan Nanofibers. Biomacromolecules 2007, *8*, 594-601.

[126] Schiffman, J.D.; Schauer, C.L. One-Step Electrospinning of Cross-Linked Chitosan Fibers. Biomacromolecules 2007, *8*, 2665-2667.

[127] Sangsanoh, P.; Supaphol, P. Stability Improvement of Electrospun Chitosan Nanofibrous Membranes in Neutral Or Weak Basic Aqueous Solutions. Biomacromolecules 2006, *7*, 2710-2714.

[128] Hasegawa, M.; Isogai, A.; Onabe, F.; Usuda, M. Dissolving States of Cellulose and Chitosan in Trifluoroacetic Acid. J Appl Polym Sci 1992, *45*, 1857-1863.

[129] Queen, H., 1982-. Electrospinning Chitosan-Based Nanofibers for Biomedical Applications [Electronic Resource]. 2006.

APPENDICES

Appendix A

Acid-base Titration Readings to Determine the Degree of Deacetylation of Chitosan

The Table below includes the titration reading for the DD-70%, DD-81%, and DD-90%. It includes the conductivity reading which was shown on the conductometric instrument with corresponding to the amount of NaOH solution added. Refer to experimental section where this method is explained in detail.

Table 19 Titration Reading for different degrees of deacetylated chitosans

DD-70%			**DD-81%**			**DD-90%**		
#	**NaOH (ml)**	**Conductivity (µS/cm)**	**#**	**NaOH (ml)**	**Conductivity (µS/cm)**	**#**	**NaOH (ml)**	**Conductivity (µS/cm)**
1	0	2600	**1**	0	2450	**1**	0	2360
2	0.2	2500	**2**	0.2	2320	**2**	0.2	2310
3	0.4	2470	**3**	0.4	2300	**3**	0.4	2250
4	0.6	2420	**4**	0.6	2270	**4**	0.6	2200
5	0.8	2360	**5**	0.8	2190	**5**	0.8	2130
6	1	2300	**6**	1	2130	**6**	1	2070
7	1.2	2230	**7**	1.2	2070	**7**	1.2	2000
8	1.4	2170	**8**	1.4	2010	**8**	1.4	1945
9	1.6	2120	**9**	1.6	1944	**9**	1.6	1886
10	1.8	2050	**10**	1.8	1885	**10**	1.8	1822

Table 19 (Continued)

DD-70%			DD-81%			DD-90%		
#	NaOH (ml)	Conductivity (µS/cm)	#	NaOH (ml)	Conductivity (µS/cm)	#	NaOH (ml)	Conductivity (µS/cm)
11	2	1965	**11**	2	1827	**11**	2	1771
12	2.2	1914	**12**	2.2	1754	**12**	2.2	1702
13	2.4	1836	**13**	2.4	1718	**13**	2.4	1645
14	2.6	1774	**14**	2.6	1651	**14**	2.6	1590
15	2.8	1717	**15**	2.8	1587	**15**	2.8	1527
16	3	1663	**16**	3	1527	**16**	3	1478
17	3.2	1600	**17**	3.2	1472	**17**	3.2	1418
18	3.4	1532	**18**	3.4	1414	**18**	3.4	1359
19	3.6	1477	**19**	3.6	1350	**19**	3.6	1301
20	4	1416	**20**	3.8	1294	**20**	3.8	1254
21	4.1	1375	**21**	4	1240	**21**	4	1201
22	4.2	1354	**22**	4.1	1213	**22**	4.1	1165
23	4.3	1326	**23**	4.2	1179	**23**	4.2	1137
24	4.4	1296	**24**	4.3	1160	**24**	4.3	1108
25	4.5	1271	**25**	4.4	1133	**25**	4.4	1076
26	4.6	1236	**26**	4.5	1102	**26**	4.5	1060
27	4.7	1214	**27**	4.6	1075	**27**	4.6	1032

Table 19 (Continued)

DD-70%			DD-81%			DD-90%		
#	NaOH (ml)	Conductivity (µS/cm)	#	NaOH (ml)	Conductivity (µS/cm)	#	NaOH (ml)	Conductivity (µS/cm)
28	4.8	1196	**28**	4.7	1052	**28**	4.7	1008
29	4.9	1152	**29**	4.8	1037	**29**	4.8	984
30	5	1131	**30**	4.9	996	**30**	4.9	965
31	5.1	1110	**31**	5	978	**31**	5	948
32	5.2	1085	**32**	5.1	959	**32**	5.1	935
33	5.3	1063	**33**	5.2	942	**33**	5.2	928
34	5.4	1041	**34**	5.3	933	**34**	5.3	925
35	5.5	1026	**35**	5.4	928	**35**	5.4	924
36	5.6	1019	**36**	5.5	927	**36**	5.5	926
37	5.7	1017	**37**	5.6	929	**37**	5.6	928
38	5.8	1017	**38**	5.7	931	**38**	5.7	932
39	5.9	1019	**39**	5.8	934	**39**	5.8	935
40	6	1021	**40**	5.9	938	**40**	5.9	938
41	6.1	1025	**41**	6	943	**41**	6	943
42	6.2	1030	**42**	6.1	946	**42**	6.1	948
43	6.3	1034	**43**	6.2	951	**43**	6.2	951
44	6.4	1039	**44**	6.3	954	**44**	6.3	956

Table 19 (Continued)

DD-70%			DD-81%			DD-90%		
#	NaOH (ml)	Conductivity (µS/cm)	#	NaOH (ml)	Conductivity (µS/cm)	#	NaOH (ml)	Conductivity (µS/cm)
45	6.5	1043	**45**	6.4	959	**45**	6.4	960
46	6.6	1046	**46**	6.5	964	**46**	6.5	963
47	6.7	1051	**47**	6.6	967	**47**	6.6	969
48	6.8	1055	**48**	6.7	971	**48**	6.7	973
49	6.9	1058	**49**	6.8	974	**49**	6.8	977
50	7	1063	**50**	6.9	979	**50**	6.9	981
51	7.1	1068	**51**	7	983	**51**	7	984
52	7.2	1072	**52**	7.1	987	**52**	7.1	989
53	7.3	1075	**53**	7.2	990	**53**	7.2	991
54	7.4	1080	**54**	7.3	994	**54**	7.3	995
55	7.5	1083	**55**	7.4	998	**55**	7.4	999
56	7.6	1087	**56**	7.5	1001	**56**	7.5	1001
57	7.7	1089	**57**	7.6	1004	**57**	7.6	1004
58	7.8	1093	**58**	7.7	1006	**58**	7.7	1006
59	7.9	1095	**59**	7.8	1010	**59**	7.8	1009
60	8	1098	**60**	7.9	1012	**60**	7.9	1012
61	8.1	1101	**61**	8	1015	**61**	8	1014

Table 19 (Continued)

DD-70%			DD-81%			DD-90%		
#	NaOH (ml)	Conductivity (µS/cm)	#	NaOH (ml)	Conductivity (µS/cm)	#	NaOH (ml)	Conductivity (µS/cm)
62	8.2	1106	**62**	8.1	1017	**62**	8.1	1017
63	8.3	1109	**63**	8.2	1019	**63**	8.2	1021
64	8.4	1111	**64**	8.3	1022	**64**	8.3	1023
65	8.5	1113	**65**	8.4	1024	**65**	8.4	1025
66	8.6	1116	**66**	8.5	1028	**66**	8.5	1028
67	8.7	1119	**67**	8.6	1030	**67**	8.6	1031
68	8.8	1121	**68**	8.7	1032	**68**	8.7	1035
69	8.9	1125	**69**	8.8	1035	**69**	8.8	1037
70	9	1128	**70**	8.9	1037	**70**	8.9	1040
71	9.1	1131	**71**	9	1040	**71**	9	1042
72	9.2	1134	**72**	9.1	1043	**72**	9.1	1046
73	9.3	1137	**73**	9.2	1044	**73**	9.2	1048
74	9.4	1144	**74**	9.3	1048	**74**	9.3	1050
75	9.5	1150	**75**	9.4	1050	**75**	9.4	1053
76	9.7	1180	**76**	9.5	1054	**76**	9.5	1057
77	9.9	1213	**77**	9.6	1056	**77**	9.6	1060
78	10	1232	**78**	9.7	1064	**78**	9.7	1064

Table 19 (Continued)

DD-70%			DD-81%			DD-90%		
#	NaOH (ml)	Conductivity (µS/cm)	#	NaOH (ml)	Conductivity (µS/cm)	#	NaOH (ml)	Conductivity (µS/cm)
79	10.2	1277	**79**	9.8	1067	**79**	9.8	1067
80	10.4	1304	**80**	9.9	1070	**80**	9.9	1070
81	10.6	1340	**81**	10	1075	**81**	10	1076
82	10.8	1380	**82**	10.2	1112	**82**	10.1	1081
83	11	1426	**83**	10.4	1152	**83**	10.2	1095
84	11.2	1456	**84**	10.6	1186	**84**	10.3	1106
85	11.4	1504	**85**	10.8	1229	**85**	10.4	1121
86	11.5	1532	**86**	11	1260	**86**	10.5	1135
87	12	1622	**87**	11.2	1305	**87**	10.6	1162
88	12.5	1712	**88**	11.4	1337	**88**	10.8	1195
89	13	1804	**89**	11.6	1380	**89**	11	1227
90	13.5	1894	**90**	11.8	1414	**90**	11.2	1266
91	14	1984	**91**	12	1450	**91**	11.4	1306
92	14.5	2080	**92**	12.5	1538	**92**	11.6	1345
93	15	2160	**93**	13	1629	**93**	11.8	1383
			94	13.5	1724	**94**	12	1417
			95	14	1823	**95**	12.5	1512

Table 19 (Continued)

DD-70%			DD-81%			DD-90%		
#	NaOH (ml)	Conductivity (µS/cm)	#	NaOH (ml)	Conductivity (µS/cm)	#	NaOH (ml)	Conductivity (µS/cm)
			96	14.5	1902	**96**	13	1607
			97	15	1987	**97**	13.5	1693
			98	15.5	2080	**98**	14	1784
			99	16	2160	**99**	14.5	1875
			100	16.5	2250	**100**	15	1963
			101	17	2340	**101**	15.5	2050
			102	17.5	2400	**102**	16	2140
			103	18	2500	**103**	16.5	2220
						104	17	2310
						105	17.5	2390
						106	18	2480

Appendix B

Rheological Data for Measuring the Zero-Shear Rate Viscosities of Chitosan Solutions Containing Acetic Acid

The rheological properties of chitosan solutions were measured using ATS Rheosystem Stresstech HR Rheometer at 25°C. A 50 mm parallel plate system with a gap of 0.4 mm was use for the all the samples. The following table provides the viscosity data as a function of share rate for a concentration of 3wt% with different of deacetylation DD81% and DD-90%. The zero shear rate viscosity (η_o) was calculated from Newtonian plateau region. These tables are given as examples. The zero shear viscosities and the corresponding specific viscosities for DD-81% and DD-90% at different concentrations are provided in Table 14.

Table 20 Rheological data of the chitosan solution (DD-81%) at a concentration of 3 wt% in 90% acetic acid/water as solvent

Time	**Temperature**	**Stress**	**Shear rate**	**Viscosity**	**APP**	**Torque**
s	**°C**	**Pa**	**1/s**	**cP**		**Nm**
37.6	25	1.00E+00	3.21E-01	3.12E+03	0.994	2.39E-05
75.2	25.1	1.27E+00	4.08E-01	3.12E+03	0.998	3.03E-05
112.8	25	1.62E+00	5.18E-01	3.12E+03	0.999	3.86E-05
150.5	25	2.06E+00	6.61E-01	3.11E+03	1.001	4.90E-05
188.1	25	2.61E+00	8.49E-01	3.08E+03	1.004	6.23E-05
225.8	25	3.32E+00	1.08E+00	3.06E+03	1.005	7.92E-05

Table 20 (Continued)

263.5	25	4.22E+00	1.42E+00	2.97E+03	1.008	1.01E-04
301.1	25	5.37E+00	1.84E+00	2.92E+03	1.008	1.28E-04
338.7	25.1	6.82E+00	2.41E+00	2.83E+03	1.007	1.63E-04
398.9	25	8.68E+00	2.93E+00	2.96E+03	0.966	2.07E-04
436.5	25	1.10E+01	3.69E+00	2.99E+03	0.994	2.63E-04
496.6	25	1.40E+01	5.05E+00	2.78E+03	1.031	3.34E-04
534.3	24.9	1.78E+01	6.34E+00	2.81E+03	1.01	4.25E-04
576	25	2.27E+01	8.32E+00	2.73E+03	1.007	5.41E-04
613.7	25	2.88E+01	1.09E+01	2.65E+03	1.004	6.87E-04
651.4	25	3.66E+01	1.45E+01	2.53E+03	1.006	8.74E-04
691.9	25	4.66E+01	1.95E+01	2.39E+03	0.995	1.11E-03
748.9	25	5.92E+01	2.94E+01	2.01E+03	1.007	1.41E-03
786.6	24.9	7.53E+01	4.08E+01	1.85E+03	0.994	1.80E-03
846.8	25	9.57E+01	5.08E+01	1.88E+03	0.952	2.28E-03
894.1	25	1.22E+02	6.83E+01	1.78E+03	0.991	2.90E-03
931.7	24.9	1.55E+02	9.56E+01	1.62E+03	0.994	3.69E-03
969.4	24.9	1.97E+02	1.36E+02	1.45E+03	0.994	4.69E-03
1007	25	2.50E+02	1.97E+02	1.27E+03	0.992	5.96E-03

Table 21 Rheological data of the chitosan solution (DD-90%) at a concentration of 3 wt% in 90% acetic acid/water as solvent

Time	**Temperature**	**Stress**	**Shear rate**	**Viscosity**	**APP**	**Torque**
s	**ºC**	**Pa**	**1/s**	**cP**		**Nm**
37.6	25.1	1.00E+00	6.07E-01	1.65E+03	1	2.39E-05
75.3	25	1.27E+00	7.72E-01	1.65E+03	0.998	3.03E-05
112.9	24.9	1.62E+00	9.78E-01	1.65E+03	0.998	3.86E-05
150.5	25	2.06E+00	1.24E+00	1.66E+03	0.999	4.90E-05
188.2	25	2.61E+00	1.57E+00	1.66E+03	0.998	6.23E-05
225.8	25	3.32E+00	1.99E+00	1.67E+03	1.001	7.92E-05
263.4	25.1	4.22E+00	2.53E+00	1.67E+03	0.997	1.01E-04
301	25	5.37E+00	3.19E+00	1.68E+03	0.995	1.28E-04
338.7	25	6.82E+00	4.07E+00	1.68E+03	0.999	1.63E-04
376.3	24.9	8.68E+00	5.19E+00	1.67E+03	1.001	2.07E-04
417.1	24.9	1.10E+01	6.61E+00	1.67E+03	0.99	2.63E-04
454.8	24.9	1.40E+01	8.46E+00	1.66E+03	0.997	3.34E-04
492.4	25	1.78E+01	1.09E+01	1.64E+03	0.999	4.25E-04
530.1	24.9	2.27E+01	1.41E+01	1.61E+03	1.006	5.41E-04
567.8	25	2.88E+01	1.81E+01	1.59E+03	0.993	6.87E-04
605.5	24.9	3.66E+01	2.41E+01	1.52E+03	1.009	8.74E-04
643.1	25.1	4.66E+01	3.11E+01	1.50E+03	0.995	1.11E-03

Table 21 (Continued)

680.7	25.1	5.92E+01	4.16E+01	1.42E+03	0.993	1.41E-03
732.4	25	7.53E+01	6.32E+01	1.19E+03	1.007	1.80E-03
773.4	25.1	9.57E+01	9.44E+01	1.01E+03	0.995	2.28E-03